ASSESSMENT OF FINITE ELEMENT APPROXIMATIONS FOR NONLINEAR FLEXIBLE MULTIBODY DYNAMICS

by

DAVID THOMAS ROBERTS

B.A.E.M., University of Minnesota (1985)

SUBMITTED TO THE DEPARTMENT OF
AERONAUTICS AND ASTRONAUTICS
IN PARTIAL FULFILLMENT OF THE REQUIREMENTS
FOR THE DEGREE OF

MASTER OF SCIENCE

at the

MASSACHUSETTS INSTITUTE OF TECHNOLOGY

May 1991

Signature of Author _____
Department of Aeronautics and Astronautics
May 10, 1991

Certified by _____
David S. Kang
Technical Staff, C.S. Draper Laboratory
Thesis Supervisor

Approved by _____
John Dugundji
Professor, Department of Aeronautics and Astronautics
Thesis Supervisor

Accepted by _____
Professor Harold Y. Wachman
Chairman, Departmental Graduate Committee

ASSESSMENT OF FINITE ELEMENT APPROXIMATIONS FOR NONLINEAR FLEXIBLE MULTIBODY DYNAMICS

by

DAVID THOMAS ROBERTS

Submitted to the Department of Aeronautics and Astronautics
on May 10, 1991
in partial fulfillment of the requirements for the degree of
Master of Science in Aeronautics and Astronautics

ABSTRACT

Systematic investigation is made of effects of kinematic assumptions and finite element approximations in the context of nonlinear flexible multibody dynamics. Two nonlinear beam finite elements are consistently derived from virtual work principle using Bernoulli-Euler and Timoshenko beam kinematics. Initial assessment is made by studying convergence properties of element formulations with eigenvalue problems: free vibration, static buckling, and dynamic buckling. Equations of motion are derived for rigid central body with flexible appendage using virtual work principle. Virtual work principle allows natural and consistent discretization of flexible appendage using finite element method. Nonlinearities in flexibility are explored through dynamics examples using beam finite elements. Application of dynamics formulation is made to a realistic scenario involving space shuttle remote manipulator arm with attached payload. Contribution of nonlinear theory, in both formulation and solution, is assessed.

Thesis Supervisor: David S. Kang, Ph.D.
Technical Staff, C.S. Draper Laboratory

Acknowledgements

I would like to express my sincere gratitude to my thesis supervisor, David S. Kang, who made substantial contributions to every aspect of my education, and graciously gave his time and energy on my behalf.

I would like to acknowledge the support and friendship of my Draper Laboratory colleagues: Joe Nadeau, Van Luu, Howard Clark, Mark Henault, Dave Dellagrotte, and Ashok Patel.

Last, but not least, I would like to express my heartfelt appreciation to my family, for all the love and encouragement they have so freely given.

This thesis was supported by The Charles Stark Draper Laboratory, Inc., under Internal Research & Development 332.

David T Roberts

David T. Roberts, CAPT, USAF

Table of Contents

List of Figures

List of Tables

List of Symbols

Following is a list of symbols used throughout the text. In some instances, the same symbols have been given different meaning in different chapters. The number to the right indicates the first occurance of the symbol and the accompanying definition.

Chapter 2

Vectors are indicated by bold type. Underlined quantities indicate vector components, expressed in the body fixed frame. If a vector and its associated components are used in the text, they are listed together.

Chapter 3

Chapter 1
Introduction

1.1 Purpose/Objective of Present Work

Increasingly, formulations for flexible multibody dynamical systems are employing the finite element method in the discretization of the flexible domain. Embedded in the finite element method are assumptions regarding the assumed displacement field, and additional approximations such as mass lumping and reduced integration over the spatial domain.

A study is conducted to address the application of finite element discretization in flexible multibody dynamics. The virtual work principle is chosen as the basis for derivation of the equations of motion for a simple class of satellite-type vehicles. The reasons for choosing the virtual work principle are threefold:

- an integral representation of the governing equations of motion is embedded in the virtual work principle,
- the virtual work principle allows decomposition of dynamic system into rigid and flexible portions,
- the virtual work principle is a basis for the finite element method.

Kinematic assumptions and finite element approximations are investigated in a dynamics context through a series of eigenvalue problems. The approach emphasizes understanding of the behavior of consistently derived finite elements rather than demonstrating one formulation over another. The consistent derivation of nonlinear finite elements allows an

assessment of such 'inconsistent' assumptions as lumped mass and reduced integration. Such in-depth study of the behavior of finite elements in dynamics is not widely available in the literature.

Multibody dynamic formulations are inherently nonlinear due to the large rotations of reference frames in inertial space. When coupled with the possibility of nonlinear flexibility, the importance of one effect compared to another is unclear. The available literature is not clear in the meaning of 'nonlinear' solutions, since nonlinearity arises from both inertial and flexibility considerations. Researchers have not taken an engineering perspective; they have not made explicit statements regarding the most important effects, i.e. which effects are essential to capture the physics of the problem. The nonlinear equations of motion developed in this thesis are applied to dynamic problems with an eye toward understanding the separate effects of forcing terms and the relative importance of nonlinear flexibility.

1.2 Thesis Overview

Chapter 2 derives exact integral equations of motion for a vehicle composed of central rigid body with a rigidly attached flexible appendage. Assumptions of lumped mass and lumped mass/inertia are employed to yield equations of motion which are suitable for time integration using an implicit scheme. Solution of these equations allows assessment of the influence of centrifugal and Coriolis forcing terms and importance of nonlinear flexibility (geometric stiffness).

In chapter 3, two nonlinear beam finite elements are consistently derived from the virtual work principle. Bernoulli-Euler and Timoshenko beam kinematics are employed to give isoparametric beam finite elements with C^1 and C^0 continuity, respectively. It is shown that consistent derivation produces higher order stress resultants in the geometric stiffness matrix, which are generally ignored. For completeness, consistent nodal loads are also derived.

Systematic assessment of beam finite elements is made in chapter 4 through eigenvalue problems which include free vibration, and static and dynamic buckling. Effects of beam kinematics and finite element assumptions are explored in detail and compared with the analytical solution from Bernoulli-Euler beam theory. Results provide insight into modelling considerations typical of scenarios arising in flexible multibody dynamics.

Nonlinear dynamic problems are addressed in chapter 5 using the lumped mass/inertia formulation of chapter 2. Two examples are considered: the beam spin-up problem, and a realistic application involving the orbiter/remote manipulator system (RMS). System response is evaluated in terms of the level of discretization, and the contribution of nonlinear effects is addressed. Nonlinear effects due to rigid body motion coupled with flexible deformations are differentiated from flexible nonlinearity associated with tangent stiffness matrix. Gross overall motion of the system and flexible natural frequency are considered independently.

Six appendices are included for completeness. Stress resultants which arise in beam elements are considered in Appendix A. In Appendix

B, the Newmark integration scheme is derived for linear systems and an incremental form with Newton/Raphson iteration is derived for solution of nonlinear systems. Introduction to the explicit Runge-Kutta integration scheme is also given. Convergence data is tabulated for future reference in Appendix C. Details of the RMS finite element model are given in Appendix D. In Appendix E, the Timoshenko frequency equation (cantilevered boundary conditions) is solved, and the natural frequency convergence plots repeated with alternative normalization. Finally, a brief overview of Gauss quadrature is given in Appendix F.

1.3 Literature Review

1.3.1 Beam Theory/Finite Elements

Classical Bernoulli-Euler beam theory is known to overpredict the natural frequencies for higher modes of vibration. It also tends to overpredict natural frequencies for *all* modes for thick beams (length/thickness ≤ 10). The first problem was alleviated by Rayleigh [1], who introduced rotatory inertia of the beam cross-sections. An additional modification was introduced by Timoshenko [2, 3], allowing description of cross-section and neutral axis rotation by independent angles, thus allowing the beam to undergo shearing deformation.

The literature has focused on Timoshenko beam theory, from both analytical and finite element standpoints. The partial differential equations resulting from Timoshenko's theory are difficult to solve for anything but

prismatic beams with simple boundary conditions. Huang [4] derives frequency and normal mode equations for uniform, isotropic beams with simple boundary conditions. Noting the difficulty of solving the frequency equations, he introduces the 'frequency chart', which, for a given set of beam parameters, provides a correction factor to be applied to the Bernoulli-Euler solution for natural frequency. Frequency charts provide a quick and convenient measure of the influence of rotatory inertia and shearing deformation. Leckie and Lindberg [5] studied the effect of lumped mass assumptions on beam natural frequencies using finite difference expressions.

In the finite element literature, much emphasis has been placed on the development of higher order Timoshenko beam elements. Higher order elements [6, 7, 8] were necessary in order to satisfy all geometric and natural boundary conditions of a Timoshenko beam. The simplest shear deformable beam possible was introduced by Hughes et. al. [9]. Convergence and accuracy were demonstrated for static problems. Shear locking was avoided by use of selective reduced integration. Consistent assessment of finite element approximations for dynamics has not been undertaken in the literature.

1.3.2 Multibody Dynamics

Review and chronology of the rigid and flexible multibody dynamics literature is widely available [10, 11, 12] and will not be repeated here. The literature can be further partitioned according to the intended application. Mello [10] separated the literature into the following groups:

spacecraft, mechanisms, and robotics. There exists a body of literature whose multibody formulations are demonstrated using beam finite elements. A selection of these will be addressed.

Ryan [13] investigated a deficiency of conventional general flexible multibody programs (such as DISCOS, NBOD, TREETOPS, ALLFLEX), which fail to correctly capture the stiffening effect of rapidly spinning systems. He extended the assumed modes formulation and demonstrated the new theory by application to a deployment maneuver and the beam spin-up problem. Simo & Vu-Quoc [14, 15] developed equations of motion for a flexible beam undergoing large overall motions. In [15], the spin-up problem is addressed among other examples. Quadratic beam finite elements are used in the discretization of the flexible domain. However, no discussion is given regarding the essential features governing the correct response. Ider & Amirouche [16] also develop an algorithm for multibody systems using assumed modes and Kane's equations. Their formulation is tailored for structures with variable cross-section beam elements. They also consider the spin-up problem in their numerical examples.

Taking an analytical approach, Silverberg & Park [17] explore contributions of Coriolis and centrifugal forcing terms in the response of maneuvering spacecraft. Through development of stiffness operators, they compare natural frequencies of a spinning beam achieved by linearization about both static and dynamic equilibriums. They show that linearization about the dynamic equilibrium (same as including geometric nonlinearities) has an important effect when certain nondimensional spin and material parameters are exceeded.

Chapter 2
Flexible Body Formulation

This chapter develops the equations of motion for a rigid body with attached flexible appendage, without articulation, using the principle of virtual work. The governing equations are consistently derived, so that all terms are retained.

Since the virtual work principle is the basis for the finite element formulation, it is natural and consistent to discretize the flexible appendage using the finite element method. In this chapter, lumped mass (3 DOFs/node) and lumped mass/inertia (6 DOFs/node) assumptions are employed in the treatment of the mass distribution of the flexible appendage. Lumped masses are located at the nodes resulting from finite element discretization of the appendage stiffness. These assumptions lead to equations of motion which can be expressed in a convenient matrix form. The exact governing equations could also be fully developed using finite element method, as has been done in the literature [14, 15, 18].

The assumption of rigid central body allows governing equations of motion to be derived with respect to the body fixed frame. Alternatively, consideration of a free floating deformable body requires the application of conservation of linear and angular momentum [18], or other corotating frames [19, 20].

Equations derived in this chapter are quite general in nature, and can be applied to a wide class of problems. Many satellites, as well as the space

shuttle, can be approximated by the rigid central body assumption. The only restriction on the flexible appendage is the fixed, or cantilevered boundary condition, relative to the rigid body. Example problems using the lumped mass/inertia formulation are considered in chapter 5, where the flexible domain is discretized using the beam finite elements derived in chapter 3.

2.1 Vehicle Idealization

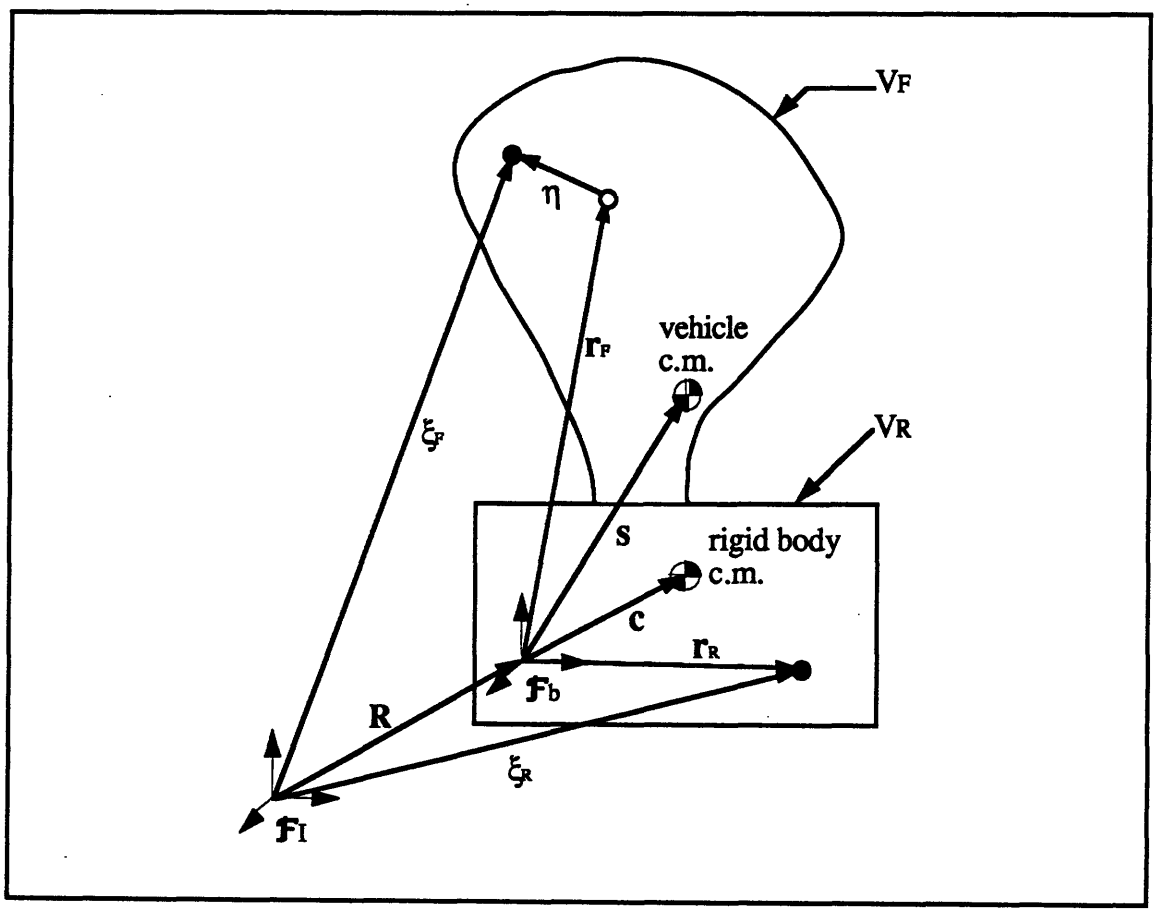

Figure 2.1. Rigid body with flexible appendage.

where

$\mathcal{F}_I$ = inertial reference frame
$\mathcal{F}_b$ = body fixed reference frame
V_R = rigid body domain
V_F = flexible body domain, reference configuration
$\xi_R(t)$ = material coordinate of rigid particle with respect to inertial frame
$\xi_F(t)$ = material coordinate of flexible particle with respect to inertial frame
$\mathbf{R}(t)$ = inertial position of body frame
$\mathbf{r}_R$ = rigid particle position with respect to body frame
$\mathbf{r}_F(t)$ = reference flexible particle position with respect to body frame
$\mathbf{c}$ = rigid c.m. with respect to body frame
$\mathbf{s}(t)$ = vehicle c.m. with respect to body frame
$\eta(t)$ = displacement of flexible particle due to deformation

Figure 2.1 shows a rigid body with attached flexible appendage in inertial space. The form of the appendage is arbitrary, as suggested by the figure. In practice, the body fixed reference frame is located as a matter of convenience, and is not normally coincident with the rigid body c.m. or the vehicle c.m.

2.2 Principle of Virtual Work

The principle of virtual work is a statement that for a body in equilibrium under the action of prescribed body and surface forces the work done by these forces through a kinematically admissible displacement is equal to the change in internal virtual work. In combination with D'Alembert's principle, the virtual work principle can be expressed as

$$\delta W_{ext} = \int_v \delta\xi \cdot (\mathbf{f} - \rho\ddot{\xi})\, dV + \int_{S_\sigma} \delta\xi \cdot \mathbf{t}\, dS = \int_v \delta\varepsilon : \sigma\, dV = \delta W_{int} \qquad (2.2.1)$$

where, in addition to the quantities previously defined,

$\mathbf{f}$ = body force (force/volume)
$\mathbf{t}$ = surface traction applied over S_σ
ρ = density
ε = strain
σ = stress

The virtual work statement is evaluated as the sum of two parts; integration over the rigid central body and integration over the flexible appendage.

2.3 Vectrix Notation

In forming the virtual work expression, several vectors must be defined. When the dynamic system involves more than one reference frame, as is the case for the vehicle of figure 2.1, it is helpful to use a notation which explicitly identifies the frame in which vector components are expressed. Toward this end, the vectrix notation [21] is used. A vector can be written as the multiplication of two column matrices: one containing the vector components, the other the frame unit directions. For example, an arbitrary vector $\mathbf{v}$ can be expressed in some reference frame $\mathcal{F}_a$, whose basis vectors are $\hat{\mathbf{a}}_1$, $\hat{\mathbf{a}}_2$, $\hat{\mathbf{a}}_3$, as

$$\mathbf{v} = v_1\hat{\mathbf{a}}_1 + v_2\hat{\mathbf{a}}_2 + v_3\hat{\mathbf{a}}_3 = \mathcal{F}_a{}^T \underline{v} = \underline{v}^T \mathcal{F}_a \qquad (2.3.1)$$

where

$$\underline{v}^T = [\ v_1 \quad v_2 \quad v_3\ ]$$

$$\mathcal{F}_a^T = [\ \hat{a}_1 \quad \hat{a}_2 \quad \hat{a}_3\ ]$$

Differentiation of vectors involving multiple reference frames introduces the vector cross product. It is convenient to express this operation as a matrix multiplication, in conjunction with vetrices. The cross product of arbitrary vectors **u** and **v**, both expressed in $\mathcal{F}_a$, is given by

$$\mathbf{u} \times \mathbf{v} = \underline{u}^T \mathcal{F}_a \times \mathcal{F}_a^T \underline{v} = \mathcal{F}_a^T (\underline{u}^\times \underline{v}) \tag{2.3.2}$$

where $\underline{v}$ is the same as above and the components of $\underline{u}$ have been formed into the skew symmetric matrix given by

$$\underline{u}^\times = \begin{bmatrix} 0 & -u_3 & u_2 \\ u_3 & 0 & -u_1 \\ -u_2 & u_1 & 0 \end{bmatrix} \tag{2.3.3}$$

The inertial time derivative of the frame is also an important relationship and is given by

$$\dot{\mathcal{F}}_b^T = \underline{\omega}^T \mathcal{F}_b \times \mathcal{F}_b^T = \mathcal{F}_b^T \underline{\omega}^\times \tag{2.3.4}$$

2.4 Vehicle Kinematics

From figure 2.1, the inertial positions of rigid and flexible material particles are given by the vectors

$$\xi_R = \mathbf{R} + \mathbf{r}_R \tag{2.4.1}$$

$$\xi_F = \mathbf{R} + \mathbf{r}_F + \eta \tag{2.4.2}$$

Inertial accelerations are obtained through time differentiation of the position vectors. Let $\frac{d}{dt}( )$ denote time differentiation in the inertial frame, and $\dot{(\,)}$ indicate time differentiation in the body fixed frame. Differentiation of equation (2.4.1) gives

$$\ddot{\xi}_R = \frac{d}{dt}\left[\frac{d\mathbf{R}}{dt} + \frac{d\mathbf{r}_R}{dt}\right] \tag{2.4.3}$$

where it is convenient to let $\mathbf{u} = \frac{d\mathbf{R}}{dt}$, the inertial velocity of the body fixed frame. Now expressing components of $\mathbf{u}$ and $\frac{d\mathbf{r}_R}{dt}$ in the body fixed frame allows the derivative to be written as

$$\ddot{\xi}_R = \frac{d}{dt}\left[\mathcal{F}_b^{\,T}\underline{u} + \frac{d}{dt}\left(\mathcal{F}_b^{\,T}\underline{r}_R\right)\right] \tag{2.4.4}$$

Application of the chain rule and using the vectrix notation gives the final form of the inertial acceleration of an arbitrary rigid material particle. The acceleration of an arbitrary flexible particle follows in an analogous manner.

$$\ddot{\xi}_R = \mathcal{F}_b^{\,T}\left[\dot{\underline{u}} + \underline{\omega}^{\times}\,\underline{u} + \dot{\underline{\omega}}^{\times}\,\underline{r}_R + \underline{\omega}^{\times}\,\underline{\omega}^{\times}\,\underline{r}_R\right] \equiv \mathcal{F}_b^{\,T}\,\underline{a}_R \tag{2.4.5}$$

$$\ddot{\xi}_F = \mathcal{F}_b^T \left[\dot{\underline{u}} + \underline{\omega}^\times \underline{u} + \dot{\underline{\omega}}^\times (\underline{r}_F + \underline{\eta}) + 2\underline{\omega}^\times \dot{\underline{\eta}} + \underline{\omega}^\times \underline{\omega}^\times (\underline{r}_F + \underline{\eta}) + \ddot{\underline{\eta}} \right] \equiv \mathcal{F}_b^T \underline{a}_F \tag{2.4.6}$$

Virtual displacements are obtained through variation of the position vectors, and can be expressed as

$$\delta\xi_R = \mathcal{F}_b^T \left[\delta\underline{x} + \delta\underline{\theta}^\times \underline{r}_R \right] \tag{2.4.7}$$

$$\delta\xi_F = \mathcal{F}_b^T \left[\delta\underline{x} + \delta\underline{\eta} + \delta\underline{\theta}^\times (\underline{r}_F + \underline{\eta}) \right] \tag{2.4.8}$$

where

$\underline{r}_R, \underline{r}_F, \underline{\eta}$ = components of $\mathbf{r}_R, \mathbf{r}_F, \eta$, expressed in the body fixed frame

$\underline{u}$ = components of the inertial velocity of the origin of the body fixed frame

$\underline{\omega}$ = components of the inertial angular velocity of the body fixed frame

$\delta\underline{x}$ = components of the variation of inertial position vector $\mathbf{R}$

$\delta\underline{\theta}$ = components of angular variation which arises as a consequence of rotation of the body frame with respect to the inertial frame

$\delta\underline{\eta}$ = components of the variation of the relative displacement vector η

$\mathcal{F}_b^T = \left[\hat{\mathbf{b}}_1 \quad \hat{\mathbf{b}}_2 \quad \hat{\mathbf{b}}_3 \right]$

All components defined above are expressed in the body fixed frame, $\mathcal{F}_b$. Note that the acceleration of a flexible particle has a high degree of coupling between rigid body motions and flexible deformations.

2.5 Exact Governing Equations

The governing equations of motion are obtained by substituting equations (2.4.5)-(2.4.8) into equation (2.2.1). Evaluation of equation (2.2.1) produces terms which can be grouped according to the variation ($\delta\underline{x}$, $\delta\underline{\theta}$, or $\delta\underline{\eta}$) multiplying each. Because of the arbitrariness of the variations, each group must independently be equal to zero. Thus the following three sets of governing equations are obtained.

Recall that no restrictions have been imposed regarding the physical shape of the flexible appendage, or on the form of the relative displacements $\underline{\eta}$.

Body Frame Translation ($\delta\underline{x}$):

$$\underline{F} + \int_{V_F} \underline{f}_F \, dV + \int_{S_{\sigma F}} \underline{t}_F \, dS = m\dot{\underline{u}} + m\underline{\omega}^{\times}\,\underline{u} + m\dot{\underline{\omega}}^{\times}\,\underline{c} + m\underline{\omega}^{\times}\,\underline{\omega}^{\times}\,\underline{c} + 2\underline{\omega}^{\times}\int_{V_F} \rho\dot{\underline{\eta}} \, dV + \int_{V_F} \rho\ddot{\underline{\eta}} \, dV \qquad (2.5.1)$$

Body Frame Rotation ($\delta\underline{\theta}$):

$$\underline{T} + \int_{V_F} (\underline{r}_F + \underline{\eta})^{\times}\,\underline{f}_F \, dV + \int_{S_{\sigma F}} (\underline{r}_F + \underline{\eta})^{\times}\,\underline{t}_F \, dS = m\underline{c}^{\times}\,\dot{\underline{u}} + m\underline{c}^{\times}\,\underline{\omega}^{\times}\,\underline{u} + \underline{I}\,\dot{\underline{\omega}} + \underline{\omega}^{\times}\,\underline{I}\,\underline{\omega} + 2\int_{V_F} \rho(\underline{r}_F + \underline{\eta})^{\times}\,\underline{\omega}^{\times}\,\dot{\underline{\eta}} \, dV + \int_{V_F} \rho(\underline{r}_F + \underline{\eta})^{\times}\,\ddot{\underline{\eta}} \, dV \qquad (2.5.2)$$

Flexible Appendage DOFs ($\delta\underline{\eta}$):

$$\int_{V_F} \delta\underline{\eta}^T \underline{f_F}\, dV + \int_{S_{\sigma F}} \delta\underline{\eta}^T \underline{t_F}\, dS = \int_{V_F} \delta\underline{\eta}^T \rho\, dV \dot{\underline{u}} + \int_{V_F} \delta\underline{\eta}^T \rho\, dV \underline{\omega}^{\times}\, \underline{u}$$
$$+ \int_{V_F} \delta\underline{\eta}^T \dot{\underline{\omega}}^{\times} (\underline{r_F} + \underline{\eta}) \rho\, dV + 2\int_{V_F} \delta\underline{\eta}^T \underline{\omega}^{\times} \dot{\underline{\eta}} \rho\, dV$$
$$+ \int_{V_F} \delta\underline{\eta}^T \underline{\omega}^{\times} \underline{\omega}^{\times} (\underline{r_F} + \underline{\eta}) \rho\, dV + \int_{V_F} \delta\underline{\eta}^T \ddot{\underline{\eta}} \rho\, dV + \int_{V_F} \delta\varepsilon : \sigma\, dV \qquad (2.5.3)$$

where

$$\underline{F} = \underline{F_B} + \underline{F_T} \qquad (2.5.4)$$

$$\underline{T} = \underline{T_B} + \underline{T_T} \qquad (2.5.5)$$

$$\underline{\underline{I}} = \underline{\underline{I}}_R + \underline{\underline{I}}_F \qquad (2.5.6)$$

$$m = \int_{V_R} \rho\, dV + \int_{V_F} \rho\, dV \qquad (2.5.7)$$

$$m\underline{c} = \int_{V_R} \rho \underline{r_R}\, dV + \int_{V_F} \rho (\underline{r_F} + \underline{\eta})\, dV \qquad (2.5.8)$$

$$\underline{\underline{I}}_R \dot{\underline{\omega}} = \int_{V_R} \rho \underline{r_R}^{\times} \dot{\underline{\omega}}^{\times} \underline{r_R}\, dV \qquad (2.5.9)$$

$$\underline{\omega}^{\times} \underline{\underline{I}}_R \underline{\omega} = \int_{V_R} \rho \underline{r_R}^{\times} \underline{\omega}^{\times} \underline{\omega}^{\times} \underline{r_R}\, dV \qquad (2.5.10)$$

$$\underline{\underline{I}}_F \dot{\underline{\omega}} = \int_{V_F} \rho (\underline{r_R} + \underline{\eta})^{\times} \dot{\underline{\omega}}^{\times} (\underline{r_R} + \underline{\eta})\, dV \qquad (2.5.11)$$

$$\underline{\omega}^{\times}\,\underline{I}_F\underline{\omega} = \int_{V_F} \rho(\underline{r}_F + \underline{\eta})^{\times}\,\underline{\omega}^{\times}\,\underline{\omega}^{\times}\,(\underline{r}_F + \underline{\eta})\,dV \tag{2.5.12}$$

along with the following definitions:

$\underline{F}$ = components of total force acting through body frame origin, due to body forces ($\underline{F}_B$) and surface tractions ($\underline{F}_T$), expressed in the body fixed frame

$\underline{T}$ = components of total torque acting about body frame origin, due to body forces ($\underline{T}_B$) and surface tractions ($\underline{T}_T$), expressed in the body fixed frame

$\underline{\underline{I}}$ = instantaneous inertia matrix of the vehicle about the body fixed frame due to rigid body ($\underline{\underline{I}}_R$) and flexible body ($\underline{\underline{I}}_F$), expressed in body fixed frame

$\underline{f}_F$ = components of body forces acting on flexible body, expressed in body frame

$\underline{t}_F$ = components of surface tractions acting on flexible body, expressed in body frame

m = total vehicle mass ($m_R + m_F$)

Equations (2.5.1)-(2.5.3) are an exact set of equations governing the idealized vehicle of figure 2.1. Discretization of the flexible domain stems from these equations. Two lumped parameter approximations will be considered: (a) discretization of the flexible domain into a collection of point masses (no rotatory inertia) interconnected by massless springs, and (b) extension of the previous model to include rotatory inertia.

In practice, mass is concentrated at locations corresponding to finite element nodes, which allows the use of the finite element stiffness matrix. For 3-D finite elements, condensation technique must be used to make the stiffness matrix compatible with approximation (a).

Finite element discretization can also be consistently applied to all integrals in Equations (2.5.1)-(2.5.3). Derivation is straightforward, but the solution procedure is more involved than lumped mass assumptions, and is therefore not considered here. This approach has been used to derive equations of motion and demonstrated through simple problems using quadratic beam elements [18].

2.6 Lumped Mass Assumption

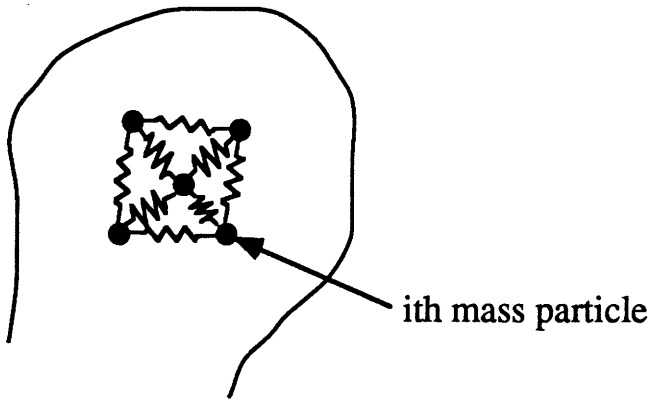

$$\underline{\eta}_i = \underline{q}_{ti} = \begin{bmatrix} u_i \\ v_i \\ w_i \end{bmatrix}$$

Figure 2.2. Lumped mass discretization of the flexible appendage.

Schematic representation of this assumption is shown in figure 2.2, where the solid line represents the surface of the flexible appendage. The flexible domain is modelled with a finite number of point mass particles, connected by massless springs. Mathematically, this is a straightforward process whereby the integrals in equations (2.5.1)-(2.5.3) over the flexible domain are replaced by summations over the number of mass particles. The location of lumped masses correspond to the nodal locations of the finite element discretization of the flexible domain.

$$\int_{V_F} f(\underline{\eta}, \dot{\underline{\eta}}, \ddot{\underline{\eta}})\rho \, dV \rightarrow \sum_{i=1}^{N} f(\underline{q}_i, \dot{\underline{q}}_i, \ddot{\underline{q}}_i)\, m_i \tag{2.6.1}$$

where

$\underline{q}_i$ = ith nodal displacements (translations only), expressed in the body fixed frame

m_i = corresponding lumped mass

The motion of a lumped mass is fully described by three translations. For 3-D finite element models of the flexible domain which include rotations as nodal DOFs, condensation technique must be used to remove rotational DOFs from the stiffness matrix. Consistent with the lumped mass approximation, external loads on the flexible body are also 'lumped' at the nodes. The exact governing equations (2.5.1)-(2.5.3) are simplified through the lumped mass assumption to give

$$\underline{F} = m\dot{\underline{u}} + m\underline{\omega}^{\times}\underline{u} + m\dot{\underline{\omega}}^{\times}\underline{c} + m\underline{\omega}^{\times}\underline{\omega}^{\times}\underline{c} + 2\sum_{i=1}^{N} m_i\, \underline{\omega}^{\times}\dot{\underline{q}}_i + \sum_{i=1}^{N} m_i\, \ddot{\underline{q}}_i \tag{2.6.2}$$

$$\underline{T} = m\underline{c}^{\times}\dot{\underline{u}} + m\underline{c}^{\times}\underline{\omega}^{\times}\underline{u} + \underline{I}\,\dot{\underline{\omega}} + \underline{\omega}^{\times}\underline{I}\,\underline{\omega} + 2\sum_{i=1}^{N} m_i\,(\underline{r}_i + \underline{q}_i)^{\times}\underline{\omega}^{\times}\dot{\underline{q}}_i$$

$$+ \sum_{i=1}^{N} m_i\,(\underline{r}_i + \underline{q}_i)^{\times}\ddot{\underline{q}}_i \tag{2.6.3}$$

$$\underline{f}_i = m_i\dot{\underline{u}} + m_i\underline{\omega}^{\times}\underline{u} + m_i\dot{\underline{\omega}}^{\times}(\underline{r}_i + \underline{q}_i) + m_i\underline{\omega}^{\times}\underline{\omega}^{\times}(\underline{r}_i + \underline{q}_i) + 2m_i\underline{\omega}^{\times}\dot{\underline{q}}_i$$

$$+ m_i\ddot{\underline{q}}_i + \sum_{j=1}^{N} \underline{K}_{ij}\,\underline{q}_i \qquad i = 1,2,\ldots,N \tag{2.6.4}$$

where

$\underline{r}_i$ = reference position of ith node, components in the body fixed frame
$\underline{f}_i$ = lumped nodal forces
$\underline{K}_{ij}$ = assembled stiffness matrix (rotation condensed out)

Equations (2.6.2)-(2.6.4) are valid for nonlinear flexible systems by interpretation of the stiffness matrix as the tangent stiffness matrix. An alternative derivation of the lumped mass equations of motion are provided in [22].

2.6.1 Equations of Motion

Equations (2.6.2)-(2.6.4) are the lumped mass equations of motion, comprising (6+3N) scalar equations. These equations can be recast into a single matrix equation of motion which can be numerically integrated.

$$\mathbf{M}\ddot{\mathbf{U}} + \mathbf{K}\mathbf{U} = \mathbf{R} \tag{2.6.5}$$

It is natural to partition the matrix equation into rigid and flexible body contributions and rewrite equation (2.6.5) as

$$\begin{bmatrix} \mathbf{M}_{RR} & \mathbf{M}_{RF} \\ \mathbf{M}_{FR} & \mathbf{M}_{FF} \end{bmatrix} \begin{bmatrix} \ddot{\mathbf{U}}_R \\ \ddot{\mathbf{U}}_F \end{bmatrix} + \begin{bmatrix} 0 & 0 \\ 0 & \mathbf{K}_{FF} \end{bmatrix} \begin{bmatrix} \mathbf{U}_R \\ \mathbf{U}_F \end{bmatrix} = \begin{bmatrix} \mathbf{R}_R + \mathbf{R}_{RF} \\ \mathbf{R}_F \end{bmatrix} \tag{2.6.6}$$

where

$$\underset{(6\times1)}{\ddot{\mathbf{U}}_R} = \begin{bmatrix} \dot{\underline{u}} \\ \dot{\underline{\omega}} \end{bmatrix} \tag{2.6.7}$$

$$\underset{(3N\times 1)}{\ddot{\mathbf{U}}_F} = \begin{bmatrix} \ddot{\underline{q}}_1 \\ \vdots \\ \ddot{\underline{q}}_N \end{bmatrix} \tag{2.6.8}$$

$$\underset{(6\times 6)}{\mathbf{M}_{RR}} = \begin{bmatrix} m & 0 & 0 & & \\ 0 & m & 0 & & -m\underline{c}^{\times} \\ 0 & 0 & m & & \\ & & & & \\ & m\underline{c}^{\times} & & & \underset{\sim}{I} \\ & & & & \end{bmatrix} \tag{2.6.9}$$

$$\underset{(3N\times 3N)}{\mathbf{M}_{FF}} = \begin{bmatrix} m_1 & & & & & & \\ & m_1 & & & & & \\ & & m_1 & & & & \\ & & & \ddots & & & \\ & & & & m_N & & \\ & & & & & m_N & \\ & & & & & & m_N \end{bmatrix} \tag{2.6.10}$$

$$\underset{(6\times 3N)}{\mathbf{M}_{RF}} = \begin{bmatrix} m_1 & 0 & 0 & & m_N & 0 & 0 \\ 0 & m_1 & 0 & \cdots & 0 & m_N & 0 \\ 0 & 0 & m_1 & & 0 & 0 & m_N \\ & & & & & & \\ m_1(\underline{r}_1 + \underline{q}_1)^{\times} & & & \cdots & & m_N(\underline{r}_N + \underline{q}_N)^{\times} & \end{bmatrix} \tag{2.6.11}$$

$$\underset{(6\times 1)}{\mathbf{R}_R} = \begin{bmatrix} \underline{F} - m\underline{\omega}^{\times}\,\underline{u} - m\underline{\omega}^{\times}\,\underline{\omega}^{\times}\,\underline{c} \\ \underline{T} - m\underline{c}^{\times}\,\underline{\omega}^{\times}\,\underline{u} - \underline{\omega}^{\times}\,\underset{\sim}{I}\,\underline{\omega} \end{bmatrix} \tag{2.6.12}$$

$$\underset{(6\times1)}{\mathbf{R}_{RF}} = \begin{bmatrix} -2\sum_{i=1}^{N} m_i \underline{\omega}^{\times} \dot{\underline{q}}_i \\ -2\sum_{i=1}^{N} m_i (\underline{r}_i + \underline{q}_i)^{\times} \underline{\omega}^{\times} \dot{\underline{q}}_i \end{bmatrix} \tag{2.6.13}$$

$$\underset{(3N\times1)}{\mathbf{R}_{F}} = \begin{bmatrix} \underline{f}_1 - m_1 \underline{\omega}^{\times} \underline{u} - m_1 \underline{\omega}^{\times} \underline{\omega}^{\times} (\underline{r}_1 + \underline{q}_1) - 2m_1 \underline{\omega}^{\times} \dot{\underline{q}}_1 \\ \vdots \\ \underline{f}_N - m_N \underline{\omega}^{\times} \underline{u} - m_N \underline{\omega}^{\times} \underline{\omega}^{\times} (\underline{r}_N + \underline{q}_N) - 2m_N \underline{\omega}^{\times} \dot{\underline{q}}_N \end{bmatrix} \tag{2.6.14}$$

Note that the mass matrix **M** is symmetric, positive definite; the stiffness matrix **K** is symmetric, positive semi-definite and allows rigid body motion. Numerical solution can be obtained in a number of ways. For linear systems, transformation can be made to modal space, which allows truncation of both system size and high frequency modes. Modal reduction is generally not possible for nonlinear flexible systems. Thus direct integration is preferred in the present context. Also the effect of various terms can be more readily assessed in physical space.

The methods available for direct integration of equation (2.6.5) can be classified into explicit and implicit schemes. Explicit schemes are conditionally stable and require very small time steps to integrate the highest frequencies accurately [23, 24]. Implicit schemes are advantageous because they are unconditionally stable and the step size can be chosen on the basis of accuracy only. This generally allows a much larger step size than would be required by explicit schemes. Because of the relaxed integration step size afforded by unconditionally stable implicit schemes, the Newmark integration method is implemented in the examples of chapter 5. Details of the Newmark scheme are outlined in Appendix B.

2.7 Lumped Mass/Inertia Assumption

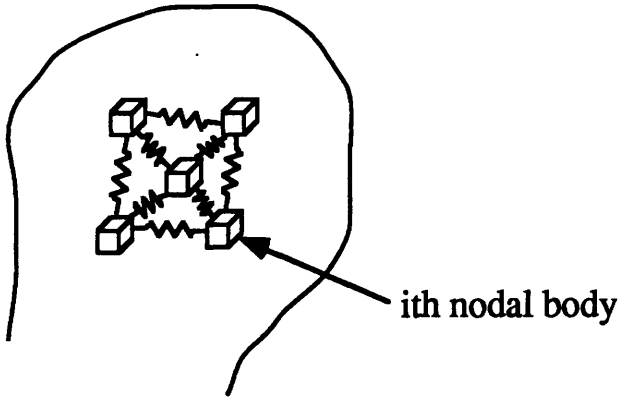

Figure 2.3. Lumped mass/inertia discretization of flexible appendage.

As in the previous derivation, integrals over the flexible domain are replaced by summations over a finite number of nodes. The nodes are now treated as small rigid bodies; they are no longer mass particles, but have both mass and inertia. Six quantities are required to describe the motion of each node.

Massless springs connect the nodal bodies just as in section 2.6. In practice, the finite element stiffness matrix provides information regarding interconnecting forces. The lumped mass/inertia formulation, as constrasted with the lumped mass formulation, has the advantage that finite element DOFs are used directly; no condensation is required in the numerical solution.

2.7.1 Kinematic Description

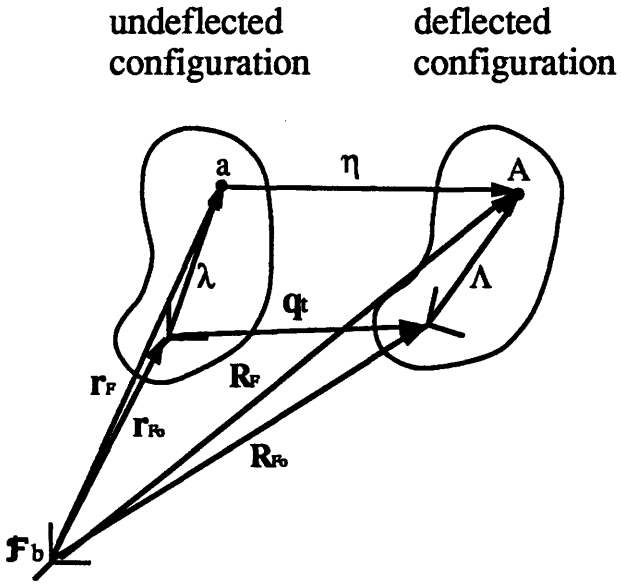

Figure 2.4. Relative displacement of ith nodal body.

Consider the rigid nodal body shown in figure 2.4 with an arbitrary material particle labelled "a" in the undeflected configuration, "A" in the deflected configuration. As measured with respect to the body fixed frame, the nodal body undergoes infinitesmal translation and rotation in moving to the deflected configuration. The location of an arbitrary material particle in the undeflected configuration is given by

$$\mathbf{r}_F = \mathbf{r}_{Fo} + \lambda \tag{2.7.1}$$

where $\mathbf{r}_{Fo}$ is the location of the nodal body reference frame in the undeflected configuration. The nodal body reference frame is aligned with the body fixed reference frame in the undeflected configuration.

In the deflected configuration, the location of A is given by

$$\mathbf{R}_F = \mathbf{R}_{Fo} + \Lambda = \mathbf{r}_{Fo} + \mathbf{q}_t + \Lambda \qquad (2.7.2)$$

where $\mathbf{R}_{Fo}$ is the location of the nodal body reference frame in the deflected configuration. The relative displacement undergone by a material particle in moving from a to A is then

$$\eta = \mathbf{R}_F - \mathbf{r}_F = \mathbf{q}_t + \Lambda - \lambda \qquad (2.7.3)$$

Rotation of the nodal body reference frame can be expressed by the skew symmetric infinitesmal rotation matrix so that

$$\Lambda = \mathbf{C}\lambda \qquad (2.7.4)$$

where

$$\mathbf{C} = \begin{bmatrix} 1 & -\theta_z & \theta_y \\ \theta_z & 1 & -\theta_x \\ -\theta_y & \theta_x & 1 \end{bmatrix}$$

Substitution of equation (2.7.4) into (2.7.3) leads to expression of the relative displacement as

$$\eta = \mathbf{q}_t + \mathbf{C}\lambda - \lambda = \mathbf{q}_t + (\mathbf{C} - \mathbf{I})\lambda \qquad (2.7.5)$$

where **I** is the identity matrix. Now since all vectors are expressed in the body fixed frame, the component notation is adopted. The matrix (**C** - **I**) above can be compared with the skew symmetric matrix (associated with vector cross products) introduced in section 2.3. Define

$$\underline{q_r} = \begin{bmatrix} \theta_x \\ \theta_y \\ \theta_z \end{bmatrix}$$

so that $\underline{q_r}^{\times} = (C - I)$. Finally, the relative displacement of a material particle, assuming infinitesmal rotation, can be written as

$$\underline{\eta} = \underline{q_t} + \underline{q_r}^{\times}\underline{\lambda} \tag{2.7.6}$$

2.7.2 Equations of Motion

The equations of motion follow from substitution of equation (2.7.6) into equations (2.5.1)-(2.5.3) and evaluating. Reduction of the exact equations is complicated somewhat by the form of the relative displacement given by equation (2.7.6). Some integrals produce higher-order terms which cannot be given simple physical interpretation. These higher-order terms are ignored. Details of integrations are not presented, and the lumped mass/inertia equations of motion in matrix form are given by

$$\begin{bmatrix} \mathbf{M_{RR}} & \mathbf{M_{RF}} \\ \mathbf{M_{FR}} & \mathbf{M_{FF}} \end{bmatrix} \begin{bmatrix} \ddot{\mathbf{U}}_R \\ \ddot{\mathbf{U}}_F \end{bmatrix} + \begin{bmatrix} 0 & 0 \\ 0 & \mathbf{K_{FF}} \end{bmatrix} \begin{bmatrix} \mathbf{U}_R \\ \mathbf{U}_F \end{bmatrix} = \begin{bmatrix} \mathbf{R}_R + \mathbf{R}_{RF} \\ \mathbf{R}_F \end{bmatrix} \tag{2.7.7}$$

where all partitions are explicitly defined below. Note that the rigid-rigid partition is the same as in section 2.6. $\mathbf{K_{FF}}$ is the full stiffness matrix produced by the finite element method. The tangent stiffness matrix is used for the solution of problems with nonlinear flexibility.

$$\underset{(6\times1)}{\ddot{\mathbf{U}}_R} = \begin{bmatrix} \ddot{\underline{u}} \\ \dot{\underline{\omega}} \end{bmatrix} \tag{2.7.8}$$

$$\underset{(6N\times 1)}{\ddot{\mathbf{U}}_F} = \begin{bmatrix} \ddot{\underline{q}}_{t1} \\ \ddot{\underline{q}}_{r1} \\ \vdots \\ \ddot{\underline{q}}_{tN} \\ \ddot{\underline{q}}_{rN} \end{bmatrix} \tag{2.7.9}$$

$$\underset{(6\times 6)}{\mathbf{M}_{RR}} = \begin{bmatrix} m & 0 & 0 & & \\ 0 & m & 0 & & -m\underline{c}^{\times} \\ 0 & 0 & m & & \\ & & & & \\ & m\underline{c}^{\times} & & & \underline{\underline{I}} \end{bmatrix} \tag{2.7.10}$$

$$\underset{(6N\times 6N)}{\mathbf{M}_{FF}} = \begin{bmatrix} m_1 & & & & & & & & \\ & m_1 & & & & & & & \\ & & m_1 & & & & & & \\ & & & \underline{\underline{I}}_1 & & & & & \\ & & & & \ddots & & & & \\ & & & & & m_N & & & \\ & & & & & & m_N & & \\ & & & & & & & m_N & \\ & & & & & & & & \underline{\underline{I}}_N \end{bmatrix} \tag{2.7.11}$$

$$\underset{(6\times 6N)}{\mathbf{M}_{RF}} = \begin{bmatrix} m_1 & & & \cdots & & m_N & & \\ & m_1 & & \cdots & & & m_N & \\ & & m_1 & \cdots & & & & \\ & & & & & & & \\ m_1(\underline{r}_1 + \underline{q}_1)^{\times} & & \underline{\underline{I}}_1 & \cdots & m_N(\underline{r}_N + \underline{q}_N)^{\times} & & & \underline{\underline{I}}_N \end{bmatrix} \tag{2.7.12}$$

$$\underset{(6\times1)}{\mathbf{R_R}} = \begin{bmatrix} \underline{F} - m\underline{\omega}^{\times}\,\underline{u} - m\underline{\omega}^{\times}\,\underline{\omega}^{\times}\,\underline{c} \\ \underline{T} - m\underline{c}^{\times}\,\underline{\omega}^{\times}\,\underline{u} - \underline{\omega}^{\times}\,\underline{\underline{I}}\,\underline{\omega} \end{bmatrix} \tag{2.7.13}$$

$$\underset{(6\times1)}{\mathbf{R_{RF}}} = \begin{bmatrix} -2\sum_{i=1}^{N} m_i\underline{\omega}^{\times}\,\underline{\dot{q}}_{ti} \\ -2\sum_{i=1}^{N} m_i(\underline{r}_i + \underline{q}_{ti})^{\times}\,\underline{\omega}^{\times}\,\underline{\dot{q}}_{ti} + \sum_{i=1}^{N} \underline{\omega}^{\times}\,\underline{\underline{I}}_i\underline{\dot{q}}_{ri} \end{bmatrix} \tag{2.7.14}$$

$$\underset{(6N\times1)}{\mathbf{R_F}} = \begin{bmatrix} \underline{f}_1 - m_1\underline{\omega}^{\times}\,\underline{u} - m_1\underline{\omega}^{\times}\,\underline{\omega}^{\times}\,(\underline{r}_1 + \underline{q}_{t1}) - 2m_1\underline{\omega}^{\times}\,\underline{\dot{q}}_{t1} + \text{h.o.t.} \\ \underline{t}_1 + \text{h.o.t.} \\ \vdots \\ \underline{f}_N - m_N\underline{\omega}^{\times}\,\underline{u} - m_N\underline{\omega}^{\times}\,\underline{\omega}^{\times}\,(\underline{r}_N + \underline{q}_{tN}) - 2m_N\underline{\omega}^{\times}\,\underline{\dot{q}}_{tN} + \text{h.o.t.} \\ \underline{t}_N + \text{h.o.t.} \end{bmatrix} \tag{2.7.15}$$

2.8 Extending Symbolic Rigid Body Codes

Implementation of the flexible body formulation can take advantage of available symbolic rigid body software. These software packages produce FORTRAN coding of the equations of motion of a user specified rigid multibody system. Some examples of symbolic manipulation rigid multibody software include SD/FAST [25], AUTOSIM [26], and AUTOLEV [27]. The use of symbolic rigid body codes allows the analyst to concentrate on a smaller set of 'hand derived' equations addressing the flexible domain [28, 29].

To show how the rigid body subroutines, generated by any one of the above programs, can be used in the flexible body implementation, the

partitioned equations of motion (2.6.6) or (2.7.7) are rewritten as a pair of matrix equations

$$\boxed{\mathbf{M_{RR}}}\,\ddot{\mathbf{U}}_R + \mathbf{M_{RF}}\,\ddot{\mathbf{U}}_F = \boxed{\mathbf{R_R}} + \mathbf{R_{RF}} \qquad (2.8.1a)$$

$$\mathbf{M_{FR}}\,\ddot{\mathbf{U}}_R + \mathbf{M_{FF}}\,\ddot{\mathbf{U}}_F + \mathbf{K_{FF}}\,\mathbf{U}_F = \mathbf{R_F} \qquad (2.8.1b)$$

where it is noted that $\mathbf{M_{RR}}$ and $\mathbf{R_R}$ refer to the current configuration *of the vehicle,* i.e the rigid body + flexible appendage is assumed rigid in the current configuration.

The rigid body code produces a set of subroutines to solve the rigid equations of motion

$$\mathbf{M_{RR}}\,\ddot{\mathbf{U}}_R = \mathbf{R_R} \qquad (2.8.2)$$

2.8.1 For Second Order Integration Schemes

When a second order integration scheme is used in the solution of the vehicle equations of motion, the rigid subroutine is necessary only in the calculation of $\mathbf{M_{RR}}$ and $\mathbf{R_R}$. The current configuration vehicle c.m. and inertia matrix are provided as inputs to the subroutine. If the vehicle undergoes large flexible displacements, the configuration must be updated at each integration step.

2.8.2 For First Order Integration Schemes

A sketch of the implementation of a Runge-Kutta integration scheme in the solution of the equations of motion is offered in Appendix B. It is shown that the computational effort is concentrated on the evaluation of derivatives, in order to employ the formula given by equation (B.4.3). In section B.5, equations (2.8.1) are rearranged to yield

$$\left[\mathbf{M}_{RR} - \mathbf{M}_{RF}\,\mathbf{M}_{FF}^{-1}\,\mathbf{M}_{FR}\right]\dot{\mathbf{U}}_R = \mathbf{R}_R + \mathbf{R}_{RF} + \cdots \qquad \text{(B.5.4)}$$

and

$$\dot{\mathbf{U}}_F = \mathbf{M}_{FF}^{-1}\left[\mathbf{R}_F - \mathbf{M}_{FR}\,\dot{\mathbf{U}}_R - \mathbf{K}_{FF}\,\mathbf{U}_F\right] \qquad \text{(B.5.3)}$$

To obtain the derivatives $\dot{\mathbf{U}}_R$ and $\dot{\mathbf{U}}_F$, these two equations must be solved in the order given. Examination of equation (B.5.4) indicates that the code produced to solve equation (2.8.2) can be used in the flexible context by modification to $\mathbf{M}_{RR}$ and $\mathbf{R}_R$. Simulations using first order integration schemes can take advantage of the code produced by symbolic software to a larger extent than simulations using second order schemes.

Chapter 3
Derivation of Finite Elements

This chapter presents the derivation of two nonlinear beam finite elements. Isotropic, prismatic beam elements are allowed to stretch, bend in two planes, and undergo St. Venant torsion. For the Timoshenko beam, shearing in two planes is also allowed. To derive the beam finite elements, assume that the flexible domain of chapter 2 (see figure 2.1 and equations (2.5.1)-(2.5.3)) is a beam, which allows explicit statement of kinematic assumptions. Bernoulli-Euler kinematic assumptions comprise the "engineering theory of beams.". A distinction is made between Bernoulli-Euler and Rayleigh beam theories in dynamics (Bernoulli-Euler ignores rotatory inertia). The Timoshenko kinematic assumptions lead to a beam theory which includes the effects of rotatory inertia and shear strain within the beam.

The development proceeds from the 3-D statement of the principle of virtual work. Kinematic assumptions are explicitly introduced, and the work expression is integrated across the beam cross-section area for reduction to a 1-D theory.

The beam elements derived are generally known as 'isoparametric' elements; isoparametric meaning 'same parameters'. For the current discussion, let element geometry be interpolated from nodal values by using *shape* functions. Let element displacements be interpolated from nodal DOFs by using *interpolation* functions. Strictly speaking,

isoparametric formulations employ the same function for shape and interpolation. It should be noted that although the C^1 element to follow does not adhere to this rigorous definition (it uses both linear and cubic interpolation functions), it may be loosely referred to as isoparametric. The C^0 element is a true isoparametric element.

3.1 Principle of Virtual Work

The principle of virtual work has been previously stated in section 2.2, where it was applied to a vehicle composed of rigid central body and attached flexible appendage. Three coupled sets of integral equations were derived which govern the vehicle motion. Equations (2.5.1) and (2.5.2) govern the translation and rotation of the the rigid body. Equation (2.5.3) governs the deflections of the flexible appendage, relative to the body fixed frame. For the purpose of this derivation, consider the rigid body to be fixed in inertial space, i.e. $\underline{\omega} = \underline{u} = 0$. Thus surviving terms give the virtual work expression which governs the deflections of the beam relative to a body fixed reference frame.

$$\int_{V_F} \delta\underline{\eta}^T \underline{f_F}\, dV + \int_{S_{\sigma F}} \delta\underline{\eta}^T \underline{t_F}\, dS = \int_{V_F} \delta\underline{\eta}^T \ddot{\underline{\eta}} \rho\, dV + \int_{V_F} \delta\varepsilon{:}\sigma\, dV \qquad (3.1.1)$$

where

$\underline{\eta}$ = components of flexible displacement, with respect to the body fixed frame
$\underline{f_F}$ = force/unit volume, with respect to the body fixed frame
$\underline{t_F}$ = surface traction applied over $S_{\sigma F}$, with respect to the body fixed frame

ρ = density
V_F = reference configuration of the flexible body
ε = strain
σ = stress

3.2 Beam Theory Preliminaries

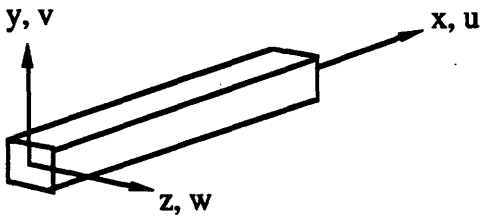

Figure 3.1. 3-D Beam Coordinate System.

Consider the beam shown in figure 3.1, with coordinate axes as shown. It is assumed that stresses σ_y and σ_z are small compared to σ_x. St. Venant torsion theory is incorporated into the displacement field (cross-sections undergo zero warping, and there is no distortion of the cross-section). The displacement field associated with the Bernoulli-Euler kinematics are

$$u(x,y,z) = u_o(x) - yv_{o,x}(x) - zw_{o,x}(x)$$

$$v(x,z) = v_o(x) - z\theta_x(x) \qquad (3.2.1)$$

$$w(x,y) = w_o(x) + y\theta_x(x)$$

and can be interpreted geometrically to mean that cross-sections remain perpendicular to the neutral axis during deformation. A representative construction is shown in figure 3.2.

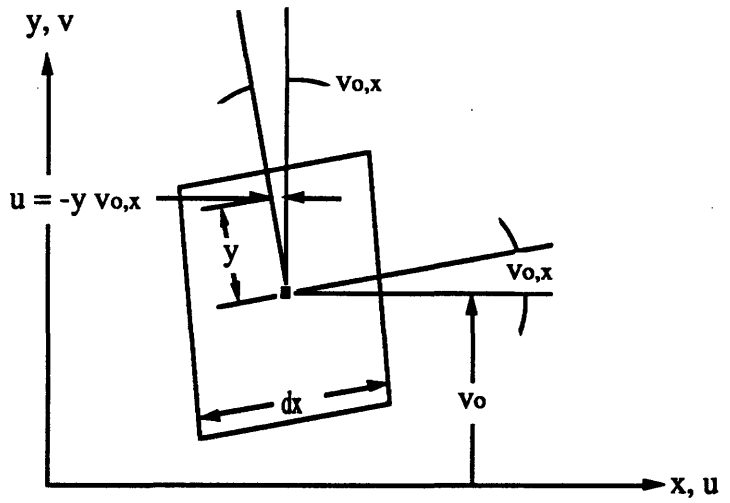

Figure 3.2. Kinematics of Bernoulli-Euler Beam Theory.

In the Timoshenko beam theory, cross-sections initially perpendicular to the neutral axis of the beam remain plane but not perpendicular to the neutral axis during deformation. This kinematic assumption is shown geometrically in figure 3.3.

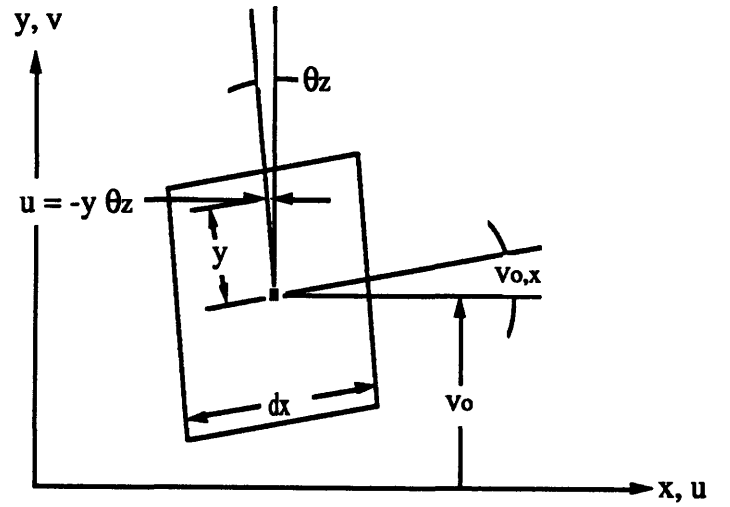

Figure 3.3. Kinematics of Timoshenko Beam Theory.

The displacement field associated with the kinematics of Timoshenko beam theory are

$$u(x,y,z) = u_o(x) - y\theta_z(x) + z\theta_y(x)$$

$$v(x,z) = v_o(x) - z\theta_x(x) \qquad (3.2.2)$$

$$w(x,y) = w_o(x) + y\theta_x(x)$$

where zero subscripts indicate displacement of the neutral axis and θ's are rotations about the subscripted axes.

Note the difference in sign of the components in the displacement field u(x,y,z) of Bernoulli-Euler and Timoshenko kinematics. Positive rotation associated with $w_{,x}$ disagrees with the right hand rule, and as a consequence, also disagrees with the right handed coordinate system used in the derivation of the vehicle equations in chapter 2. Therefore, in order to use the Bernoulli-Euler (C^1) element in the dynamic simulation, a transformation must be made so that the rotation is consistent with a right hand coordinate system.

The restriction of zero deformation of the cross-section during torsion implies that $\gamma_{yz} = 0$. The assumptions associated with both kinematic models allow reduction of the 3-D linear elastic, isotropic stress-strain relations to the simple result

$$\begin{Bmatrix} \sigma_x \\ \tau_{xy} \\ \tau_{zx} \end{Bmatrix} = \begin{bmatrix} E & & \\ & G & \\ & & G \end{bmatrix} \begin{Bmatrix} \varepsilon_x \\ \gamma_{xy} \\ \gamma_{zx} \end{Bmatrix} \qquad (3.2.3)$$

3.3 C^1 Formulation

The C^1 formulation encompasses both the Bernoulli-Euler and Rayleigh beam theories. The subtle distinction is the inclusion of rotatory inertia in *Rayleigh's equations* governing the motion of a beam [30]. It will be shown that consistent derivation using the virtual work principle produces the Rayleigh theory. By convention, Bernoulli-Euler theory excludes rotatory inertia.

From small deflection theory, the non-zero strains associated with the displacement field of equation (3.2.1) are

$$\begin{aligned}
\varepsilon_x &= u_{,x} = u_{o,x}(x) - y v_{o,xx}(x) - z w_{o,xx}(x) \\
\gamma_{xy} &= u_{,y} + v_{,x} = - z\theta_{x,x}(x) \\
\gamma_{zx} &= w_{,x} + u_{,z} = y\theta_{x,x}(x)
\end{aligned} \tag{3.3.1}$$

Substituting equations (3.3.1) and (3.2.1) and constitutive relations (3.2.3) into the right hand side of (3.1.1) gives the internal virtual work expression in the volume integral form

$$\begin{aligned}
\int_v \{ & \rho[(\delta u_o - y\delta v_{o,x} - z\delta w_{o,x})(\ddot{u}_o - y\ddot{v}_{o,x} - z\ddot{w}_{o,x}) + (\delta v_o - z\delta\theta_x)(\ddot{v}_o - z\ddot{\theta}_x) \\
& + (\delta w_o + y\delta\theta_x)(\ddot{w}_o + y\ddot{\theta}_x)] \\
& + E(\delta u_{o,x} - y\delta v_{o,xx} - z\delta w_{o,xx})(u_{o,x} - y v_{o,xx} - z w_{o,xx}) \\
& + G(-z\delta\theta_{x,x})(-z\theta_{x,x}) + G(y\delta\theta_{x,x})(y\theta_{x,x})\} \, dV = RHS
\end{aligned} \tag{3.3.2}$$

where the domain is understood to be the flexible volume. The expression (3.3.2) can be integrated through the beam cross-section to give

$$\int_x \{m(\delta u_o \ddot{u}_o + \delta v_o \ddot{v}_o + \delta w_o \ddot{w}_o) + (I_{my} + I_{mz})\delta\theta_x \ddot{\theta}_x + I_{my}\delta w_{o,x}\ddot{w}_{o,x} + I_{mz}\delta v_{o,x}\ddot{v}_{o,x} + EA\delta u_{o,x}u_{o,x} + EI_y\delta w_{o,xx}w_{o,xx} + EI_z\delta v_{o,xx}v_{o,xx} + G(I_y + I_z)\delta\theta_{x,x}\theta_{x,x}\}dx = RHS \quad (3.3.3)$$

where cross-section principal axes are assumed to be aligned with element coordinate axes. Constants appearing in equation (3.3.3) are defined as follows:

$$A = \int_A dA \qquad m = \int_A \rho\, dA$$

$$I_y = \int_A z^2 dA \qquad I_z = \int_A y^2 dA \qquad J = I_y + I_z$$

$$I_{my} = \int_A \rho z^2 dA \qquad I_{mz} = \int_A \rho y^2 dA$$

where

$$\int_A y dA = \int_A z dA = \int_A yz dA = 0$$

m	=	mass/length
I_y, I_z	=	area moment of inertia
I_{my}, I_{mz}	=	mass moment of inertia

The integral equation (3.3.3) appearing above is to be evaluated over the length of the flexible domain. The flexible domain is decomposed into finite elements and equation (3.3.3) becomes a summation of integrals over the individual element domains. The continuity of assumed displacement functions is dictated by the terms appearing in the integrand. Since second

derivatives of displacement exist in the element stiffness integral, inter-element continuity requires that the displacement fields w_o and v_o be C^1 continuous. The axial displacement and twist require only C^0 continuity. (The superscript indicates the derivative through which the function or field is continuous.) The continuity condition is the integrability of equation (3.3.3) over the entire domain.

3.3.1 Discretization

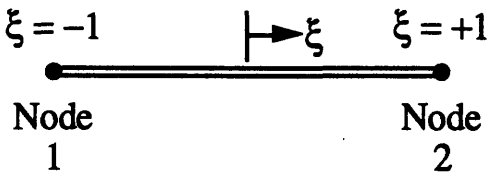

Figure 3.4. Local coordinates for 2 node beam element.

The two node element is defined by the local coordinate system shown in figure 3.4. The element has six DOFs at each node. The necessary interpolation functions are defined in terms of the local coordinate ξ. The linear interpolation functions are given by

$$N_1^0 = \frac{1}{2}(1 - \xi)$$

$$N_2^0 = \frac{1}{2}(1 + \xi) \qquad (3.3.4)$$

For the C^1 continuous displacement fields w_o and v_o, the cubic Hermitian interpolation functions are used and are defined as

$$N_1^1 = \frac{1}{4}(1 - \xi)(2 - \xi - \xi^2)$$

$$N_2^1 = \frac{1}{4}(1 - \xi)^2(\xi + 1)$$

$$N_3^1 = \frac{1}{4}(1 + \xi)(2 + \xi - \xi^2)$$

$$N_4^1 = \frac{1}{4}(1 + \xi)^2(\xi - 1) \qquad (3.3.5)$$

Element nodal DOFs are arranged as

$$\underline{q}^T = [\ \underline{q_1}^T \quad \underline{q_2}^T\ ] \qquad (3.3.6)$$

where

$$\underline{q_1}^T = [\ u_{o1} \quad v_{o1} \quad w_{o1} \quad \theta_{x1} \quad w_{o,x1} \quad v_{o,x1}\ ]$$

$$\underline{q_2}^T = [\ u_{o2} \quad v_{o2} \quad w_{o2} \quad \theta_{x2} \quad w_{o,x2} \quad v_{o,x2}\ ]$$

Also define

$$\underline{d}^T = [\ u_o \quad v_o \quad w_o \quad \theta_x \quad w_{o,x} \quad v_{o,x}\ ]$$

$$\underline{\varepsilon}^T = [\ u_{o,x} \quad \theta_{x,x} \quad w_{o,xx} \quad v_{o,xx}\ ] = [\ \varepsilon_{ox} \quad \kappa_t \quad \kappa_y \quad \kappa_z\ ]$$

where the strains, $\underline{\varepsilon}$, are defined as the work conjugates to the stress resultants (see Appendix A). These definitions allow a succinct way of defining the matrices $\underline{N}$ and $\underline{B}$, which relate the element nodal displacements to the vectors $\underline{d}$ and $\underline{\varepsilon}$.

With the interpolation functions and nodal DOFs explicitly stated, some explanation is necessary to avoid a pitfall which can be harmlessly overlooked in C^0 elements. Nodal DOFs consist of axial displacement and transverse displacements and their derivatives with respect to x, while the

interpolation functions are defined in local coordinates. Care must be taken to insure correct application of the Jacobian transformation.

To consider the problem of interpolation in a consistent manner, note that interpolation is performed using the nodal quantities $w_{o,\xi i}$ and $v_{o,\xi i}$. For example,

$$w_o = N_1^1 w_{o1} + N_2^1 w_{o,\xi 1} + N_3^1 w_{o2} + N_4^1 w_{o,\xi 2}$$

$$w_{o,\xi} = N_{1,\xi}^1 w_{o1} + N_{2,\xi}^1 w_{o,\xi 1} + N_{3,\xi}^1 w_{o2} + N_{4,\xi}^1 w_{o,\xi 2} \qquad (3.3.7)$$

$$w_{o,\xi\xi} = N_{1,\xi\xi}^1 w_{o1} + N_{2,\xi\xi}^1 w_{o,\xi 1} + N_{3,\xi\xi}^1 w_{o2} + N_{4,\xi\xi}^1 w_{o,\xi 2}$$

Note that these expressions yield the expected results when evaluated at the endpoints, $\xi = \pm 1$. In order to express each of these equations properly in physical coordinates, we must consider how derivatives transform between local and physical coordinates. Since $N_i = N_i(\xi)$, the derivative with respect to x can be written

$$\frac{dN_i}{dx} = \frac{dN_i}{d\xi}\frac{d\xi}{dx} \qquad (3.3.8)$$

where by definition, the Jacobian is $J = \frac{dx}{d\xi}$. The second derivative becomes

$$\frac{d^2N_i}{dx^2} = \frac{d^2N_i}{d\xi^2}\left(\frac{d\xi}{dx}\right)^2 + \frac{dN_i}{d\xi}\frac{d^2\xi}{dx^2} \qquad (3.3.9)$$

Likewise, displacement derivatives can be written

$$\frac{dw_o}{dx} = \frac{dw_o}{d\xi}\frac{d\xi}{dx} \qquad (3.3.10)$$

$$\frac{d^2w_o}{dx^2} = \frac{d^2w_o}{d\xi^2}\left(\frac{d\xi}{dx}\right)^2 + \frac{dw_o}{d\xi}\frac{d^2\xi}{dx^2} \tag{3.3.11}$$

where for straight beams, the Jacobian is constant and equal to L/2 in each element (L is the physical length of an arbitrary element), so that the second term of (3.3.9) and (3.3.11) is zero. Substituting equations (3.3.8)-(3.3.11) into equations (3.3.7), displacements and displacement derivatives can be rewritten in terms of physical coordinates. This gives, in matrix form,

$$\begin{bmatrix} w_o \\ w_{o,x} \\ w_{o,xx} \end{bmatrix} = \begin{bmatrix} N_1^1 & JN_2^1 & N_3^1 & JN_4^1 \\ N_{1,x}^1 & JN_{2,x}^1 & N_{3,x}^1 & JN_{4,x}^1 \\ N_{1,xx}^1 & JN_{2,xx}^1 & N_{3,xx}^1 & JN_{4,xx}^1 \end{bmatrix} \begin{bmatrix} w_{o1} \\ w_{o,x1} \\ w_{o2} \\ w_{o,x2} \end{bmatrix} \tag{3.3.12}$$

and demonstrates correct differentiation (with respect to the physical coordinate) using local cubic interpolation functions. A similar statement can be made for the displacement v_o. For displacement fields requiring only linear interpolation functions, the relationship between displacement/displacement derivatives and nodal DOFs does not involve the Jacobian. For instance,

$$\begin{bmatrix} u_o \\ u_{o,x} \end{bmatrix} = \begin{bmatrix} N_1^0 & N_2^0 \\ N_{1,x}^0 & N_{2,x}^0 \end{bmatrix} \begin{bmatrix} u_{o1} \\ u_{o2} \end{bmatrix} \tag{3.3.13}$$

Now equation (3.3.3) can be rewritten in matrix form as

$$\int_x \delta\underline{d}^T \underline{D_m}\, \ddot{\underline{d}} + \delta\underline{\varepsilon}^T \underline{D_k}\, \underline{\varepsilon}\, dx = RHS \tag{3.3.14}$$

and finally, equation (3.3.14) can be rewritten in terms of the nodal DOFs to give

$$\delta \underline{q}^T \underline{M} \ddot{\underline{q}} + \delta \underline{q}^T \underline{K} \underline{q} = \text{RHS}$$

where

$\underline{M}$ = consistent mass matrix
$\underline{K}$ = stiffness matrix

and the element level consistent mass matrix and material stiffness matrix are given by

$$\underline{M} = \int_x \underline{N}^T \underline{D_m} \underline{N} \, dx \tag{3.3.15}$$

$$\underline{K} = \int_x \underline{B}^T \underline{D_k} \underline{B} \, dx \tag{3.3.16}$$

where

$$\underline{D_m} = \begin{bmatrix} m & & & & & & \\ & m & & & & & \\ & & m & & & & \\ & & & (I_{my} + I_{mz}) & & & \\ & & & & I_{my} & & \\ & & & & & I_{mz} & \end{bmatrix}$$

and

$$\underline{D_k} = \begin{bmatrix} EA & & & & \\ & GJ & & & \\ & & EI_y & & \\ & & & EI_z & \end{bmatrix}$$

The matrices $\underline{N}$ and $\underline{B}$ relate element nodal displacements to the vectors $\underline{d}$ and $\underline{\varepsilon}$ and are defined by the equations

$$\underline{d} = \underline{N}\,\underline{q} \tag{3.3.17}$$

$$\underline{\varepsilon} = \underline{B}\,\underline{q} \tag{3.3.18}$$

These matrices are formed by appropriate placement of the linear and Hermitian interpolation functions and their derivatives. For the C^1 element formulation, they are

$$\underline{N} = \begin{bmatrix} N_1^0 & 0 & 0 & 0 & 0 & 0 & N_2^0 & 0 & 0 & 0 & 0 & 0 \\ 0 & N_1^1 & 0 & 0 & 0 & JN_2^1 & 0 & N_3^1 & 0 & 0 & 0 & JN_4^1 \\ 0 & 0 & N_1^1 & 0 & JN_2^1 & 0 & 0 & 0 & N_3^1 & 0 & JN_4^1 & 0 \\ 0 & 0 & 0 & N_1^0 & 0 & 0 & 0 & 0 & 0 & N_2^0 & 0 & 0 \\ 0 & 0 & N_{1,x}^1 & 0 & JN_{2,x}^1 & 0 & 0 & 0 & N_{3,x}^1 & 0 & JN_{4,x}^1 & 0 \\ 0 & N_{1,x}^1 & 0 & 0 & 0 & JN_{2,x}^1 & 0 & N_{3,x}^1 & 0 & 0 & 0 & JN_{4,x}^1 \end{bmatrix}$$

and

$$\underline{B} = \begin{bmatrix} N^0_{1,x} & 0 & 0 & 0 & 0 & 0 & N^0_{2,x} & 0 & 0 & 0 & 0 & 0 \\ 0 & 0 & 0 & N^0_{1,x} & 0 & 0 & 0 & 0 & 0 & N^0_{2,x} & 0 & 0 \\ 0 & 0 & N^1_{1,xx} & 0 & JN^1_{2,xx} & 0 & 0 & 0 & N^1_{3,xx} & 0 & JN^1_{4,xx} & 0 \\ 0 & N^1_{1,xx} & 0 & 0 & 0 & JN^1_{2,xx} & 0 & N^1_{3,xx} & 0 & 0 & 0 & JN^1_{4,xx} \end{bmatrix}$$

The preceding equations are properly known as the beam theory of Rayleigh. By convention, Bernoulli-Euler theory sets the rotatory inertias $I_{my} = I_{mz} = 0$.

The above expressions for element level consistent mass matrix and the material stiffness matrix contain local interpolation functions differentiated with respect to the physical coordinate x. Proper introduction of the Jacobian yields integrals in a form which can be numerically integrated using Gaussian quadrature (Appendix F). Assembled matrices are obtained by summing over all element matrices.

3.4 C^0 Formulation

The C^0 formulation is derived based on the kinematic assumptions of Timoshenko beam theory. Rotation of beam cross-sections are independent of transverse displacements (recall figure 3.3). This produces a beam theory which has nonzero shearing strains. This formulation is more accurate when the thickness of the beam is large compared to its length, and for higher vibration modes (wavelength/thickness → small).

From small deflection theory, the non-zero strains associated with the displacement field of equation (3.2.2) are

$$\varepsilon_x = u_{,x} = u_{o,x}(x) - y\theta_{z,x}(x) + z\theta_{y,x}(x)$$

$$\gamma_{xy} = u_{,y} + v_{,x} = -\theta_z(x) + v_{o,x}(x) - z\theta_{x,x}(x) \qquad (3.4.1)$$

$$\gamma_{zx} = w_{,x} + u_{,z} = w_{o,x}(x) + y\theta_{x,x}(x) + \theta_y(x)$$

Substituting equations (3.4.1) and (3.2.2) and constitutive relations (3.2.3) into the right hand side of equation (3.1.1) gives the internal virtual work expression in the volume integral form

$$\int_V \{\rho[(\delta u_o - y\delta\theta_z + z\delta\theta_y)(\ddot{u}_o - y\ddot{\theta}_z + z\ddot{\theta}_y) + (\delta v_o - z\delta\theta_x)(\ddot{v}_o - z\ddot{\theta}_x) + (\delta w_o + y\delta\theta_x)(\ddot{w}_o + y\ddot{\theta}_x)] + E(\delta u_{o,x} - y\delta\theta_{z,x} + z\delta\theta_{y,x})(u_{o,x} - y\theta_{z,x} + z\theta_{y,x}) + G(-\delta\theta_z + \delta v_{o,x} - z\delta\theta_{x,x})(-\theta_z + v_{o,x} - z\theta_{x,x}) + G(\delta\theta_y + \delta w_{o,x} + y\delta\theta_{x,x})(\theta_y + w_{o,x} + y\theta_{x,x})\} dV = RHS \qquad (3.4.2)$$

where the domain is understood to be the flexible volume. The expression (3.4.2) can be integrated through the beam cross-section to give

$$\int_x \{m(\delta u_o\ddot{u}_o + \delta v_o\ddot{v}_o + \delta w_o\ddot{w}_o) + (I_{my} + I_{mz})\delta\theta_x\ddot{\theta}_x + I_{my}\delta\theta_y\ddot{\theta}_y + I_{mz}\delta\theta_z\ddot{\theta}_z + EA\delta u_{o,x}u_{o,x} + EI_y\delta\theta_{y,x}\theta_{y,x} + EI_z\delta\theta_{z,x}\theta_{z,x} + G(I_y + I_z)\delta\theta_{x,x}\theta_{x,x} + GA\delta(v_{o,x} - \theta_z)(v_{o,x} - \theta_z) + GA\delta(w_{o,x} + \theta_y)(w_{o,x} + \theta_y)\}dx = RHS \qquad (3.4.3)$$

where cross-section principal axes are assumed to be aligned with element coordinate axes. Constants appearing in equation (3.4.3) are the same as defined in section 3.3 (see page 51).

The integration to be carried out in equation (3.4.3) is again evaluated as the summation over the finite elements which constitute the flexible domain. Examination of the integrand reveals that only C^0 continuity is required.

3.4.1 Discretization

A schematic of the finite element model is shown in figure 3.4. Because cross-sectional rotations are independent of the transverse displacements, only the linear interpolation functions are necessary. In local coordinates the interpolation functions have the form

$$N_1^0 = \frac{1}{2}(1 - \xi)$$

$$N_2^0 = \frac{1}{2}(1 + \xi) \qquad (3.4.4)$$

Element nodal DOFs are arranged as

$$\underline{q}^T = [\ \underline{q_1}^T \quad \underline{q_2}^T\ ] \qquad (3.4.5)$$

where

$$\underline{q_1}^T = [\ u_{o1} \quad v_{o1} \quad w_{o1} \quad \theta_{x1} \quad \theta_{y1} \quad \theta_{z1}\ ]$$

$$\underline{q_2}^T = [\ u_{o2} \quad v_{o2} \quad w_{o2} \quad \theta_{x2} \quad \theta_{y2} \quad \theta_{z2}\ ]$$

The C^0 displacements and strains are given by

$$\underline{d}^T = [\ u_o \quad v_o \quad w_o \quad \theta_x \quad \theta_y \quad \theta_z\ ]$$

$$\underline{\varepsilon}^T = [\ u_{o,x} \quad \theta_{x,x} \quad \theta_{y,x} \quad \theta_{z,x} \quad (v_{o,x} - \theta_z) \quad (w_{o,x} + \theta_y)\ ]$$

$$= [\ \varepsilon_{xo} \quad \kappa_t \quad -\kappa_y \quad \kappa_z \quad \gamma_{xyo} \quad \gamma_{xzo}\ ]$$

where the additional terms in this strain vector, compared to the previous section, are the shear strains arising from the Timoshenko kinematics. Forming these vectors from the element nodal displacements defines the matrices $\underline{N}$ and $\underline{B}$. These matrices are composed of the linear interpolation functions and their derivatives.

$$\underline{d} = \underline{N}\,\underline{q} \tag{3.4.6}$$

$$\underline{\varepsilon} = \underline{B}\,\underline{q} \tag{3.4.7}$$

Explicitly, the $\underline{N}$ and $\underline{B}$ matrix are given by

$$\underline{N} = \begin{bmatrix} N_1^0 & 0 & 0 & 0 & 0 & 0 & N_2^0 & 0 & 0 & 0 & 0 & 0 \\ 0 & N_1^0 & 0 & 0 & 0 & 0 & 0 & N_2^0 & 0 & 0 & 0 & 0 \\ 0 & 0 & N_1^0 & 0 & 0 & 0 & 0 & 0 & N_2^0 & 0 & 0 & 0 \\ 0 & 0 & 0 & N_1^0 & 0 & 0 & 0 & 0 & 0 & N_2^0 & 0 & 0 \\ 0 & 0 & 0 & 0 & N_1^0 & 0 & 0 & 0 & 0 & 0 & N_2^0 & 0 \\ 0 & 0 & 0 & 0 & 0 & N_1^0 & 0 & 0 & 0 & 0 & 0 & N_2^0 \end{bmatrix}$$

$$\underline{B} = \begin{bmatrix} N^0_{1,x} & 0 & 0 & 0 & 0 & 0 & N^0_{2,x} & 0 & 0 & 0 & 0 & 0 \\ 0 & 0 & 0 & N^0_{1,x} & 0 & 0 & 0 & 0 & 0 & N^0_{2,x} & 0 & 0 \\ 0 & 0 & 0 & 0 & N^0_{1,x} & 0 & 0 & 0 & 0 & 0 & N^0_{2,x} & 0 \\ 0 & 0 & 0 & 0 & 0 & N^0_{1,x} & 0 & 0 & 0 & 0 & 0 & N^0_{2,x} \\ 0 & N^0_{1,x} & 0 & 0 & 0 & -N^0_1 & 0 & N^0_{2,x} & 0 & 0 & 0 & -N^0_2 \\ 0 & 0 & N^0_{1,x} & 0 & N^0_1 & 0 & 0 & 0 & N^0_{2,x} & 0 & N^0_2 & 0 \end{bmatrix}$$

Now equation (3.4.3) can be rewritten in matrix form

$$\int_x \delta\underline{d}^T \underline{D_m}\, \ddot{\underline{d}} + \delta\underline{\varepsilon}^T \underline{D_k}\, \underline{\varepsilon}\, dx = RHS \tag{3.4.8}$$

and finally, equation (3.4.8) can be rewritten in terms of the nodal DOFs to give

$$\delta\underline{q}^T \underline{M}\ddot{\underline{q}} + \delta\underline{q}^T \underline{K}\underline{q} = RHS$$

where

$\underline{M}$ = consistent mass matrix
$\underline{K}$ = stiffness matrix

and the element level consistent mass matrix and material stiffness matrix are given by

$$\underline{M} = \int_x \underline{N}^T \underline{D_m}\, \underline{N}\, dx \tag{3.4.9}$$

$$\underline{K} = \int_x \underline{B}^T \underline{D_k}\, \underline{B}\, dx \tag{3.4.10}$$

where

$$\underline{D_m} = \begin{bmatrix} m & & & & & & \\ & m & & & & & \\ & & m & & & & \\ & & & (I_{my} + I_{mz}) & & & \\ & & & & I_{my} & & \\ & & & & & I_{mz} & \end{bmatrix}$$

and

$$\underline{D_k} = \begin{bmatrix} EA & & & & & & \\ & GJ & & & & & \\ & & EI_y & & & & \\ & & & EI_z & & & \\ & & & & GA & & \\ & & & & & GA & \end{bmatrix}$$

The expression for the material stiffness matrix contains local interpolation functions differentiated with respect to the physical coordinate x. Jacobian transformation must be introduced in order to properly express the integrand in terms of x. The integrals can then be numerically integrated using Gaussian quadrature (Appendix F). Assembled matrices are obtained by summing over all element matrices.

3.5. Geometric Stiffness Matrix

For problems involving geometric nonlinearities, system equilibrium must be satisfied in the deformed configuration. In terms of the virtual

work principle, the deformed, or current configuration, is represented by consideration of both linear and nonlinear strain terms. Derivation of the geometric stiffness matrix is accomplished through incremental linearization of the internal virtual work principle at the current configuration of the flexible domain [31]. All terms are retained in the consistent derivation. The incremental virtual work statement is

$$\Delta\delta W_{int} = \int_{V_F} \left(\delta\Delta\varepsilon : \Delta\sigma + \delta\Delta e : \sigma_T\right) dV$$

$$= \int_{V_F} \delta\Delta\underline{\xi}\cdot\left(\Delta\underline{f}_F - \rho\Delta\ddot{\underline{\xi}}\right) dV + \int_{S_{\sigma F}} \delta\Delta\underline{\xi}\cdot\Delta\underline{t}_F \, dS = \Delta\delta W_{ext} \qquad (3.5.1)$$

where

$$\Delta\varepsilon_{ij} = \frac{1}{2}\left(\frac{\partial\Delta u_i}{\partial x_j} + \frac{\partial\Delta u_j}{\partial x_i}\right)$$

$$\Delta e_{ij} = \frac{1}{2}\left(\frac{\partial\Delta u_k}{\partial x_i}\right)\left(\frac{\partial\Delta u_k}{\partial x_j}\right)$$

σ_T = total accumulated stress
$\Delta\underline{f}_F$ = increment in prescribed body forces, components expressed in body fixed frame
$\Delta\underline{t}_F$ = increment in prescribed tractions, components expressed in body fixed frame

The first term of the incremental internal virtual work above becomes the material stiffness matrix previously obtained. The second term leads to the geometric stiffness matrix and will be derived in this section. The nonlinear strain increments, Δe_{ij}, may be formed from either

set of kinematic assumptions without great difficulty. In accordance with thin beam assumptions noted earlier, σ_y and σ_z are small compared to σ_x and may be neglected. St. Venant torsion theory does not allow distortion of the cross-section, which implies that $\gamma_{yz} = 0$ and leads to $\tau_{yz} = 0$. Zero warping is also assumed, although this is strictly true only for beams of circular cross-section.

Using Timoshenko kinematics, the nonlinear strain increments are substituted into the second term of equation (3.5.1), and after some algebra, the volume integral can be reduced to

Timoshenko kinematics:

$$\int_V \delta e : \sigma_T \, dV = \int_x \{ N_x(\delta\varepsilon_{xo}\varepsilon_{xo} + \delta v_{o,x} v_{o,x} + \delta w_{o,x} w_{o,x})$$

$$+ M_z(\delta\kappa_z\varepsilon_{xo} + \delta\varepsilon_{xo}\kappa_z - \delta\kappa_t w_{o,x} - \delta w_{o,x}\kappa_t)$$

$$+ M_y(\delta\kappa_y\varepsilon_{xo} + \delta\varepsilon_{xo}\kappa_y + \delta\kappa_t v_{o,x} + \delta v_{o,x}\kappa_t)$$

$$+ P_z(\delta\kappa_z\kappa_z + \delta\kappa_t\kappa_t) + P_y(\delta\kappa_y\kappa_y + \delta\kappa_t\kappa_t)$$

$$+ P_{yz}(\delta\kappa_y\kappa_z + \delta\kappa_z\kappa_y)$$

$$+ V_y(-\delta\theta_z\varepsilon_{xo} - \delta\varepsilon_{xo}\theta_z + \delta\theta_x w_{o,x} + \delta w_{o,x}\theta_x)$$

$$+ V_z(\delta\theta_y\varepsilon_{xo} + \delta\varepsilon_{xo}\theta_y - \delta\theta_x v_{o,x} - \delta v_{o,x}\theta_x)$$

$$+ R_{yy}(\delta\kappa_z\theta_z + \delta\theta_z\kappa_z + \delta\kappa_t\theta_x + \delta\theta_x\kappa_t)$$

$$+ R_{yz}(-\delta\kappa_z\theta_y - \delta\theta_y\kappa_z) + R_{zy}(\delta\kappa_y\theta_z + \delta\theta_z\kappa_y)$$

$$+ R_{zz}(-\delta\kappa_y\theta_y - \delta\theta_y\kappa_y + \delta\kappa_t\theta_x + \delta\theta_x\kappa_t)\} \, dx \qquad (3.5.2)$$

A similar expression can be obtained by substituting Bernoulli-Euler kinematics into equation (3.5.1). Alternatively, the Bernoulli-Euler result can obtained directly from the Timoshenko result, equation (3.5.2), by letting $V_y = V_z = 0$, $\theta_z \rightarrow v_{o,x}$, $\theta_y \rightarrow - w_{o,x}$.

Bernoulli-Euler kinematics:

$$\int_V \delta e:\sigma_T \, dV = \int_x \{N_x(\delta\varepsilon_{xo}\varepsilon_{xo} + \delta v_{o,x}v_{o,x} + \delta w_{o,x}w_{o,x})$$

$$+ M_z(\delta\kappa_z\varepsilon_{xo} + \delta\varepsilon_{xo}\kappa_z - \delta\kappa_t w_{o,x} - \delta w_{o,x}\kappa_t)$$

$$+ M_y(\delta\kappa_y\varepsilon_{xo} + \delta\varepsilon_{xo}\kappa_y + \delta\kappa_t v_{o,x} + \delta v_{o,x}\kappa_t)$$

$$+ P_z(\delta\kappa_z\kappa_z + \delta\kappa_t\kappa_t) + P_y(\delta\kappa_y\kappa_y + \delta\kappa_t\kappa_t)$$

$$+ P_{yz}(\delta\kappa_y\kappa_z + \delta\kappa_z\kappa_y)$$

$$+ R_{yy}(\delta\kappa_z v_{o,x} + \delta v_{o,x}\kappa_z + \delta\kappa_t\theta_x + \delta\theta_x\kappa_t)$$

$$+ R_{yz}(\delta\kappa_z w_{o,x} + \delta w_{o,x}\kappa_z) + R_{zy}(\delta\kappa_y v_{o,x} + \delta v_{o,x}\kappa_y)$$

$$+ R_{zz}(\delta\kappa_y w_{o,x} + \delta w_{o,x}\kappa_y + \delta\kappa_t\theta_x + \delta\theta_x\kappa_t)\} \, dx \qquad (3.5.3)$$

where, in addition to the stress resultants defined in Appendix A, the following higher order resultants are defined:

$$P_y = \int_A \sigma_x z^2 dA \qquad P_{yz} = \int_A \sigma_x yz dA \qquad P_z = \int_A \sigma_x y^2 dA$$

$$R_{yy} = \int_A \tau_{xy} y dA \qquad R_{zz} = \int_A \tau_{xz} z dA$$

$$R_{yz} = \int_A \tau_{xz} y dA \qquad R_{zy} = \int_A \tau_{xy} z dA$$

Equations (3.5.2) & (3.5.3) include all terms. The higher order resultants, however, are easily computed only for simple loadings. One

instance where they can be computed is in the application of an axial load. In the buckling problem, inclusion of the P_y, P_{yz}, and P_z resultants lowers the buckling load for thick beams only very slightly, so that these terms are reasonably ignored (see tabulations in Appendix C).

It is again convenient to define a vector of quantities which will allow definition of what shall be called the $\underline{G}$ matrix. Let

C^1: $\underline{\beta}^T = [\ \varepsilon_{xo} \quad v_{o,x} \quad w_{o,x} \quad \kappa_t \quad \kappa_y \quad \kappa_z\ ]$

C^0: $\underline{\beta}^T = [\ \varepsilon_{xo} \quad v_{o,x} \quad w_{o,x} \quad \kappa_t \quad \kappa_y \quad \kappa_z \quad \theta_x \quad \theta_y \quad \theta_z\ ]$

The matrix $\underline{G}$ relates the above quantities to the element nodal displacements, and is formed by the appropriate placement of interpolation functions and their derivatives.

$$\underline{\beta} = \underline{G}\,\underline{q} \tag{3.5.4}$$

Equation (3.5.4) is valid for C^1 and C^0 formulations. Rewriting equation (3.5.2) & (3.5.3) in matrix form and introducing equation (3.5.4) allows us to write the geometric stiffness term in the following form

$$\delta\underline{q}^T \underline{K_\sigma}\, \underline{q}$$

where

$$\underline{K_\sigma} = \int_x \underline{G}^T \underline{D_g} \underline{G}\, dx \tag{3.5.5}$$

and

$\underline{K_\sigma}$ = geometric stiffness matrix

$\underline{D_g}$ = matrix of total accumulated stresses

The above form of the geometric stiffness matrix is valid for both C^1 and C^0 formulations, with substitution of appropriate expressions for $\underline{G}$ and $\underline{D_g}$. $\underline{D_g}$ is given below, where the partition made up of the first six rows and columns is appropriate to the C^1 formulation. The full matrix is the C^0 form.

$$\underline{D_g} = \begin{bmatrix} N_x & 0 & 0 & 0 & M_y & M_z & 0 & V_z & -V_y \\ 0 & N_x & 0 & M_y & 0 & 0 & -V_z & 0 & 0 \\ 0 & 0 & N_x & -M_z & 0 & 0 & V_y & 0 & 0 \\ 0 & M_y & -M_z & 0 & 0 & 0 & 0 & 0 & 0 \\ M_y & 0 & 0 & 0 & 0 & 0 & 0 & 0 & 0 \\ M_z & 0 & 0 & 0 & 0 & 0 & 0 & 0 & 0 \\ 0 & -V_z & V_y & 0 & 0 & 0 & 0 & 0 & 0 \\ V_z & 0 & 0 & 0 & 0 & 0 & 0 & 0 & 0 \\ -V_y & 0 & 0 & 0 & 0 & 0 & 0 & 0 & 0 \end{bmatrix}$$

The $\underline{G}$ matrix follows directly from equation (3.5.4). It is given explicitly below:

C^1:

$$\underline{G} = \begin{bmatrix} N^0_{1,x} & 0 & 0 & 0 & 0 & 0 & N^0_{2,x} & 0 & 0 & 0 & 0 & 0 \\ 0 & N^1_{1,x} & 0 & 0 & 0 & JN^1_{2,x} & 0 & N^1_{3,x} & 0 & 0 & 0 & JN^1_{4,x} \\ 0 & 0 & N^1_{1,x} & 0 & JN^1_{2,x} & 0 & 0 & 0 & N^1_{3,x} & 0 & JN^1_{4,x} & 0 \\ 0 & 0 & 0 & N^0_{1,x} & 0 & 0 & 0 & 0 & 0 & N^0_{2,x} & 0 & 0 \\ 0 & 0 & N^1_{1,xx} & 0 & JN^1_{2,xx} & 0 & 0 & 0 & N^1_{3,xx} & 0 & JN^1_{4,xx} & 0 \\ 0 & N^1_{1,xx} & 0 & 0 & 0 & JN^1_{2,xx} & 0 & N^1_{3,xx} & 0 & 0 & 0 & JN^1_{4,xx} \end{bmatrix}$$

C^0:

$$\underline{G} = \begin{bmatrix} N^0_{1,x} & 0 & 0 & 0 & 0 & 0 & N^0_{2,x} & 0 & 0 & 0 & 0 & 0 \\ 0 & N^0_{1,x} & 0 & 0 & 0 & 0 & 0 & N^0_{2,x} & 0 & 0 & 0 & 0 \\ 0 & 0 & N^0_{1,x} & 0 & 0 & 0 & 0 & 0 & N^0_{2,x} & 0 & 0 & 0 \\ 0 & 0 & 0 & N^0_{1,x} & 0 & 0 & 0 & 0 & 0 & N^0_{2,x} & 0 & 0 \\ 0 & 0 & 0 & 0 & -N^0_{1,x} & 0 & 0 & 0 & 0 & 0 & -N^0_{2,x} & 0 \\ 0 & 0 & 0 & 0 & 0 & N^0_{1,x} & 0 & 0 & 0 & 0 & 0 & N^0_{2,x} \\ 0 & 0 & 0 & N^0_1 & 0 & 0 & 0 & 0 & 0 & N^0_2 & 0 & 0 \\ 0 & 0 & 0 & 0 & N^0_1 & 0 & 0 & 0 & 0 & 0 & N^0_2 & 0 \\ 0 & 0 & 0 & 0 & 0 & N^0_1 & 0 & 0 & 0 & 0 & 0 & N^0_2 \end{bmatrix}$$

3.6. Consistent Nodal Loads

For completeness, the derivation of consistent nodal loads is considered. The left hand side of equation (3.1.1) is rewritten below

$$\text{LHS} = \int_{V_F} \delta\underline{\eta}^T \underline{f_E}\, dV + \int_{S_{\sigma F}} \delta\underline{\eta}^T \underline{t_E}\, dS \qquad (3.6.1)$$

where, as a reminder,

$\underline{\eta}$ = flexible displacement of material particle, with respect to the body fixed frame
$\underline{f}_F$ = force/unit volume, with respect to the body fixed frame
$\underline{t}_F$ = surface traction applied over $S_{\sigma F}$, with respect to the body fixed frame
V_F = reference configuration of the flexible body

It should be noted that equation (3.6.1) is referred to the entire flexible body. With the introduction of Timoshenko beam kinematics, the volume integral associated with the body force can be written

$$\int_V \delta\underline{\eta}^T \underline{f}_F \, dV = \int_V \left[\left(\delta u_o - y\delta\theta_z + z\delta\theta_y\right) f_x + \left(\delta v_o - z\delta\theta_x\right) f_y + \left(\delta w_o + y\delta\theta_x\right) f_z \right] dV \tag{3.6.2}$$

Integration through the cross-section along with the assumption that beam cross-section principle axes are aligned with the beam coordinate system yields

$$\int_V \delta\underline{\eta}^T \underline{f}_F \, dV = \int_x \left(\delta u_o f_x + \delta v_o f_y + \delta w_o f_z\right) dx = \int_x \begin{bmatrix} \delta u_o & \delta v_o & \delta w_o \end{bmatrix} \begin{Bmatrix} f_x \\ f_y \\ f_z \end{Bmatrix} dx \tag{3.6.3}$$

It is easily verified that Bernoulli-Euler kinematics produce the same equation (3.6.3). If we now consider the integral in (3.6.3) as a sum of integrals over all element domains, all that remains is to express $[\delta u_o \; \delta v_o \; \delta w_o]$ in terms of the element nodal DOFs.

$$\begin{Bmatrix} u_o \\ v_o \\ w_o \end{Bmatrix} = \underline{N_B}\,\underline{q}$$

where

$$C^1: \quad \underline{N_B} = \begin{bmatrix} N_1^0 & 0 & 0 & 0 & 0 & 0 & N_2^0 & 0 & 0 & 0 & 0 & 0 \\ 0 & N_1^1 & 0 & 0 & 0 & JN_2^1 & 0 & N_3^1 & 0 & 0 & 0 & JN_4^1 \\ 0 & 0 & N_1^1 & 0 & JN_2^1 & 0 & 0 & 0 & N_3^1 & 0 & JN_4^1 & 0 \end{bmatrix}$$

$$C^0: \quad \underline{N_B} = \begin{bmatrix} N_1^0 & 0 & 0 & 0 & 0 & 0 & N_2^0 & 0 & 0 & 0 & 0 & 0 \\ 0 & N_1^0 & 0 & 0 & 0 & 0 & 0 & N_2^0 & 0 & 0 & 0 & 0 \\ 0 & 0 & N_1^0 & 0 & 0 & 0 & 0 & 0 & N_2^0 & 0 & 0 & 0 \end{bmatrix}$$

Thus, the volume integral associated with body forces becomes

$$\int_{V_F} \delta\underline{\eta}^T \underline{f_F}\, dV = \delta\underline{q}^T \int_x \underline{N_B}^T \underline{f_F}\, dx = \delta\underline{q}^T \underline{Q_B}$$

where

$$\underline{Q_B} = \int_x \underline{N_B}^T \underline{f_F}\, dx \tag{3.6.4}$$

The surface integral is dealt with in the same manner. After substitution of tractions into the surface integral, an expression can be derived just as for the body forces. Equation (3.6.1) can then be written as

$$\text{LHS} = \delta\underline{q}^T \left(\underline{Q_B} + \underline{Q_S}\right) = \delta\underline{q}^T\, \underline{Q} \tag{3.6.5}$$

where

$$\underline{Q_S} = \int_{S_e} \underline{N_S}^T \underline{t_F} \, dS$$

$$\underline{Q} = \underline{Q_B} + \underline{Q_S}$$

and comparison with earlier sections shows that $\underline{Q}$ is the element consistent nodal load vector.

The external loads on a structure can also be specified in an 'inconsistent' fashion. External loads can be lumped directly at the nodes. Direct nodal loading can be handled as an additional term added to the external virtual work. No interpolation functions are involved in the discretization since the load is applied directly to the element nodal DOFs. In practice, nodal loads are added directly to the corresponding element of the assembled force vector.

Chapter 4
Eigenvalue Problems

A set of problems has been addressed to examine the beam kinematic assumptions and finite element approximations. For a beam with cantilever boundary conditions, the following problems have been solved: free vibration, and static and dynamic buckling.

A study of the beam finite elements derived in the previous chapter has been accomplished for two beams whose physical and material parameters are indicated in table 4.1. The first beam has L/h = 10 (length/thickness) and borders the Bernoulli-Euler assumptions. Parameter set 2 differs only in the beam thickness; this beam has L/h = 100 and its behavior should be consistent with Bernoulli-Euler beam theory. This choice of parameters allows clearer insight into the effects of kinematic assumptions and treatment of the mass matrix and level of integration.

Table 4.1. Beam material properties for eigenvalue problems.

	Parameter Set 1	Parameter Set 2
E	10^7	10^7
ν	0.3	0.3
ρ	1	1
L	10	10
b	1	1
h	1	0.1
I	1/12	$1/12\ (0.1)^3$
I_m	1/12	$1/12\ (0.1)^3$

4.1 Free Vibration

Considering only the flexible domain, the virtual work expression gives rise to the following dynamic equilibrium equation

$$\underline{M}\ddot{\underline{q}} + \underline{K}\underline{q} = \underline{Q}$$

where

$\underline{M}$ = consistent mass matrix
$\underline{K}$ = stiffness matrix
$\underline{Q}$ = consistent nodal loads (may include lumped loads)

Solutions to the homogeneous problem can be obtained by letting $\underline{q} = \underline{y}e^{i\omega t}$, where $\underline{y}$ is the column matrix of amplitudes. Substitution leads to a general eigenvalue problem

$$(-\omega^2\underline{M} + \underline{K})\,\underline{y} = 0 \qquad (4.1.1)$$

where the eigenvalue is the square of the natural frequency of vibration, and $\underline{y}$ the associated eigenvector. The exact solution for natural vibration of a Bernoulli-Euler beam is given by [32]

$$\omega = \left(\frac{\lambda}{L}\right)^2 \left(\frac{EI}{m}\right)^{1/2} \qquad (4.1.2)$$

where λ is found from solution of the characteristic equation

$$\cos\lambda \cosh\lambda + 1 = 0 \qquad (4.1.3)$$

The natural modes of vibration are shown in figure 4.14 and are given analytically by

$$Y(x) = A[(\sin\lambda - \sinh\lambda)(\sin\lambda x/L - \sinh\lambda x/L) + (\cos\lambda - \cosh\lambda)(\cos\lambda x/L - \cosh\lambda x/L)] \quad (4.1.4)$$

where

$$A = \frac{C_1}{\sin\lambda - \sinh\lambda}$$

Equation (4.1.2) yields an infinite number of frequencies, however the higher frequencies obtained become increasingly invalid as the kinetic energy associated with rotation of the beam cross-sections becomes significant. Recall that the Bernoulli-Euler assumptions ignore rotatory inertia; kinetic energy comes only from transverse deflections. The frequencies obtained from equation (4.1.2) also neglect shear, which is important as frequency increases, i.e. as the ratio of wavelength/thickness decreases.

To assess the effects of each variation, the natural frequency was normalized by the exact result from Bernoulli-Euler beam theory, and plotted against the number of elements comprising the beam† (in some literature convergence is plotted against number of DOFs – equivalent). The following eight types of beam elements have been formulated:

1) C^0: consistent mass, full integration of mass and stiffness
2) C^0: consistent mass, reduced integration of stiffness

† A slightly different perspective is given in Appendix E, where the natural frequencies are normalized by the exact result from Timoshenko beam theory.

3) C^0: consistent mass, 1-point integration of mass and stiffness
4) C^0: lumped mass, full integration of mass and stiffness
5) C^0: lumped mass, reduced integration of stiffness
6) C^0: lumped mass, 1-point integration of mass and stiffness
7) C^1: consistent mass, full integration of mass and stiffness (with rotatory inertia - Rayleigh)
8) C^1: consistent mass, full integration of mass and stiffness (without rotatory inertia - Bernoulli-Euler)

Recall that the C^0 consistent mass and material stiffness matrices were defined in equations (3.4.9) and (3.4.10), respectively. The C^1 consistent mass and material stiffness matrices were defined in equations (3.3.15) and (3.3.16), respectively.

By convention, Bernoulli-Euler theory neglects rotatory inertia and corresponds directly to case 8. Although consistent application of the finite element method leads to fully integrated consistent mass and stiffness matrices, in practice a reduced level of integration is used to evaluate the C^0 stiffness matrix to avoid element locking. Reduced integration is applied to all terms of the stiffness matrix, and is differentiated from 'selective reduced integration,' in which only the shear related terms are evaluated using reduced integration. Appendix F provides a brief overview of Gauss quadrature, and gives the integration rule corresponding to full and reduced integration of the beam finite elements. Use of the lumped mass matrix is normally dictated by the reduced cost of computing eigenvalues.

Case 1 is the consistent application of the finite element method to the C^0 beam element, and the convergence is shown in figure 4.1. Generally, natural frequencies converge very slowly, even for the first

mode. The increasing influence of shear and rotatory inertia with mode number can also be seen, as the higher modes do not converge to the B.E. result. When the L/h ratio is increased by an order of magnitude, shear and rotatory inertia effects are virtually eliminated, and the problem of shear locking becomes more apparent, as shown in figure 4.2.

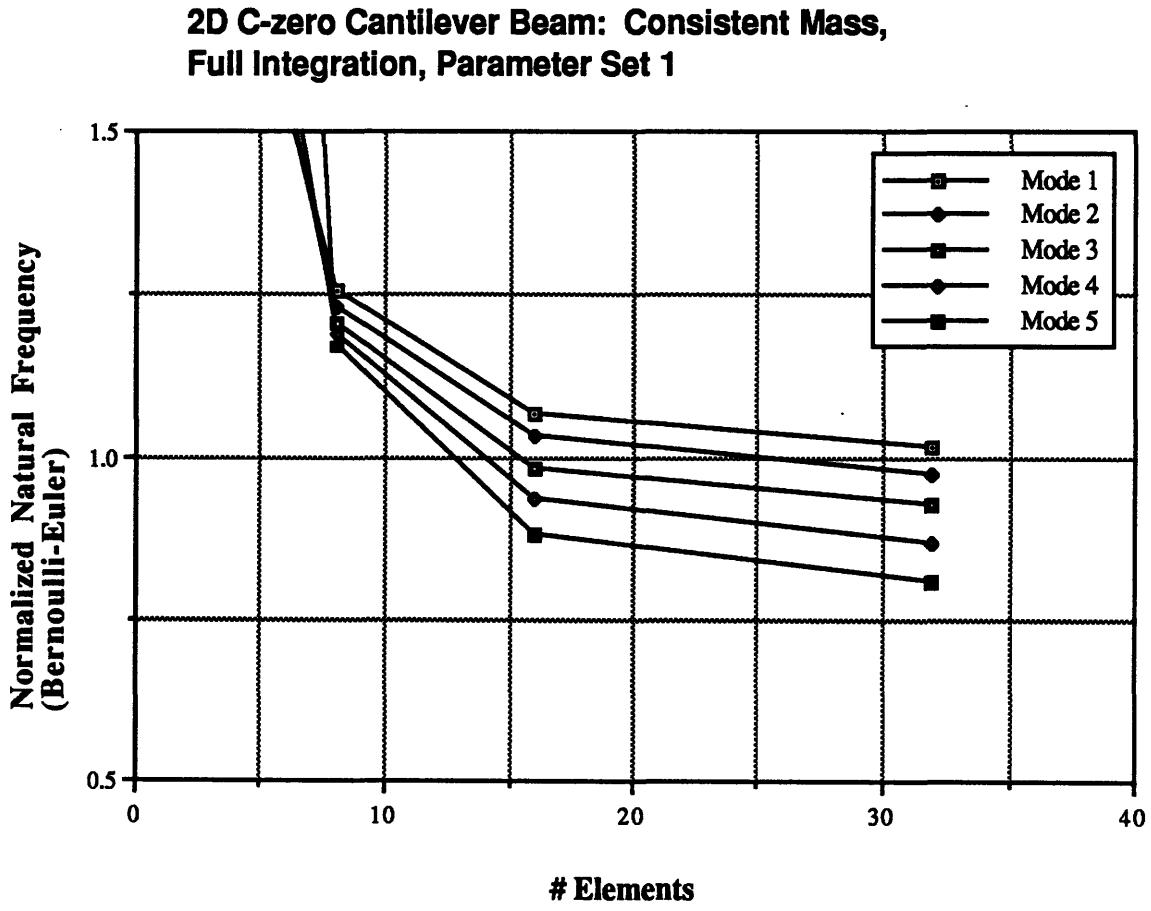

Figure 4.1. Convergence for C^0 beam, consistent mass, full integration.

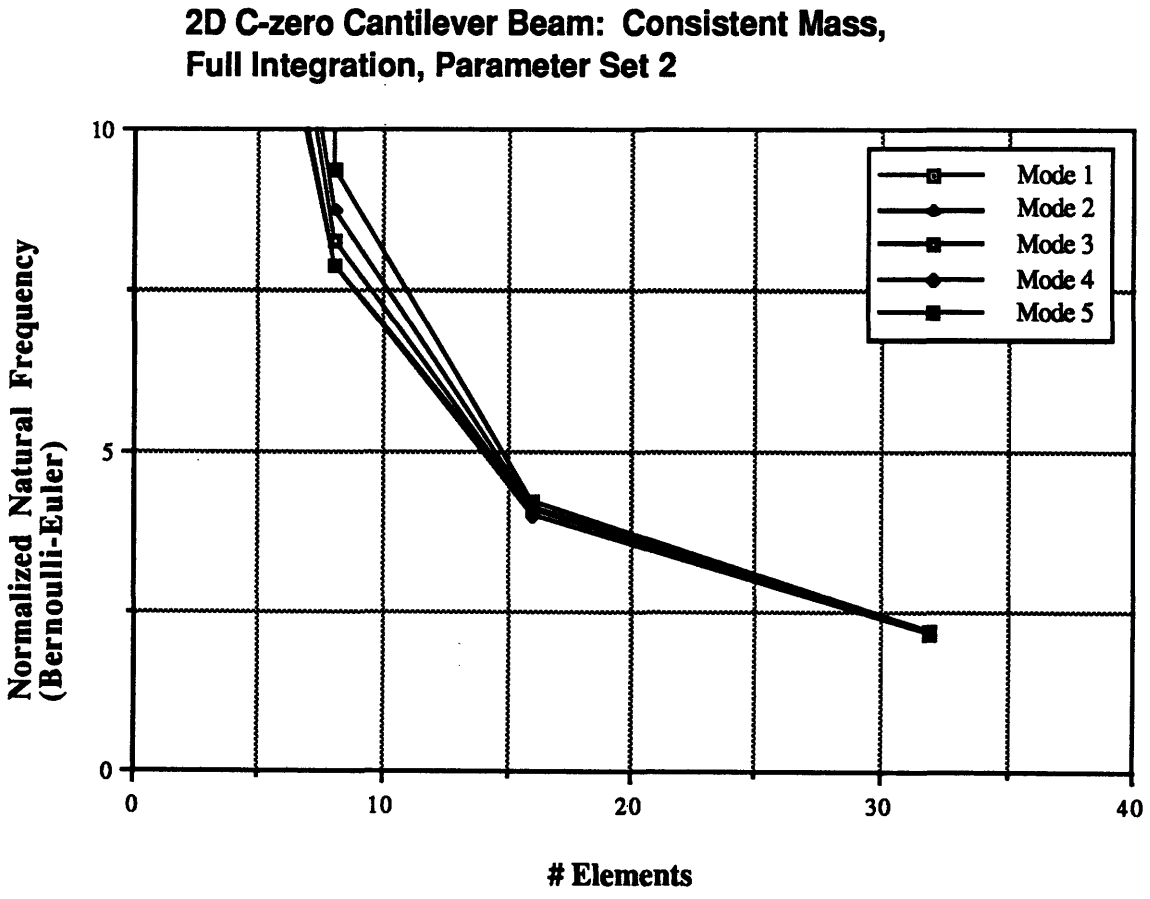

Figure 4.2. Convergence for C^0 beam, consistent mass, full integration.

Case 2 is shown in figure 4.3, and demonstrates the effect reduced stiffness has on the C^0 beam element. The first mode is essentially captured with one element. Again the influence of shear with increasing frequency is apparent, but it can also be seen that good convergence is achieved with a relatively coarse mesh. With parameter set 2, the shear and rotatory inertia effects are negligible, and convergence is achieved with a fine mesh, as shown in figure 4.4. Locking is still observed in the higher modes.

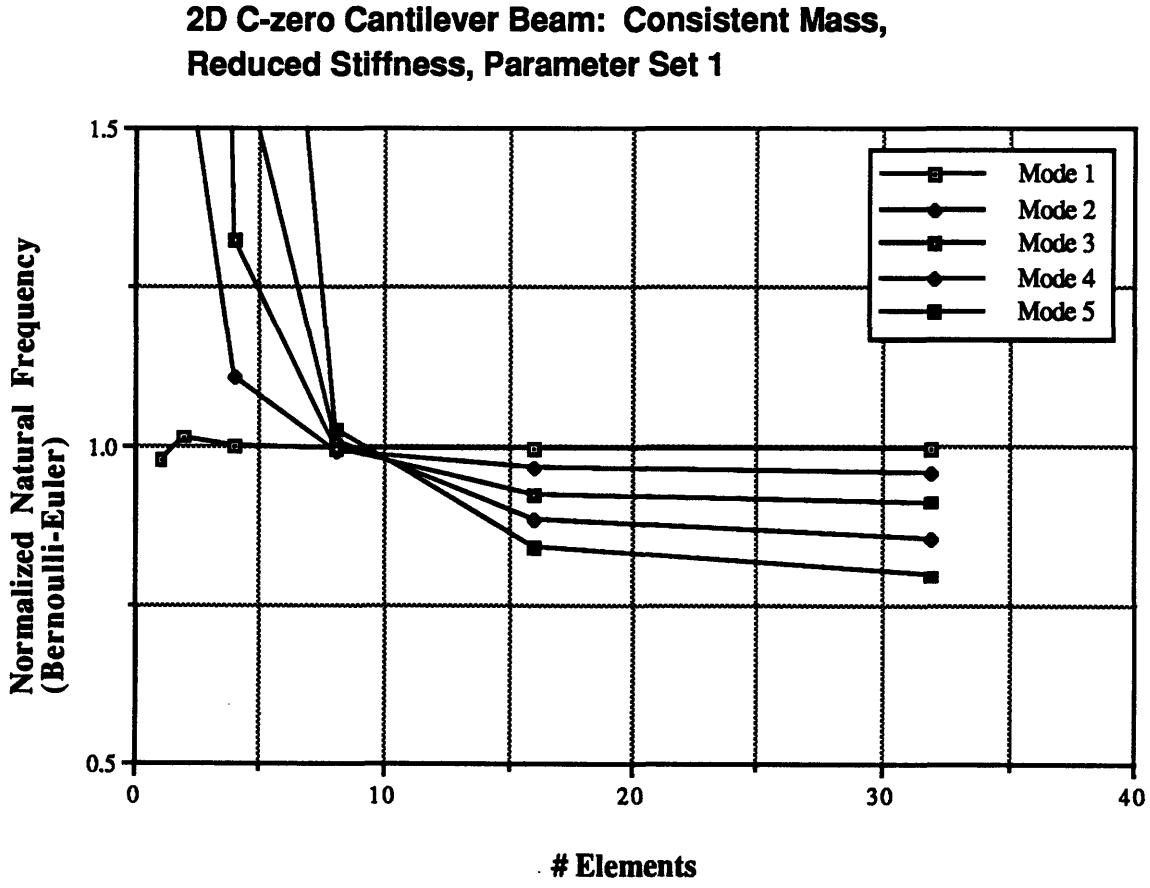

Figure 4.3. Convergence for C^0 beam, consistent mass, reduced stiffness.

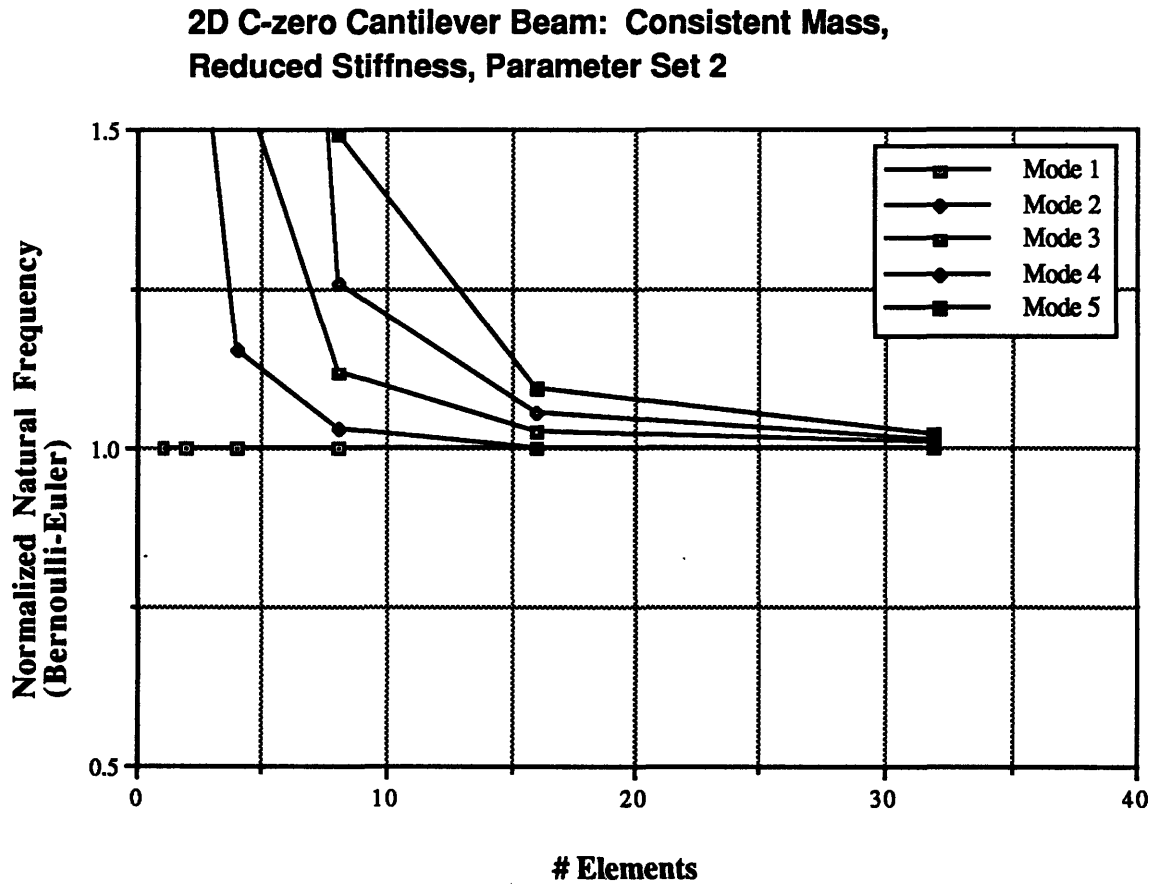

Figure 4.4. Convergence for C^0 beam, consistent mass, reduced stiffness.

The convergence plots associated with case 3 are very similar to those associated with case 2 for the higher modes. Mode 1 now converges from above and requires at least four elements before locking on to the Bernoulli-Euler result. These results are given as figures 4.5 and 4.6.

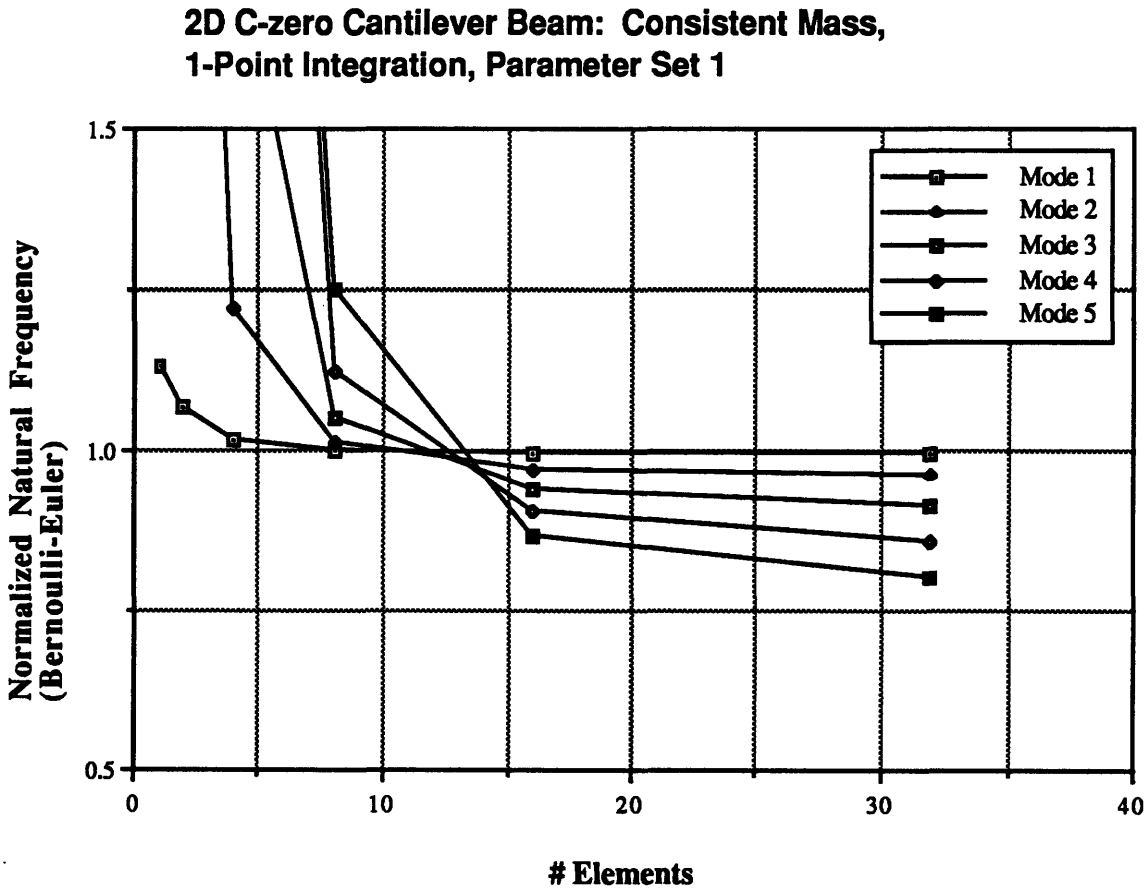

Figure 4.5. Convergence for C^0 beam, consistent mass, uniform 1-point integration.

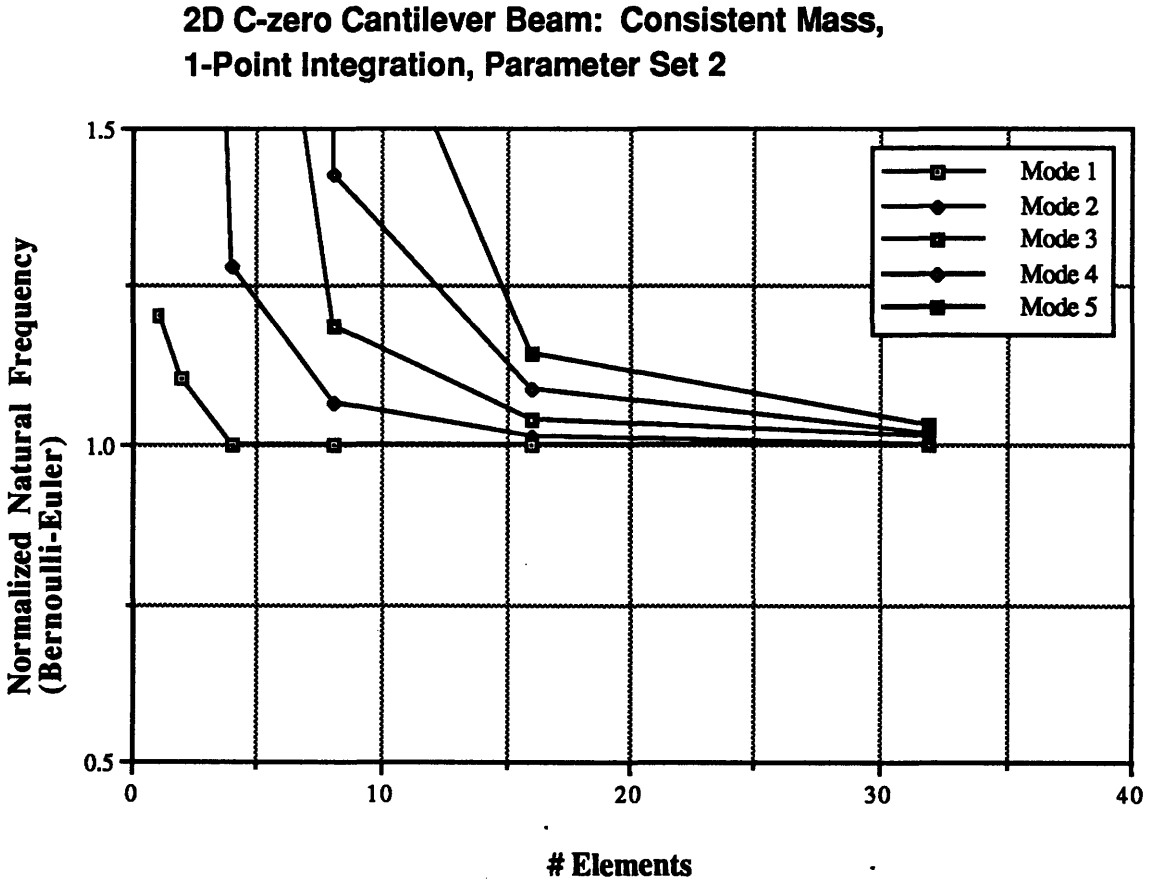

Figure 4.6. Convergence for C^0 beam, consistent mass, uniform 1-point integration.

Convergence for case 4 is shown in figure 4.7. The lumped mass assumption (no lumped inertia) isolates the shear effect. Comparison with figure 4.1 indicates that rotatory inertia has little influence on the frequencies of vibration. The result for parameter set 2 is shown in figure 4.8, and is very similar to the consistent mass result shown in figure 4.2, which indicates that locking is not remedied by mass assumptions.

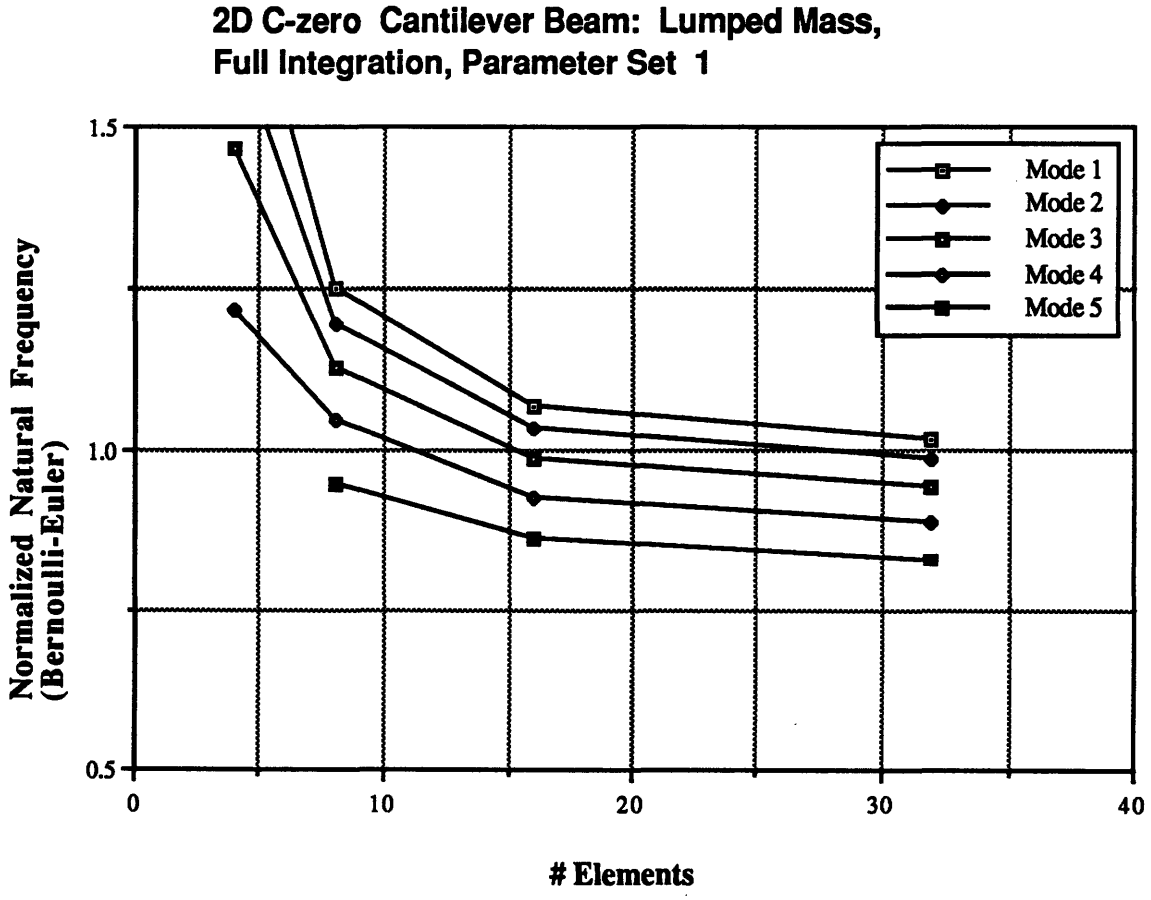

Figure 4.7. Convergence for C^0 beam, lumped mass, full integration.

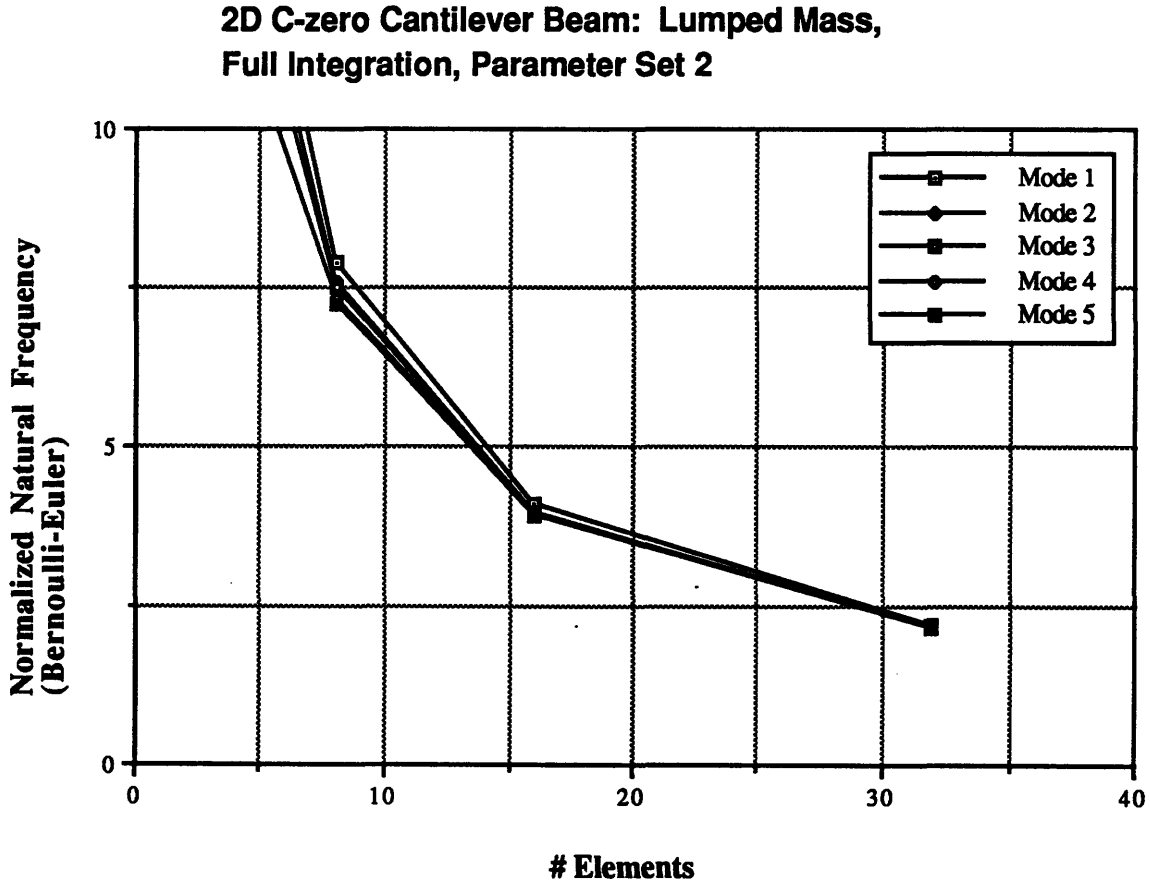

Figure 4.8. Convergence for C^0 beam, lumped mass, full integration.

The last set of C^0 formulations to be discussed is that of lumped mass/reduced stiffness. (Cases 5 & 6 are one and the same, since by the lumped mass assumption, the mass matrix is not subject to integration). Note that only the effect of shear is present, lumped inertia being neglected. One striking feature is the convergence of Mode 1 from below, rather than from above. Convergence is achieved with relatively course mesh, with shear still apparent in the higher modes. The effect of L/h is clearly shown in figure 4.10, where shear is not an important factor, and convergence to the B.E. result is observed.

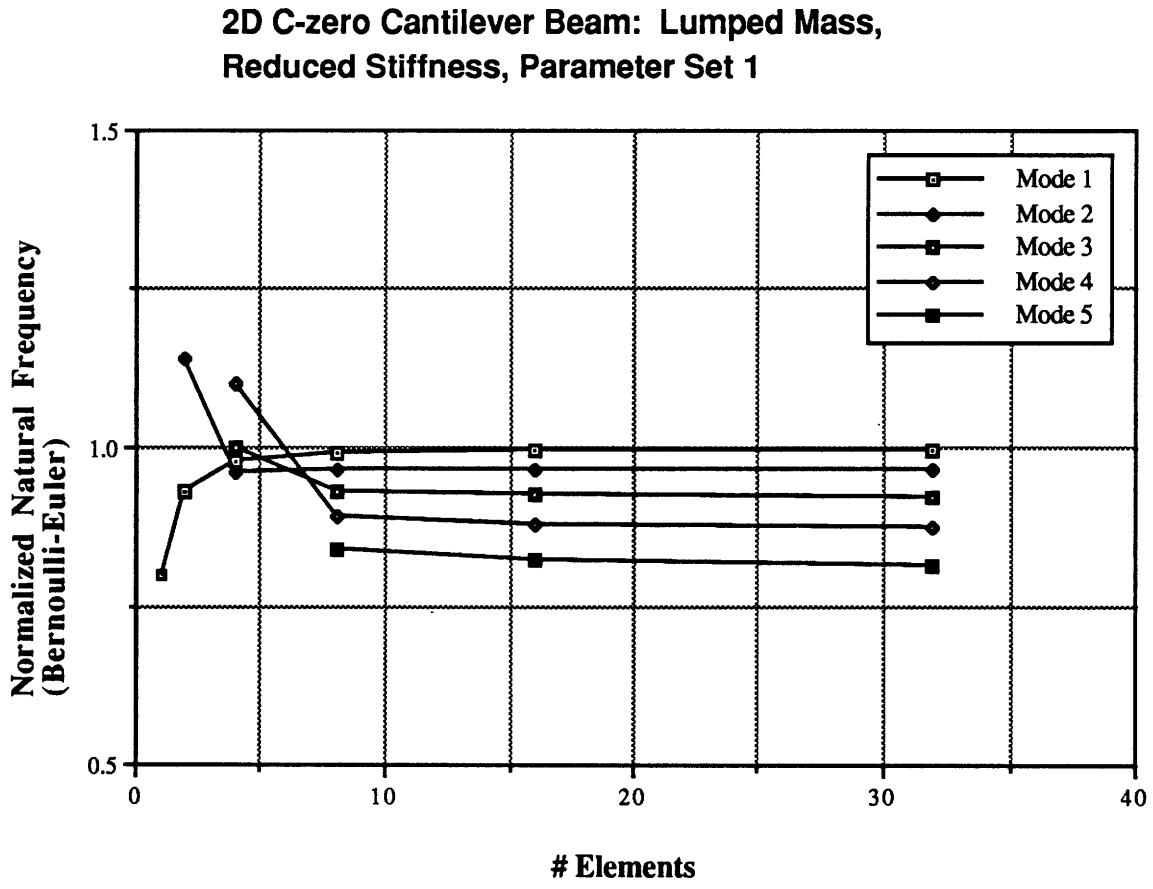

Figure 4.9. Convergence for C^0 beam, lumped mass, reduced stiffness.

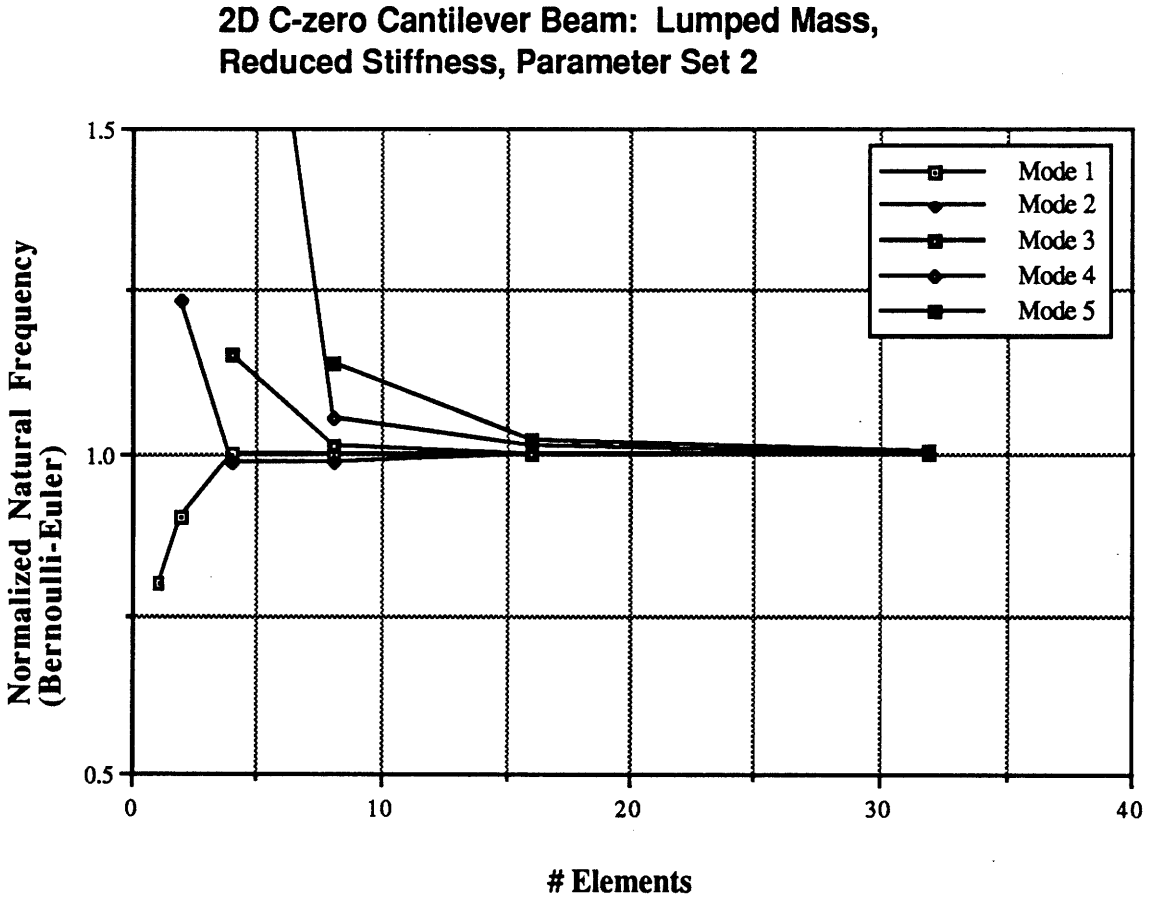

Figure 4.10. Convergence for C^0 beam, lumped mass, reduced stiffness.

The last two cases are those of the C^1 elements. Both are fully integrated, and use the consistent mass matrix. The only difference is the treatment of rotatory inertia. The Rayleigh formulation using parameter set 1 is shown in figure 4.11. The influence of rotatory inertia can be seen to lower the frequency of the higher modes. The so-called Bernoulli-Euler beam theory has $I_{my} = I_{mz} = 0$. With regard to the previous derivation, the last three terms on the diagonal of matrix $\underline{D_m}$ are set equal to zero . It can be seen (figure 4.12) that convergence is very rapid, and all modes are converged with no more than eight elements. Bernoulli-

Euler and Rayleigh beam theories become indistinguishable as L/h increases. Figure 4.13 is representative of both Rayleigh and Bernoulli-Euler formulations for parameter set 2.

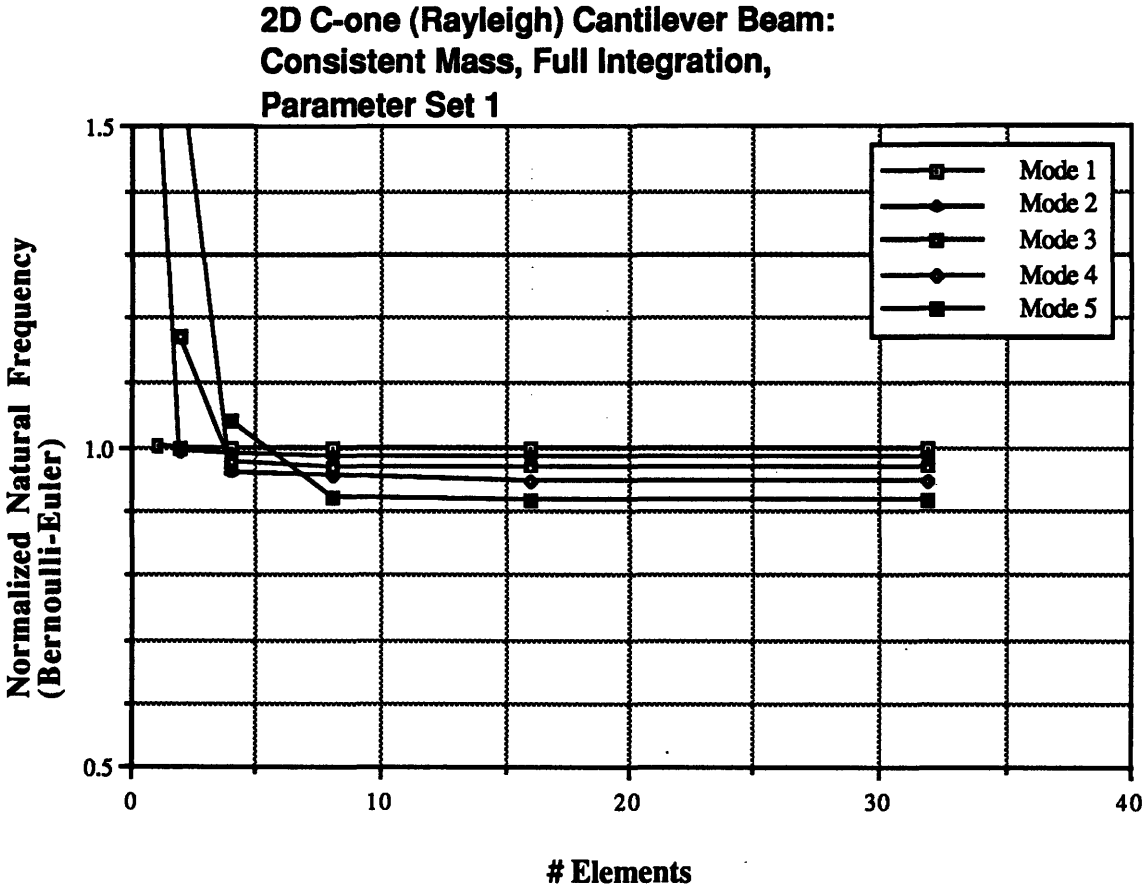

Figure 4.11. Convergence for C^1 beam (Rayleigh), consistent mass, full integration.

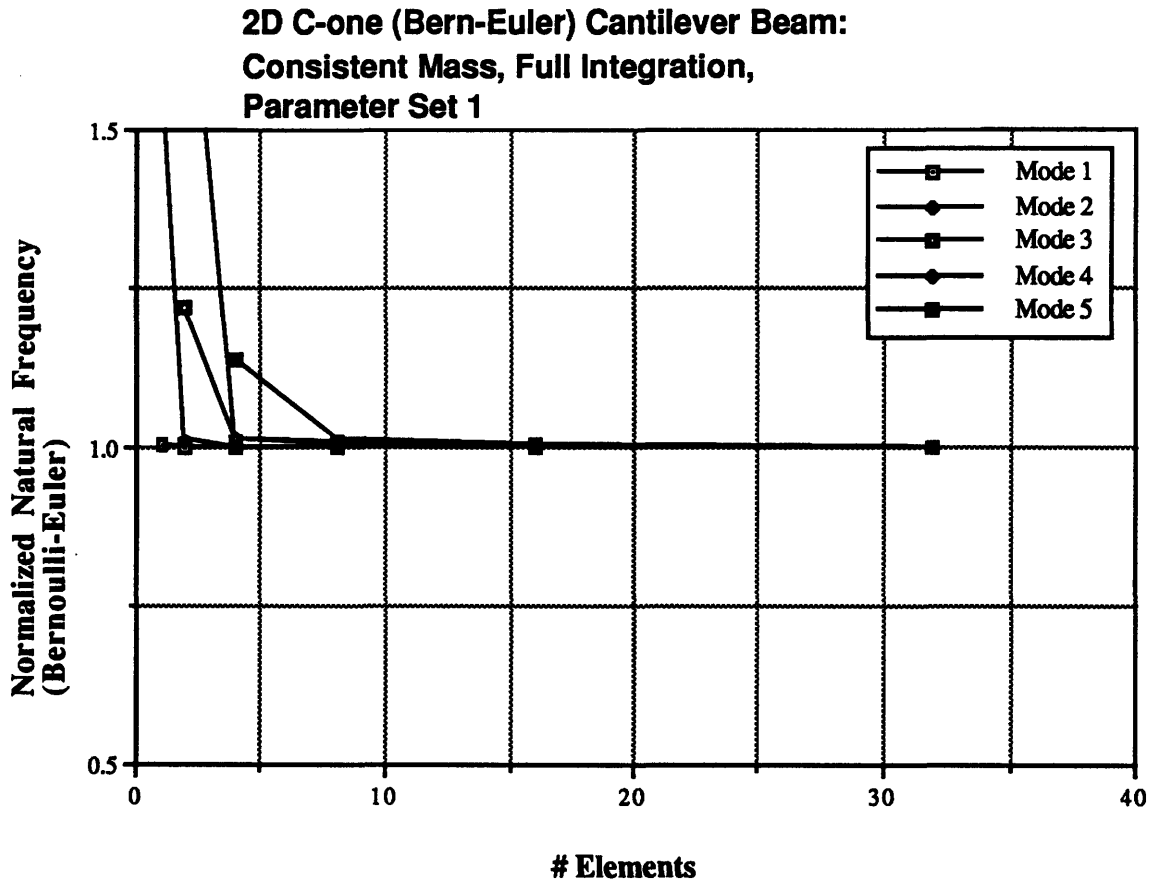

Figure 4.12. Convergence for C^1 beam (B.E.), consistent mass, full integration.

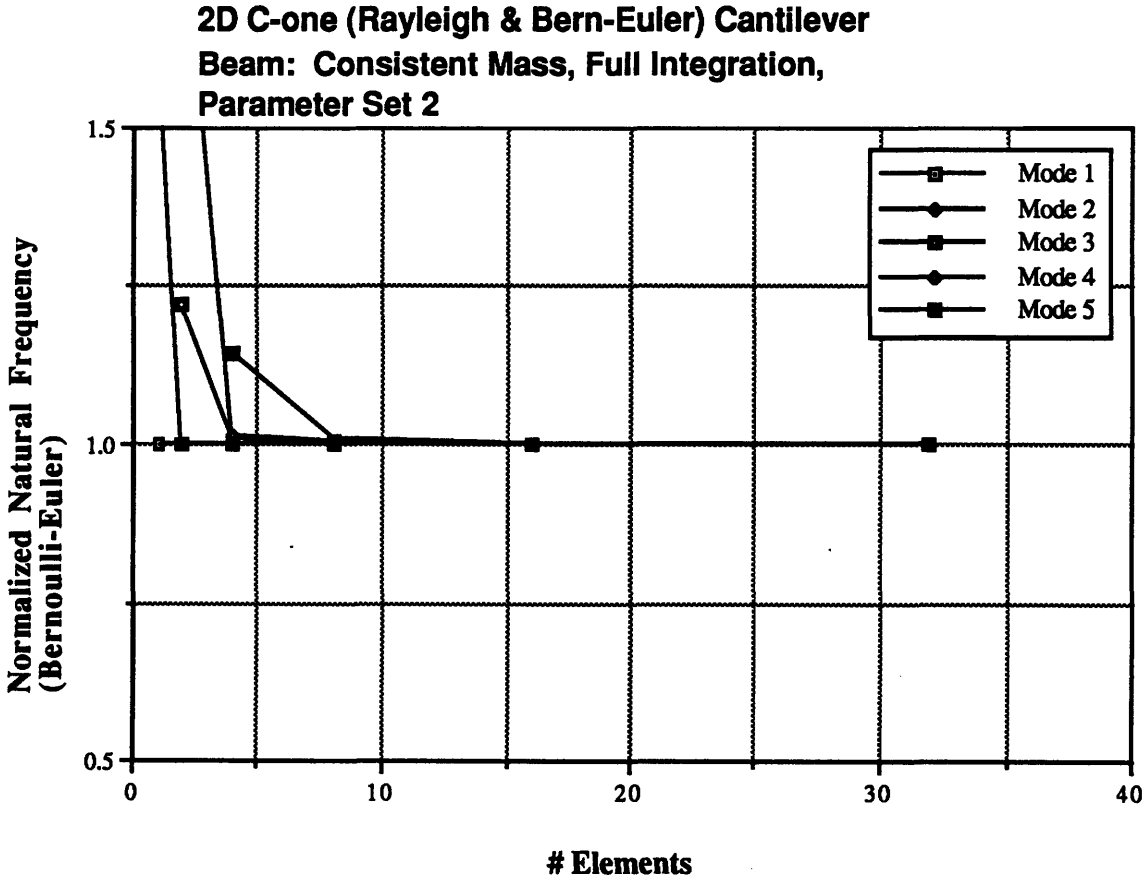

Figure 4.13. Convergence for C^1 beam, consistent mass, full integration.

4.1.1 Importance of Shear and Rotatory Inertia

The results show that consideration of shear and rotatory inertia cause a reduction of natural frequency compared to the analytical Bernoulli-Euler theory. The influence of shear and rotatory inertia can be quantified, to a degree, in terms of the 'effective length'/thickness, which allows all modes and beam parameters to be judged according to the same criteria. The effective length is taken to be the approximate wavelength, obtained from figure 4.14. Table 4.2 shows an estimation of the wavelength and the corresponding ratios of wavelength/thickness. For the

purpose of discussion, modes 1 & 2 were considered to be 1/4 and 1/2 waves, respectively.

Table 4.2. Effective (wavelength/thickness).

Mode	Wave-length	Effective length/thick	
		Set 1	Set 2
1	40	40	400
2	20	20	200
3	8	8	80
4	5.5	5.5	55
5	4.75	4.75	47.5

Correlation of the values in table 4.2 with the results given in the preceding figures shows that departure from Bernoulli-Euler theory occurs when the effective length/thickness < 40. This is demonstrated in figures 4.9 & 4.10, where rotatory inertia effects are absent; it is also seen in figure 4.11, where only the shear effect is neglected. Note that shear has a larger influence on natural frequency than does rotatory inertia. As a rule of thumb, the consideration of effective length/thickness provides an aid in the selection of an appropriate finite element model.

4.1.2 Mesh Estimate for C^0 Elements

An estimate of the mesh requirements for C^0 element discretization can be made with the help of figure 4.14. The figure represents the exact mode shapes for the first five frequencies of transverse vibration for a Bernoulli-Euler beam with cantilevered boundary conditions. Amplitudes

shown are arbitrary. Since C^0 elements can model only linear variation of transverse displacement, the number of straight line segments (or elements) required to model a given frequency can be estimated. Discretization based on this method of mesh estimation suggests using beam elements of various lengths, in order to efficiently capture the target mode shapes.

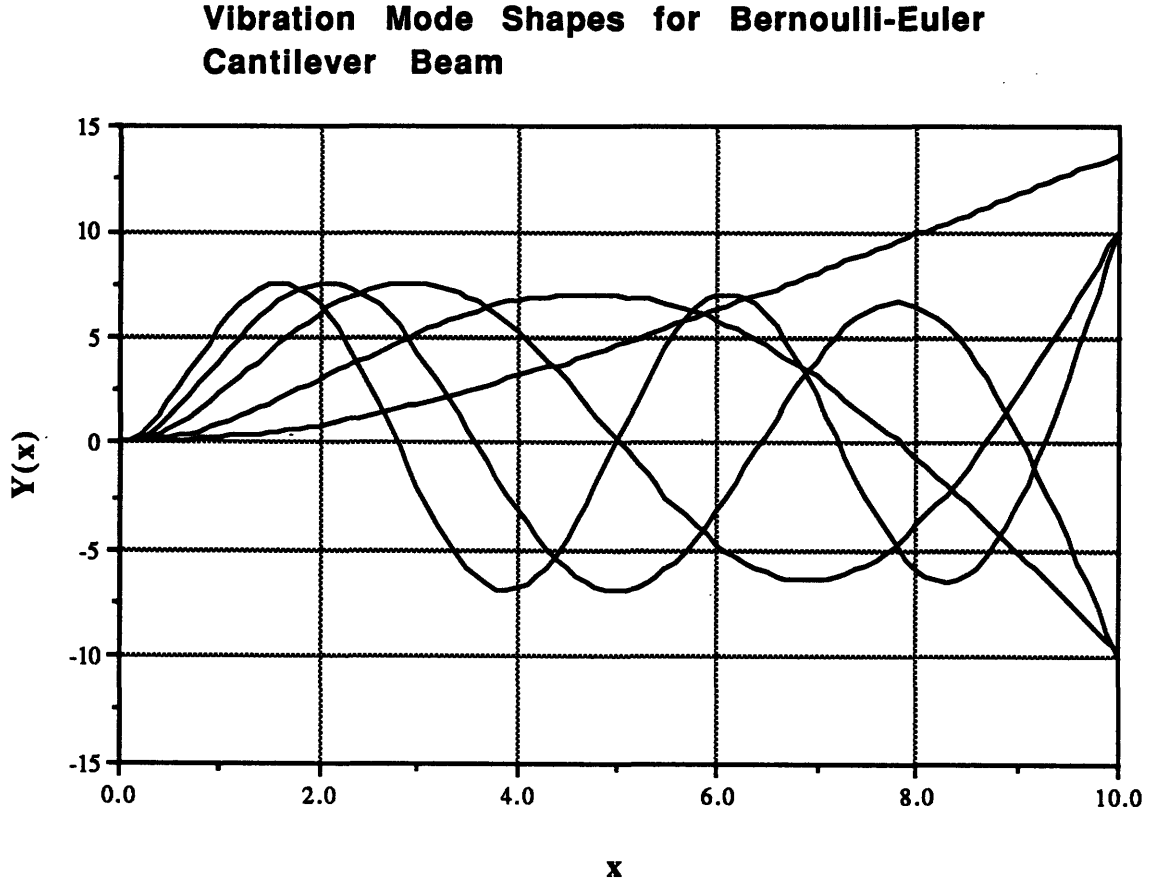

Figure 4.14. Exact vibration mode shapes, Bernoulli-Euler theory.

4.2 Static Buckling

The effect of large initial stress and contribution of nonlinear strains must be considered in order to solve the static buckling problem. The geometric stiffness matrix was derived in section 3.5, and now provides the mechanism by which the second eigenvalue problem is formed. The new equation can be written

$$(\underline{K} + P\underline{K_\sigma})\,\underline{y} = 0 \tag{4.2.1}$$

where the only nonzero element of $\underline{K_\sigma}$ is some reference axial stress resultant N_{xref}. The critical buckling load is then $P_{cr} = \lambda N_{xref}$, where λ is the smallest eigenvalue. The exact solution for Bernoulli-Euler beam with clamped/free boundary conditions is given by [33]

$$P_{cr} = \frac{\pi^2 EI}{4L^2}(2n - 1)^2 \qquad n = 1, 2, 3, \ldots \tag{4.2.2}$$

where the associated mode shapes are given by

$$v = \begin{cases} c_1\left(1 - \cos\dfrac{\pi x}{2L}\right) & n = 1 \\ c_1\left(1 - \cos\dfrac{2n - 1}{2}\dfrac{x}{L}\right) & n = 2, 3, 4, \ldots \end{cases} \tag{4.2.3}$$

where c_1 is arbitrary as long as the deflections are consistent with the theory of small displacements.

Because the static buckling problem does not involve the mass matrix, and because the load is constant over the length of the beam, only three different formulations are presented for this example:

1) C^0: full integration of stiffness matrices
2) C^0: reduced integration of material stiffness
3) C^1: full integration of stiffness matrices

Buckling loads have been normalized by the exact Bernoulli-Euler buckling load. Although only the critical mode is important in the simple example considered, the higher modes may become important in more complex structures, and are thus included in the following figures. Convergence of static buckling load is very similar to the convergence of natural frequencies obtained from consistent mass formulations - compare figures 4.15-4.20 to figures 4.1-4.6 and figures 4.12-4.13.

Comments made earlier also apply here, however, a couple of additional comments are made. Figure 4.16 shows very clearly the problem of shear locking associated with the fully integrated C^0 material stiffness matrix. Figures 4.17 and 4.18 differ from figures 4.3 and 4.4 only in that the critical buckling is not captured with one element. It requires at least eight elements to lock on to the Bernoulli-Euler result. The C^1 formulation captures the critical buckling load with one element.

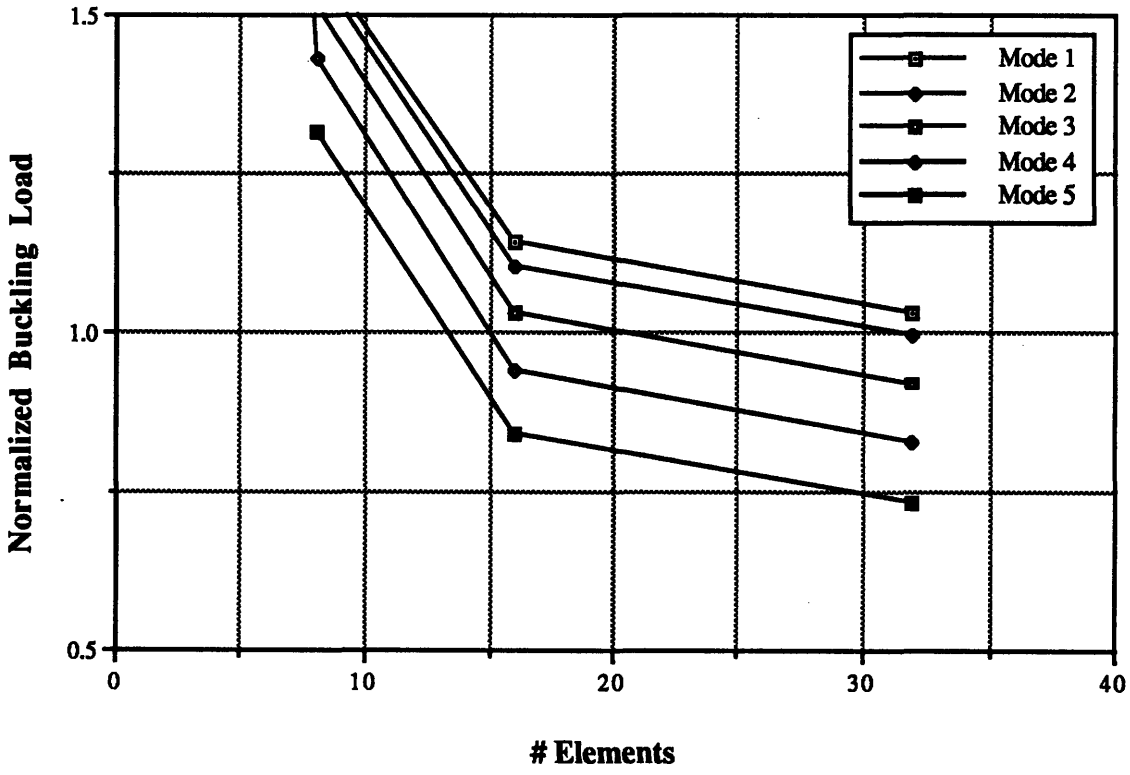

Figure 4.15. Convergence for C^0 beam, full integration of stiffness.

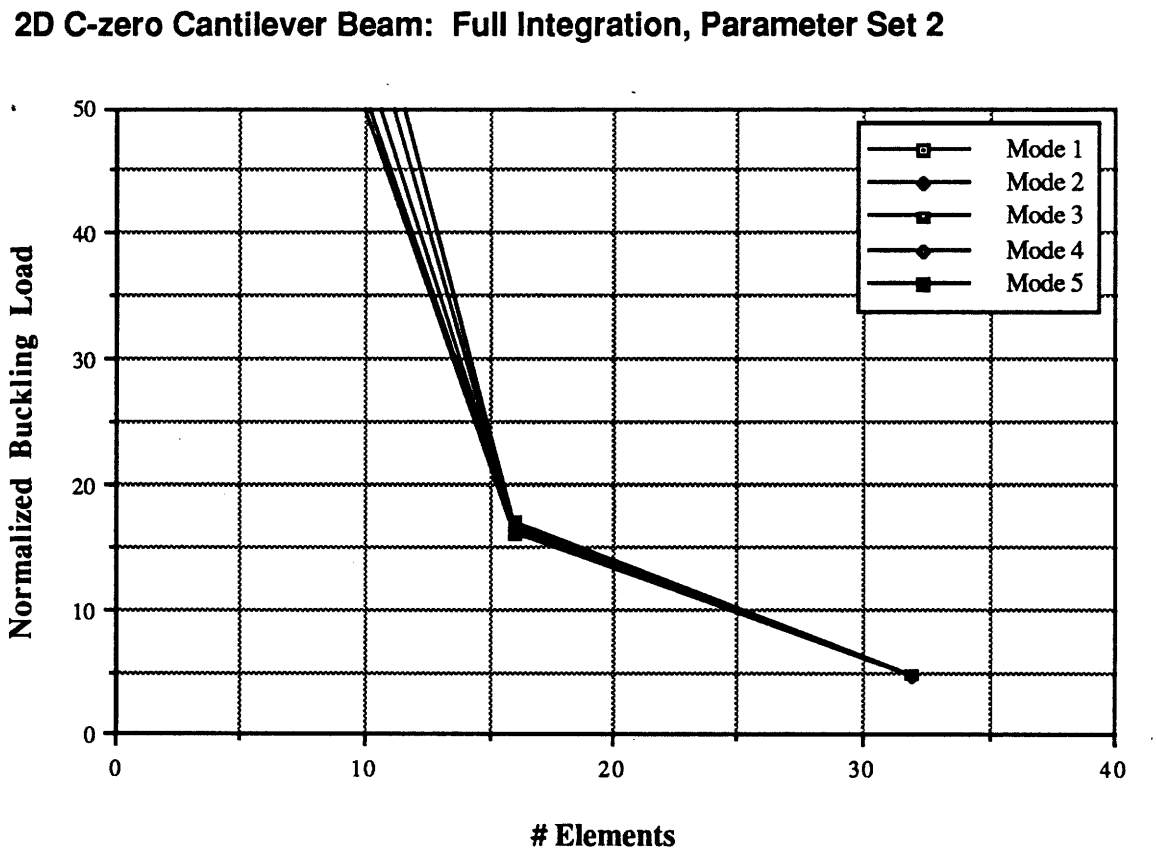

Figure 4.16. Convergence for C^0 beam, full integration of stiffness.

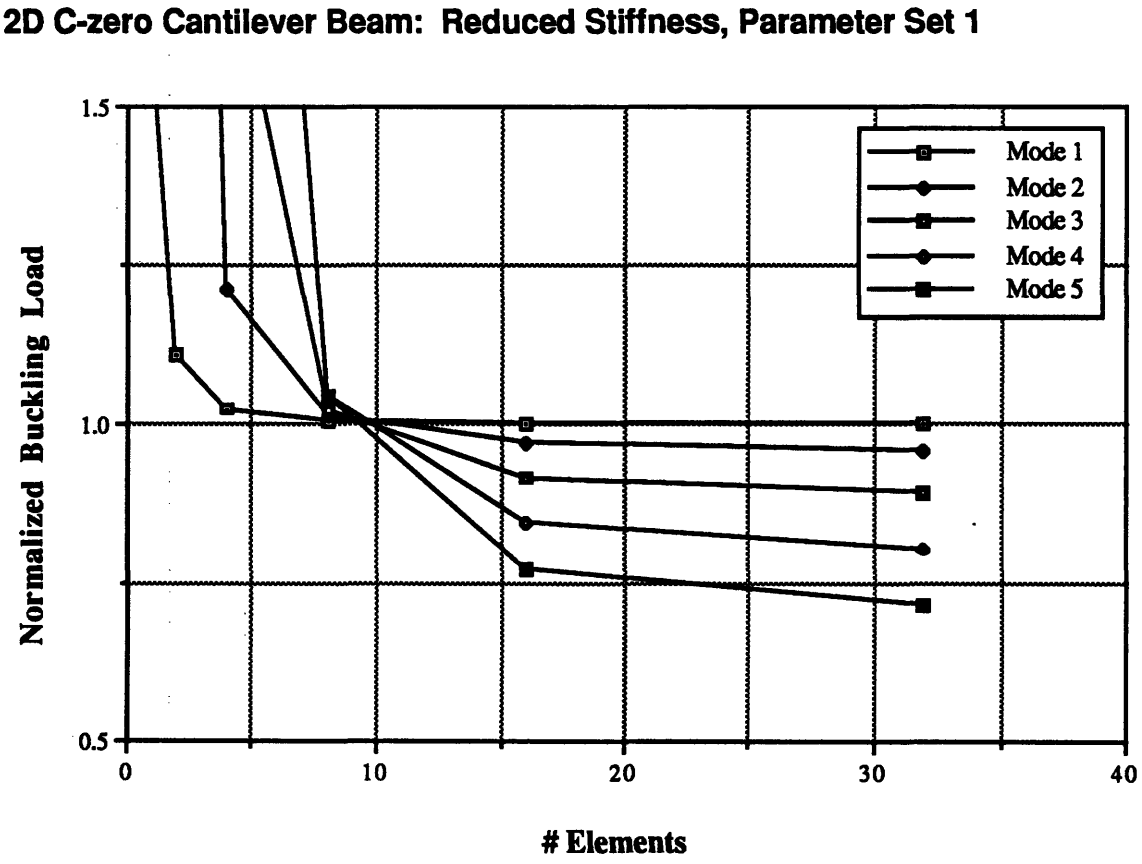

Figure 4.17. Convergence for C^0 beam, reduced integration of stiffness.

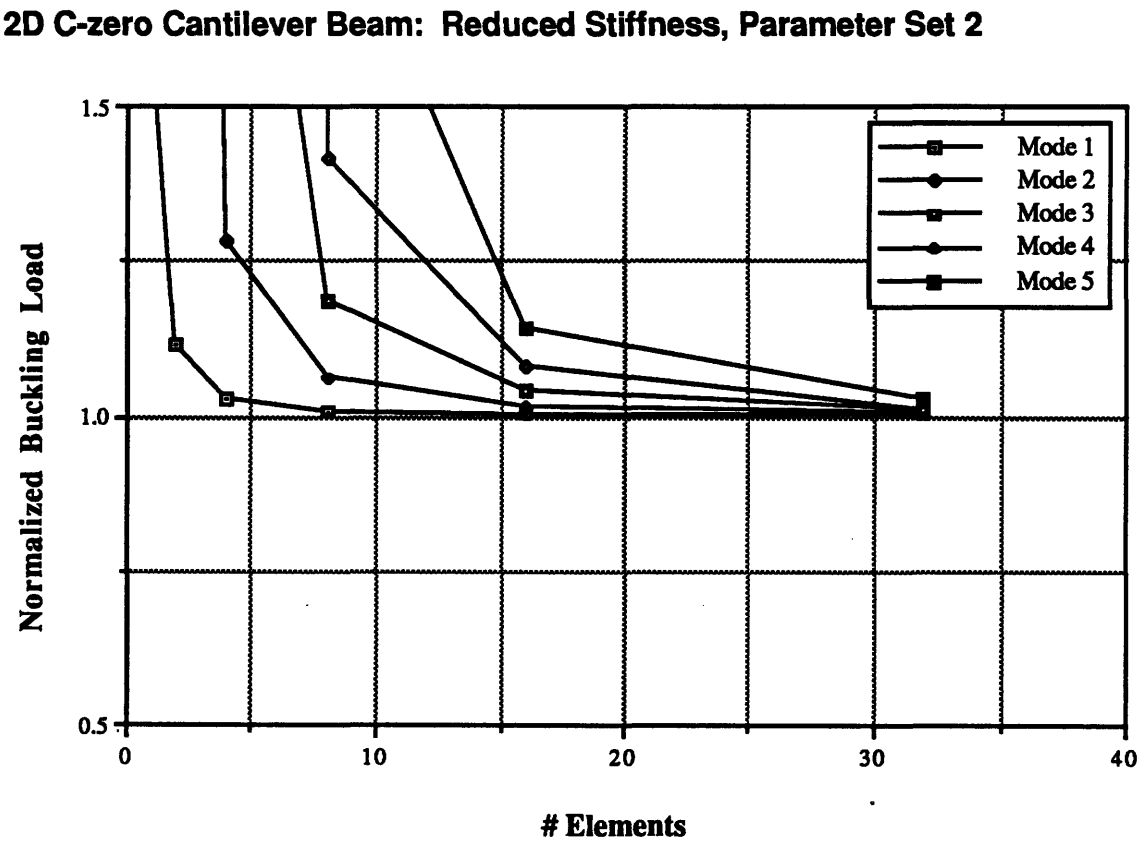

Figure 4.18. Convergence for C^0 beam, reduced integration of stiffness.

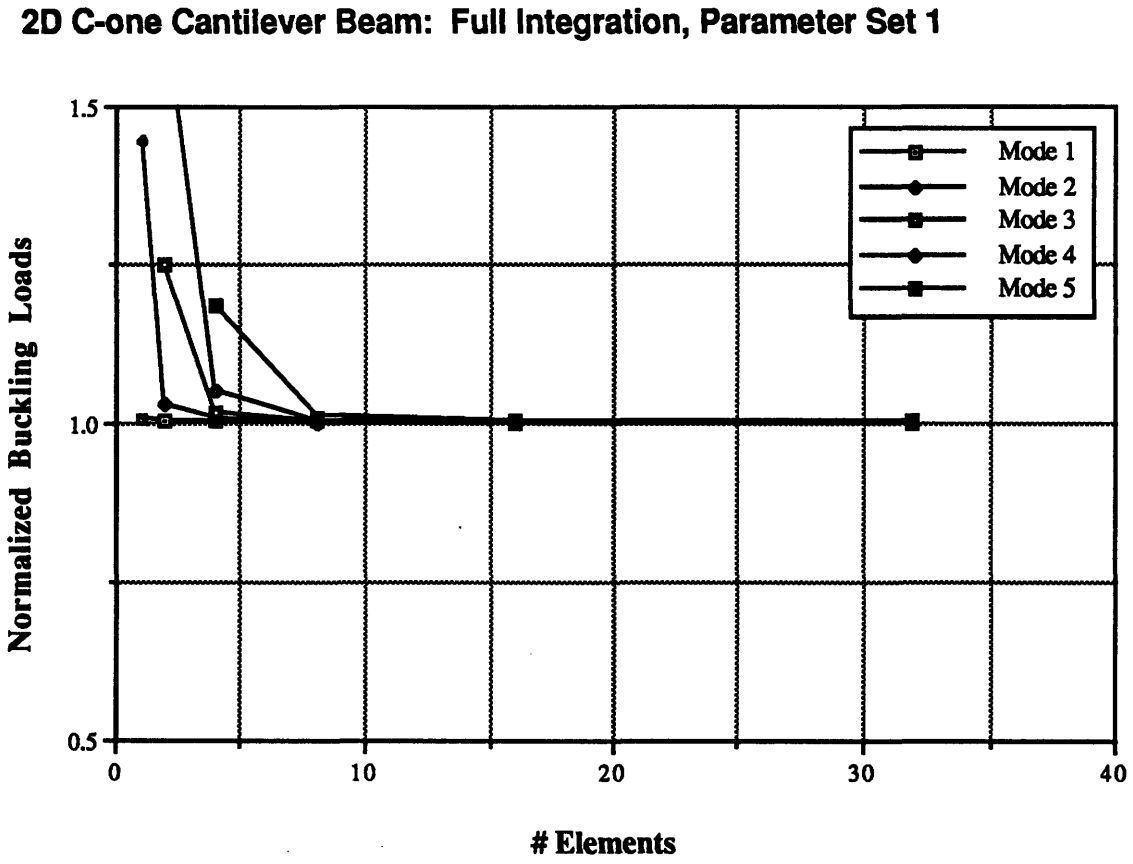

Figure 4.19. Convergence for C^1 beam, full integration of stiffness.

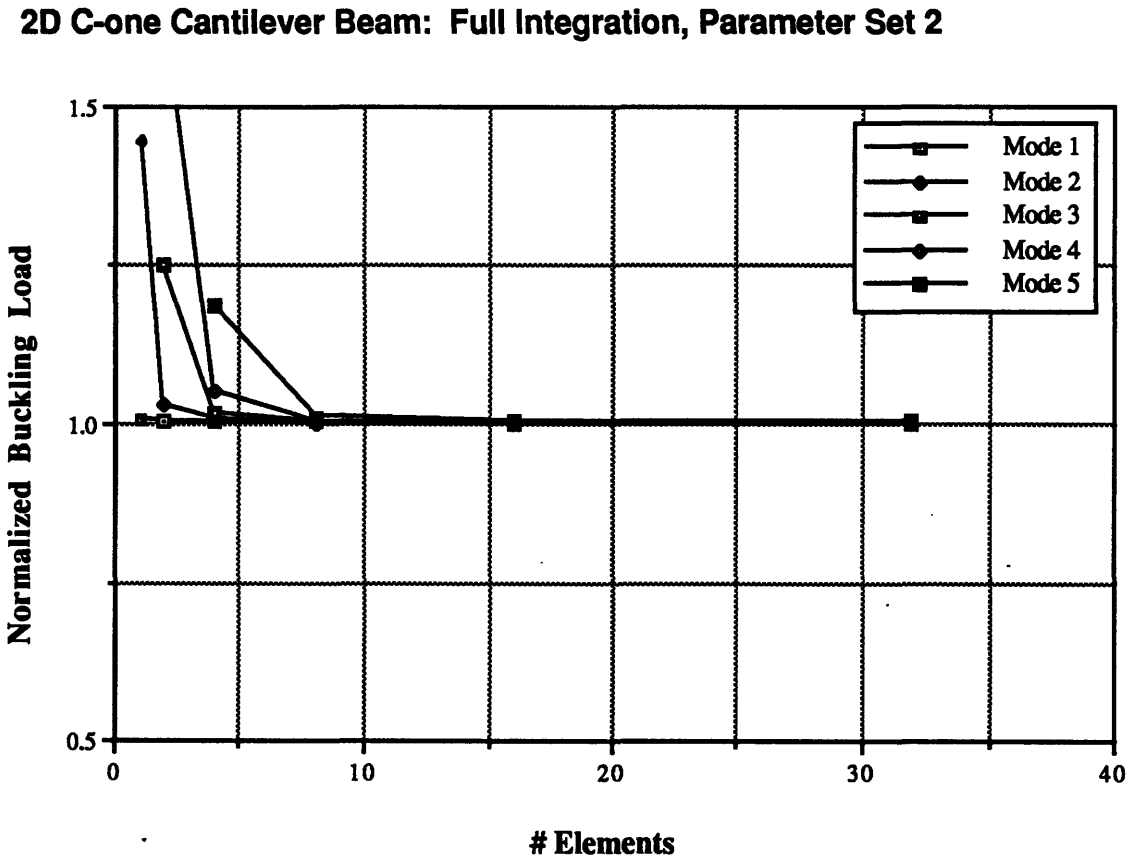

Figure 4.20. Convergence for C^1 beam, full integration of stiffness.

4.3 Dynamic Buckling

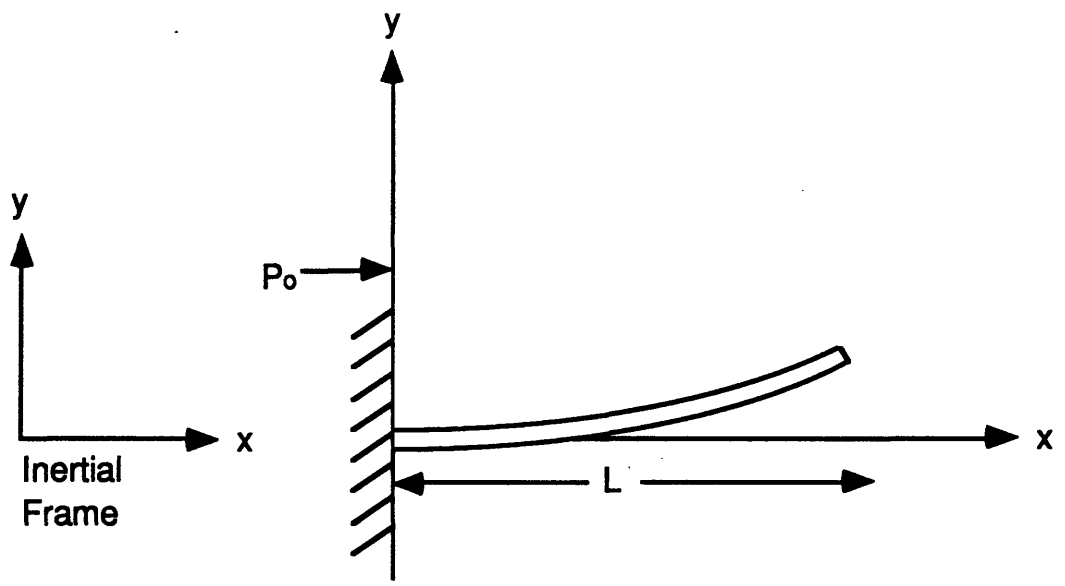

Figure 4.21. Cantilevered beam under distributed axial load.

Yet a third eigenvalue problem can be formulated which involves all three principal finite element matrices. Consider an inextensible beam with cantilevered boundary conditions which is free to translate in space. A constant axial load is applied to the cantilevered end as shown in figure 4.21 which produces the following distributed axial loading.

$$P(x) = P_o\left(1 - \frac{x}{L}\right) \tag{4.3.1}$$

For a given static loading determined by P_o, the frequencies of natural vibration can be computed. It will be seen that compressive axial stress has a 'softening' effect. The eigenvalue problem is similar to the case of free vibration considered in section 4.1. Now the effect of internal force is included in the stiffness and the eigenvalue problem can be written as

$$[-\omega^2 \underline{M} + (\underline{K} + \underline{K_\sigma})]\, \underline{y} = 0 \qquad (4.3.2)$$

where the internal force distribution is embedded in the geometric stiffness matrix. When $P_o = 0$, the geometric stiffness matrix becomes the null matrix and the simple free vibration problem is recovered. For $P_o < P_{cr}$, the eigenvalue problem of equation (4.3.2) gives the frequencies of natural vibration. As P_o is increased to P_{cr}, the fundamental frequency goes to zero, as shown in figure 4.22. Dynamic buckling occurs at $P_o = P_{cr}$, which corresponds to the zero frequency. This is equivalent to a static buckling problem of the type considered in section 4.2 in which the axial load distribution is given by equation (4.3.1).

Buckling of a vertical cantilevered beam due to its own weight was considered by Timoshenko [34] and is here used as the exact solution for the Bernoulli-Euler beam. The critical load was given as

$$P_{cr} = 7.837 \frac{EI}{L^2} \qquad (4.3.3)$$

A more general formulation for the buckling of a beam under axial acceleration with rigid mass attached to the free end was considered by Storch and Gates [35]. In the degenerate case, with zero tip mass, the critical load has the same form as given above except the factor becomes 7.8664.

An investigation of the performance of a single element is shown in figure 4.22. Data displayed in the figure is tabulated in table 4.3. Examination of the data shows that the mass matrices from B.E. and Rayleigh theory do indeed yield different frequencies, although the difference is very small. A comparison of performance would be

incomplete without considering the fully integrated C^0 beam, however, a single element is so stiff that plotted on the scale of figure 4.22 the curve would begin well up (171) and end well to the right (196,033) of all the other curves. Reducing the integration of the stiffness matrices reduces the locking problem so apparent with full integration. The curve with reduced stiffness compares quite favorably to the Bernoulli-Euler result. Overrelaxation is observed in the C^0 formulation with both reduced stiffness and lumped mass approximation for small axial loads.

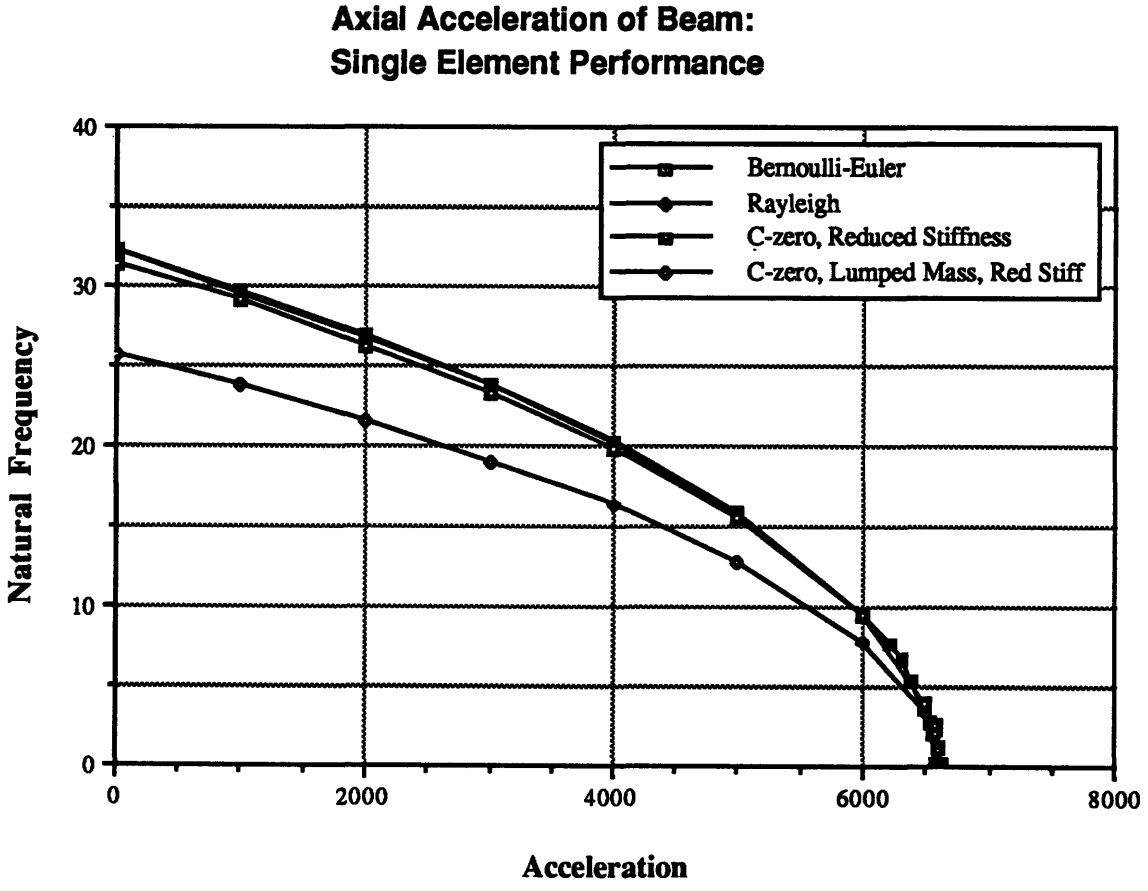

Figure 4.22. Natural frequencies for $P_o < P_{cr}$, parameter set 1.

Figure 4.23 shows the convergence of the critical acceleration for several beam element formulations. Bernoulli-Euler and Rayleigh beam assumptions (B.E. has zero rotatory inertia) produce identical results for critical acceleration, since this corresponds to a static buckling problem with load distribution given by equation (4.3.1). The C^0 formulation with full integration shows clearly the element locking problem, while reduced integration of the stiffness matrices produces better convergence. The loss of monotonicity of convergence due to reduced integration is also observed.

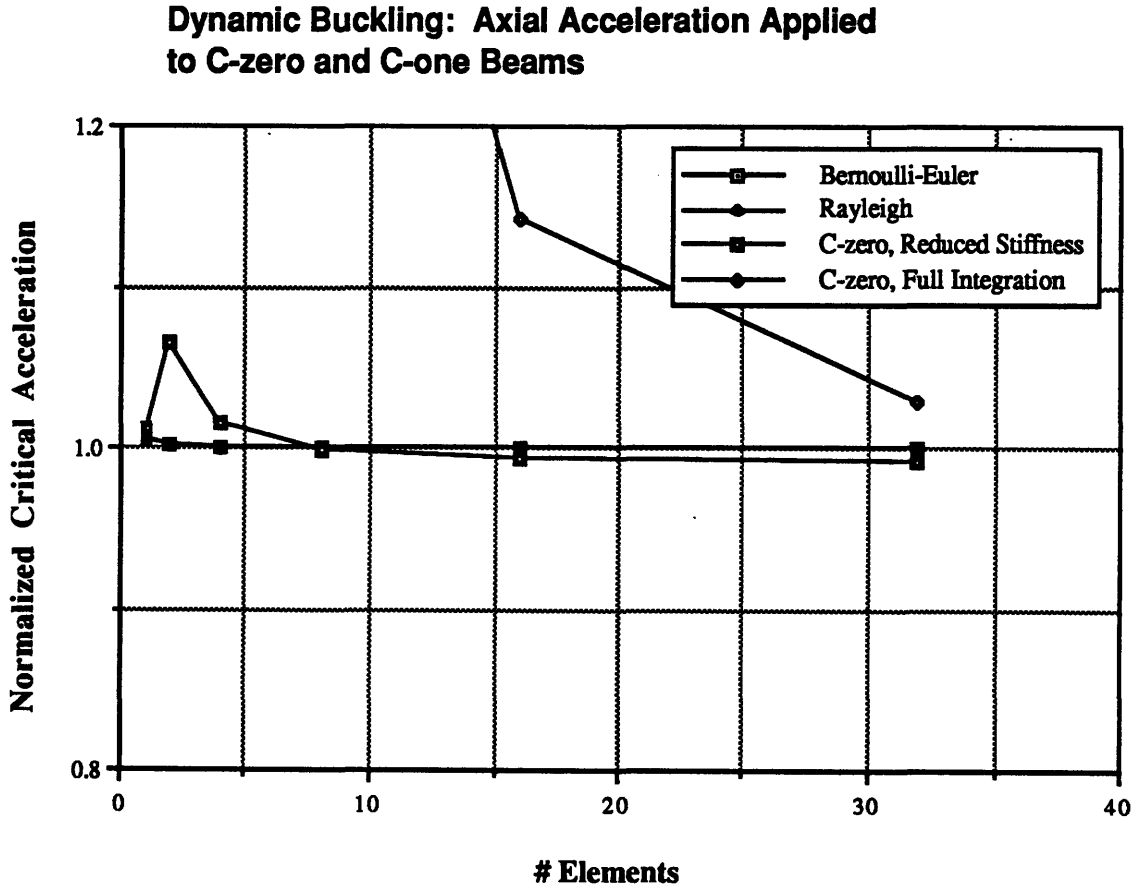

Figure 4.23. Convergence for dynamic buckling, parameter set 1.

Table 4.3. Data displayed in figure 4.22.

	Fundamental Frequency			
Acceleration	Bernoulli-Euler	Rayleigh	C^0, reduced stiffness	C^0, reduced lumped mass
0	32.2	32.2	31.4	25.7
500	-	30.9	-	-
1000	29.7	29.6	29	23.7
2000	26.9	26.8	26.3	21.5
3000	23.8	23.7	23.2	19
4000	20.2	20.1	19.8	16.2
5000	15.8	15.8	15.5	12.7
5700	11.8	11.7	-	-
6000	9.53	9.51	9.54	7.81
6200	7.69	7.68	-	-
6300	6.59	6.57	-	-
6400	5.25	5.24	-	-
6500	3.42	3.42	4.04	3.31
6530	2.64	2.64	-	-
6550	1.95	1.95	-	-
6570	-	-	2.43	1.98
6574.1	0.138	0.0555	-	-
6600	-	-	1.18	0.967
6609.3	-	-	0.094	0.0769

Chapter 5
Dynamic Problems

The eigenvalue problems of the previous chapter provide insight regarding the behavior of nonlinear beam finite elements in the context of dynamics. The next step in the systematic assessment of finite element approximations is a benchmark nonlinear dynamic simulation. The example chosen was originally proposed by Kane [36, 13] to demonstrate the physical behavior of rapidly spinning systems known as 'centrifugal stiffening.' The result reported by Ryan [36] was obtained using an assumed modes formulation. Other researchers who have also published a solution to the spin-up problem are Simo & Vu-Quoc (nonlinear finite element method) [15], and Ider & Amirouche (also assumed modes) [16]. These published results provide comparison for the present solution. The focus is on understanding the influence of the Coriolis and centrifugal forcing terms, and the contribution of the geometric stiffness matrix.

Application of the dynamics formulation is also made to a space shuttle/remote manipulator arm/payload model which demonstrates a practical application of the theory. A realistic torque is applied to the orbiter and realistic payload mass properties are used.

5.1 Dynamics Simulation

5.1.1 Specification of Equations of Motion

An exact set of governing equations was derived in section 2.5. The succeeding sections introduced two alternative modelling assumptions with regards to the flexible appendage mass distribution: lumped mass (§2.6) and lumped mass/inertia (§2.7). In either case the stiffness matrix is provided by 3-D finite elements. The lumped mass/inertia equations of section 2.7 are chosen for implementation, which eliminates the necessity of condensing rotational DOFs from the stiffness matrix. In the spin-up problem, all rigid body DOFs are prescribed. For the orbiter/RMS problem, a rigid body torque is prescribed while the remaining rigid body DOFs are constrained.

To facilitate discussion of the results to follow, equation (2.7.15) is rewritten below along with identification of terms appearing in the forcing vector associated with flexible translational DOFs.

$$\underset{(6N\times 1)}{\mathbf{R}_F} = \begin{bmatrix} \underline{f}_1 - m_1\underline{\omega}^{\times}\,\underline{u} - \overbrace{m_1\underline{\omega}^{\times}\,\underline{\omega}^{\times}\,\underline{r}_1}^{\text{centrifugal force}} - \overbrace{2m_1\underline{\omega}^{\times}\,\dot{\underline{q}}_{t1}}^{\text{Coriolis force}} + \text{h.o.t.} \\ \underline{t}_1 + \text{h.o.t.} \\ \vdots \\ \underline{f}_N - m_N\underline{\omega}^{\times}\,\underline{u} - m_N\underline{\omega}^{\times}\,\underline{\omega}^{\times}\,\underline{r}_N - 2m_N\underline{\omega}^{\times}\,\dot{\underline{q}}_{tN} + \text{h.o.t.} \\ \underline{t}_N + \text{h.o.t.} \end{bmatrix} \qquad (5.1.1)$$

Note that the relative displacements $\underline{q}_{ti}$ are omitted from the centrifugal force term. It is assumed that flexible deformations are small

so that vehicle geometry is adequately represented by the undeformed, or original configuration. For the dynamics problems considered, the undeformed configuration is the reference configuration. This implies that the rigid/flex coupling matrix given by equation (2.7.12) is constant and need be determined only once in the original configuration. Also, the instantaneous vehicle inertia appearing in the M_{RR} matrix is constant and need be computed only once in the original configuration.

5.1.2 Incremental Solution

The equations of motion (2.7.7) are well suited for solution by the second order Newmark integration scheme. Derivation of Newmark integration for linear systems is outlined in Appendix B, as well as an incremental form which is required for the solution of nonlinear equations. The incremental form with modified Newton-Raphson iteration has been implemented in the dynamic simulation.

From equation (B.2.10), note that the incremental solution algorithm requires calculation of a nodal force vector corresponding to the state of internal stress. For the finite element discretization of stiffness, the internal force vector is given by

$$F_{int} = \int_x \underline{B}^T \sigma \, dx \tag{5.1.2}$$

where

$\underline{B}$ = strain-displacement matrix encountered in chapter 3 ($\underline{\varepsilon} = \underline{B}\,\underline{q}$)

σ = vector of stress resultants

Assuming material linearity, the stress resultants can be found using equation (A.7).

5.1.3 Computer Implementation

The computer implementation of the dynamics formulation noted above proceeds as shown in figure 5.1. For all problems the integration step size used was $\Delta t = 0.01$, and the convergence criteria used was

$$\|\Delta \mathbf{U}^k\| \leq \text{tolerance} \tag{5.1.3}$$

where $\Delta \mathbf{U}^k$ is the vector of incremental displacements corresponding to the kth iteration (see Appendix B). Thus the solution is converged when the norm of $\Delta \mathbf{U}^k$ is less than some tolerance. The displacement tolerance for both dynamic problems was equal to 0.000001.

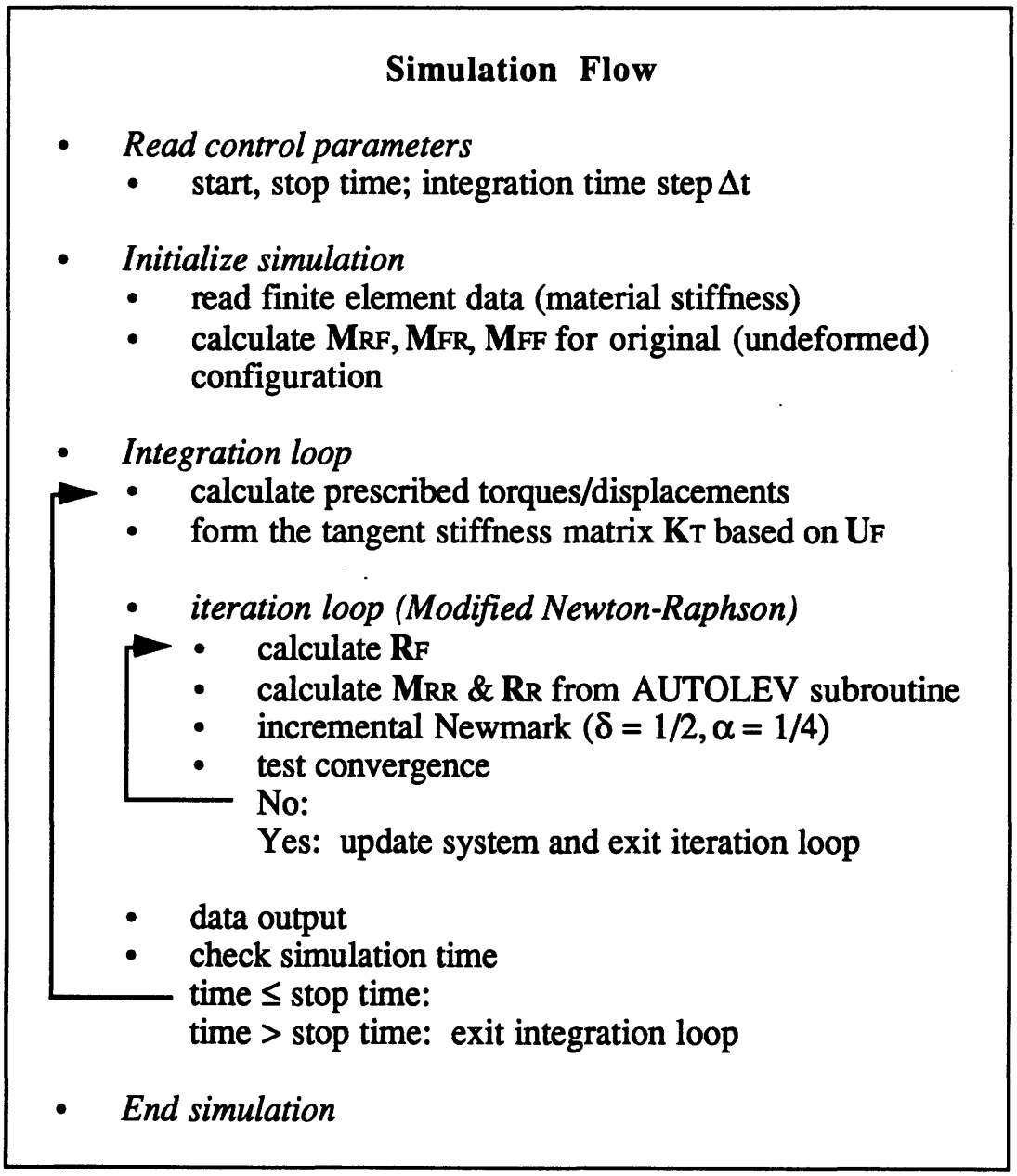

Figure 5.1. Flow diagram for dynamic simulations.

5.2 Spin-Up Problem

5.2.1 Problem Description

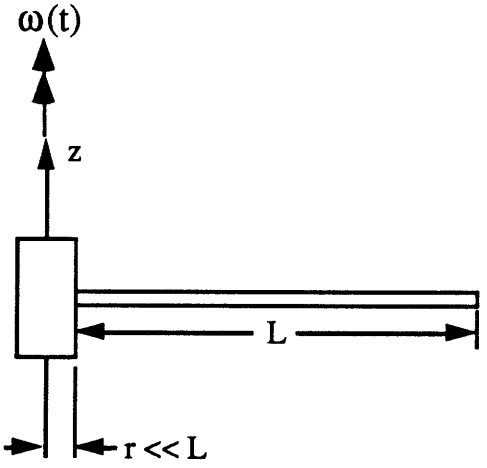

Figure 5.2. Spin-up of cantilever beam.

Schematic of the physical problem is shown in figure 5.2. A rigid central body has a rigidly attached flexible beam. The hub radius is small compared with the length of the beam and may be ignored. The central body is constrained against translation, while hub rotation is a prescribed function of time, equation (5.2.1) specifying a smooth transition from zero hub motion to constant angular speed of 6 rad/sec. The prescribed rotation is also shown graphically in figure 5.3.

$$\omega(t) = \begin{cases} 0.4\left[t - (7.5/\pi)\sin(\pi t/7.5)\right] \text{ rad/sec} & 0 < t < 15 \text{ sec} \\ 6 \text{ rad/sec} & 15 < t < 30 \text{ sec} \end{cases} \qquad (5.2.1)$$

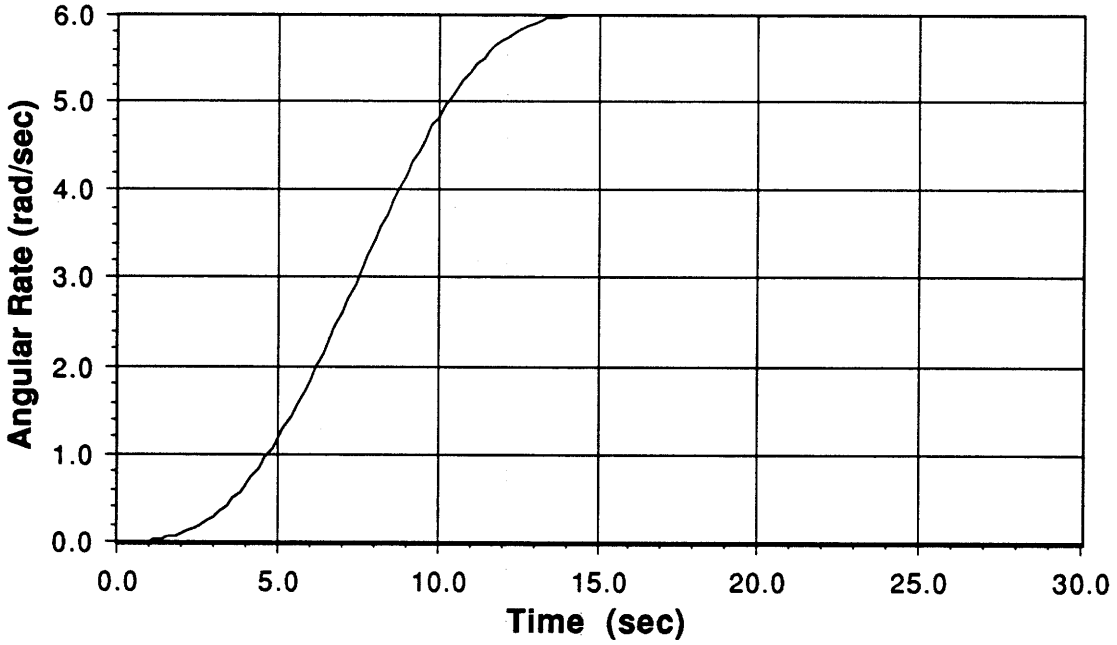

Figure 5.3. Hub motion prescribed by equation (5.2.1).

5.2.2 Finite Element Model

The beam has uniform cross-section and is discretized using uniformly sized C^0 finite elements. Both material and geometric stiffness matrices are evaluated by reduced integration to avoid shear locking. Material properties are chosen to correspond with previously published results, and are given in table 5.1. (k is the shear correction factor, ρ is the per volume density).

Table 5.1. Beam material properties for spin-up problem.

E	7×10^{10}
k	1/1.2
ν	1/6
ρ	1.2
L	10
area	4×10^{-4}
I	2×10^{-7}
I_m	6×10^{-4}

A schematic of the finite element model in the undeformed (reference) configuration is shown in figure 5.4. The body fixed frame is coincident with the rigid central body. Flexible mass distribution is treated using the lumped mass/inertia assumption. Note that the vehicle c.m. in figure 5.4 has only one nonzero component in the body fixed frame. Lumped masses are equally spaced along the length of the beam.

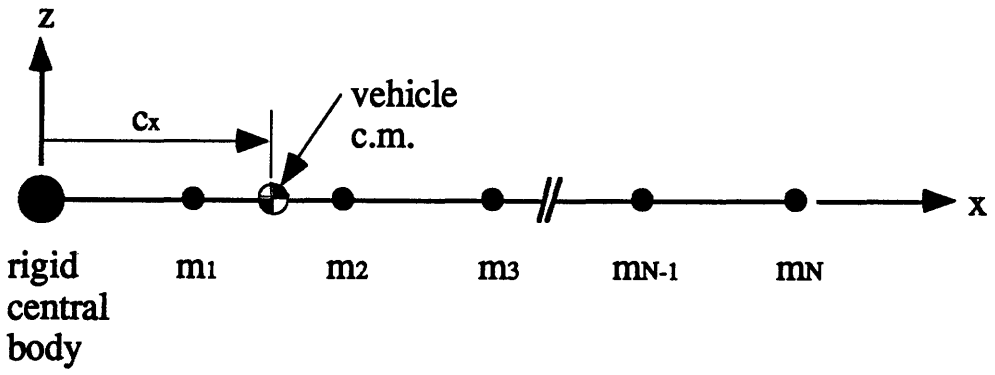

Figure 5.4. Schematic of finite element model, analogous to figure 2.1.

5.2.3 Spin-Up Results & Discussion

The study of the spin-up problem is accomplished through consideration of the following cases:

1) full solution – including all forcing terms, geometric stiffness matrix, incremental integration scheme (Newton-Raphson iteration)
2) neglect Coriolis forcing term
3) neglect centrifugal & Coriolis forcing terms
4) neglect geometric stiffness matrix

In all of the above cases, the effect of mesh refinement is also examined. The motion shown in the following figures corresponds to the axial and transverse displacements of the beam tip, relative to the body fixed frame. Transverse displacement is perpendicular to the axis of rotation.

Tip displacements for case 1 are shown in figures 5.5-5.12. The gross behavior is captured well by a course mesh, as seen in figures 5.5 and 5.6. Axial displacement appears to settle into a steady-state elongation at constant spin-rate. Increasing the number of elements brings out the detail of this motion, however, and it is seen that an oscillatory motion is superposed onto the steady-state deflection. Steady-state axial deflection converges from above; in other words, a course mesh overpredicts the axial deflection.

The transverse behavior of the beam is characterized by an increase in deflection until the midpoint of the spin-up (corresponding to the maximum angular acceleration), after which the tip catches up to the body fixed frame and oscillates about zero relative deflection. This behavior is also captured with a course mesh. Two tendencies are noted with respect

to mesh refinement: the peak deflection (absolute value) converges from above, and the steady state frequency associated with bending vibration converges from below. For future reference, case 1 is summarized in table 5.2.

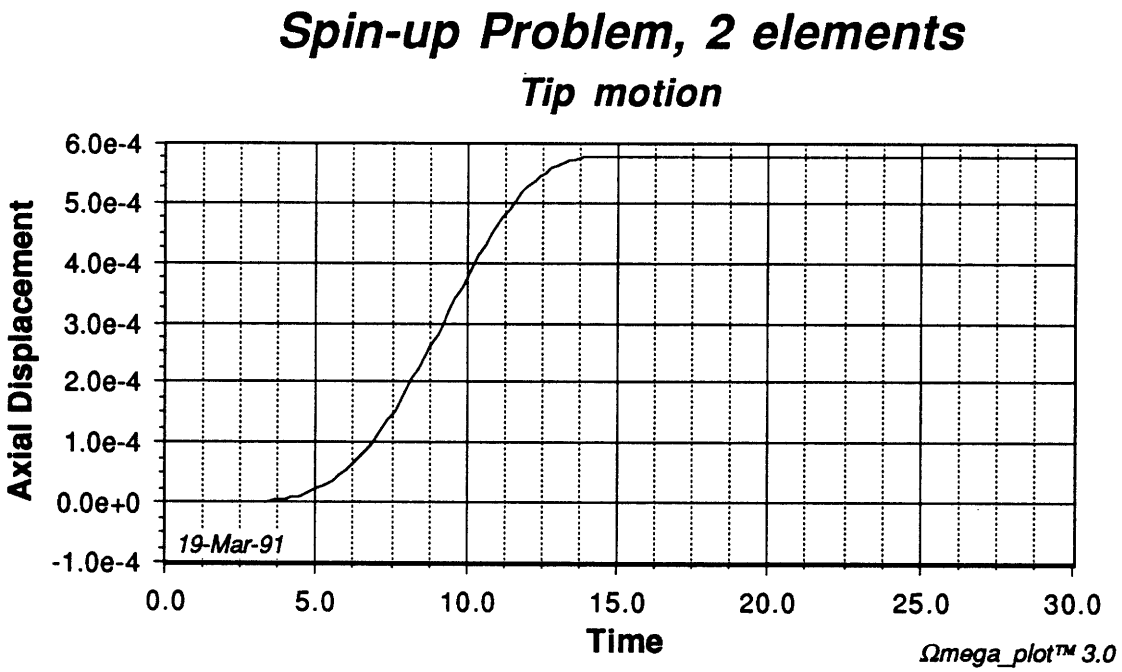

Figure 5.5. Axial displacement of beam tip for case 1, 2 elements.

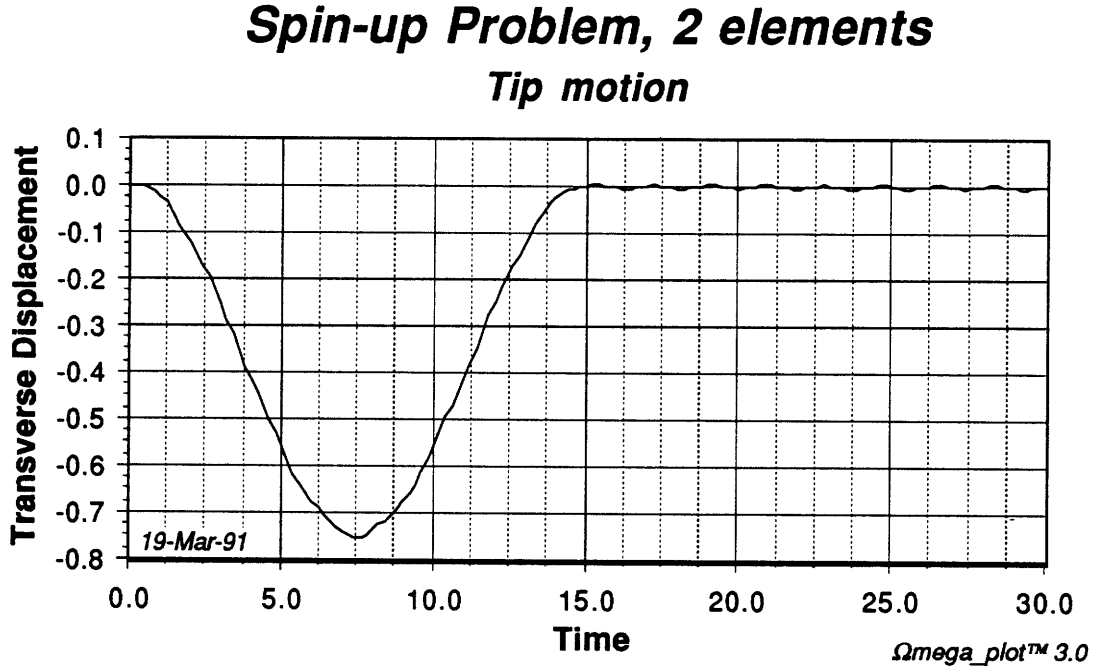

Figure 5.6. Transverse displacement of beam tip for case 1, 2 elements.

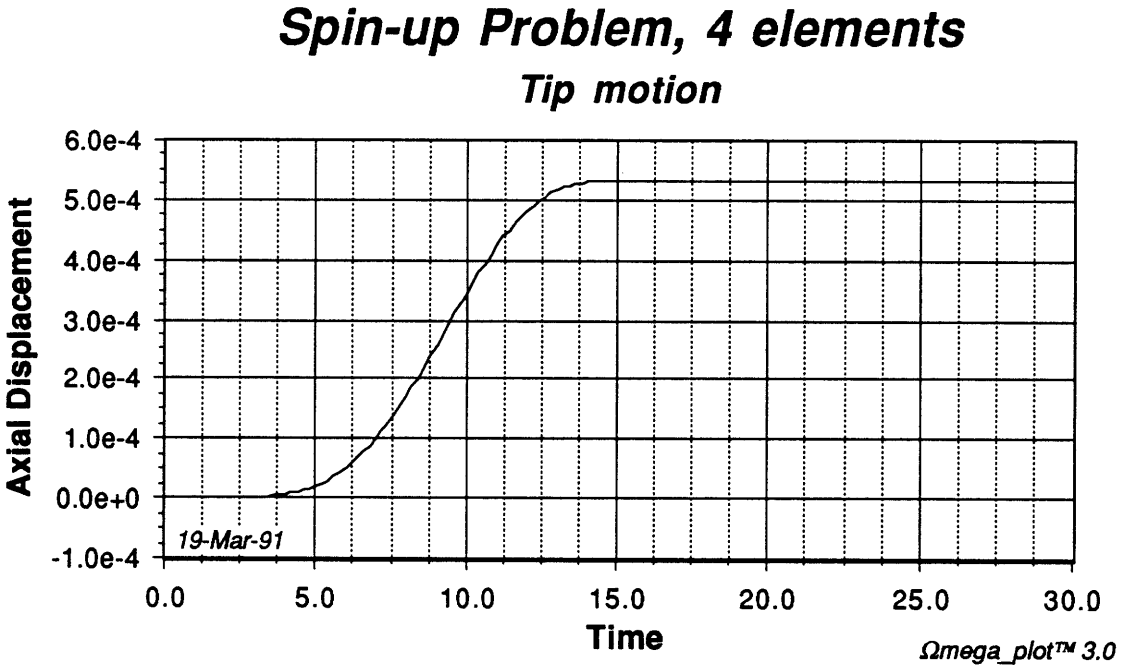

Figure 5.7. Axial displacement of beam tip for case 1, 4 elements.

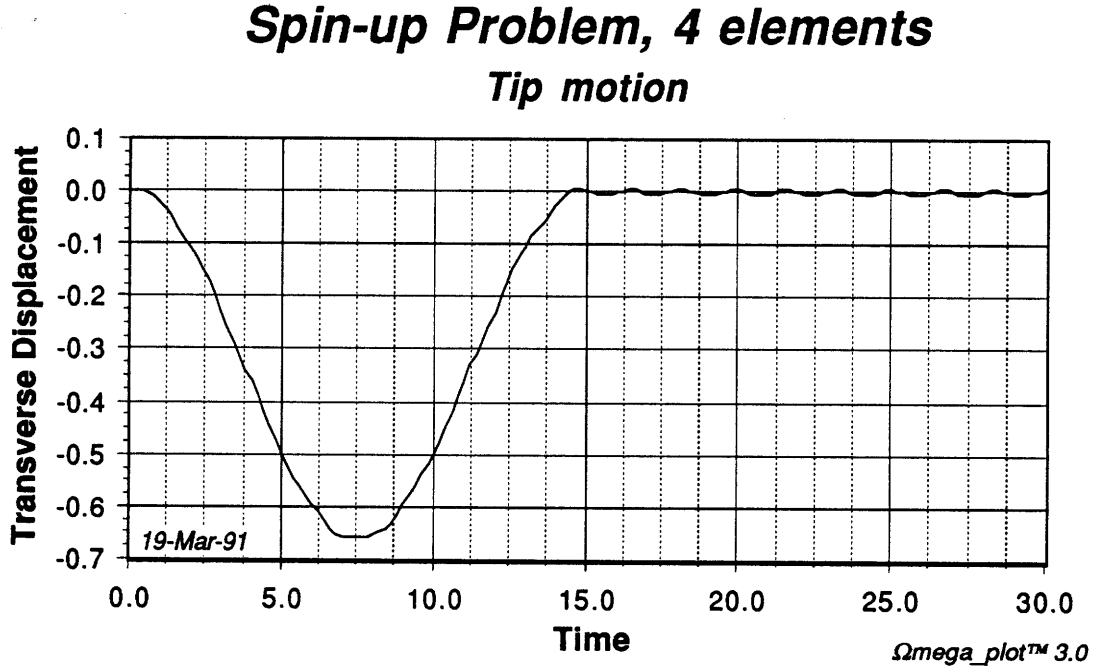

Figure 5.8. Transverse displacement of beam tip for case 1, 4 elements.

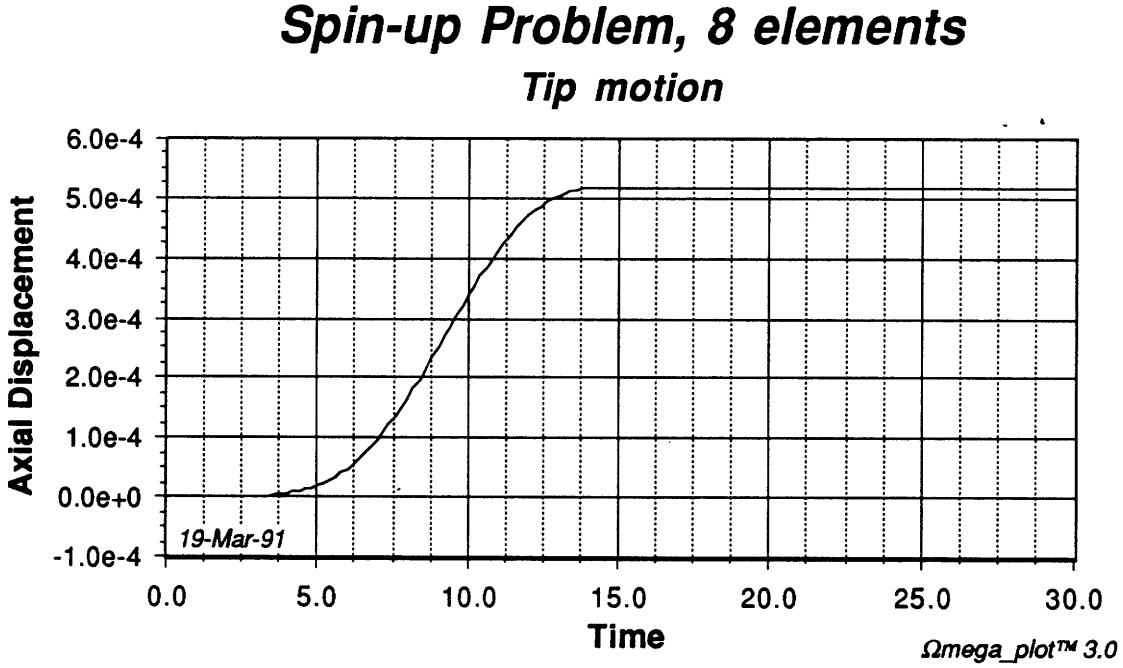

Figure 5.9. Axial displacement of beam tip for case 1, 8 elements.

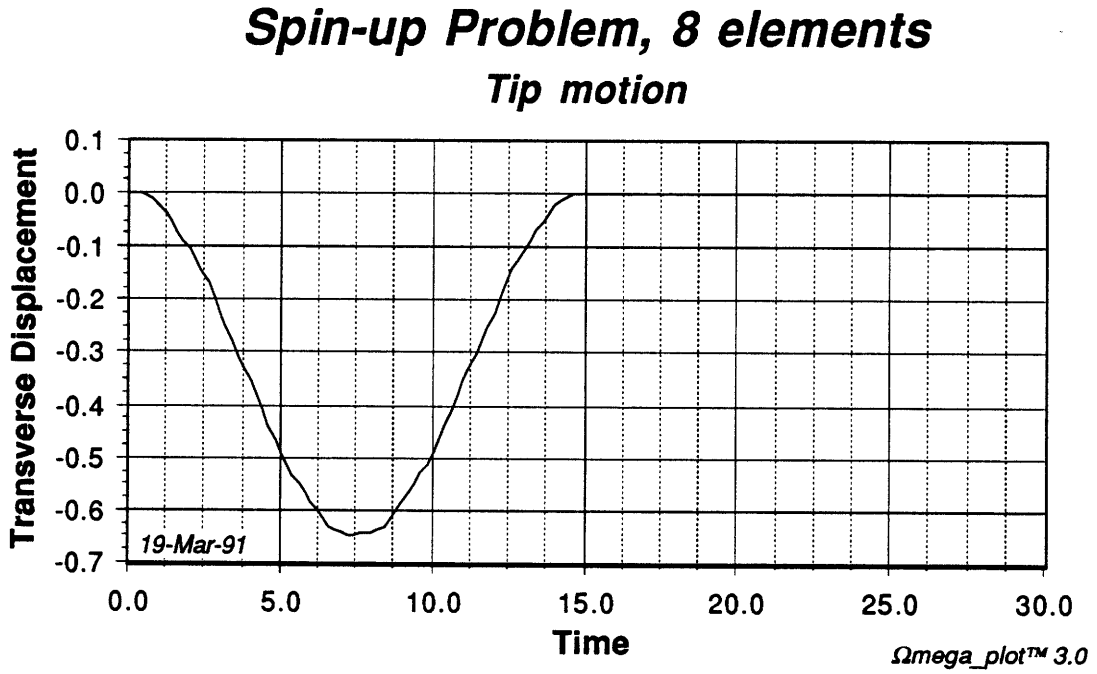

Figure 5.10. Transverse displacement of beam tip for case 1, 8 elements.

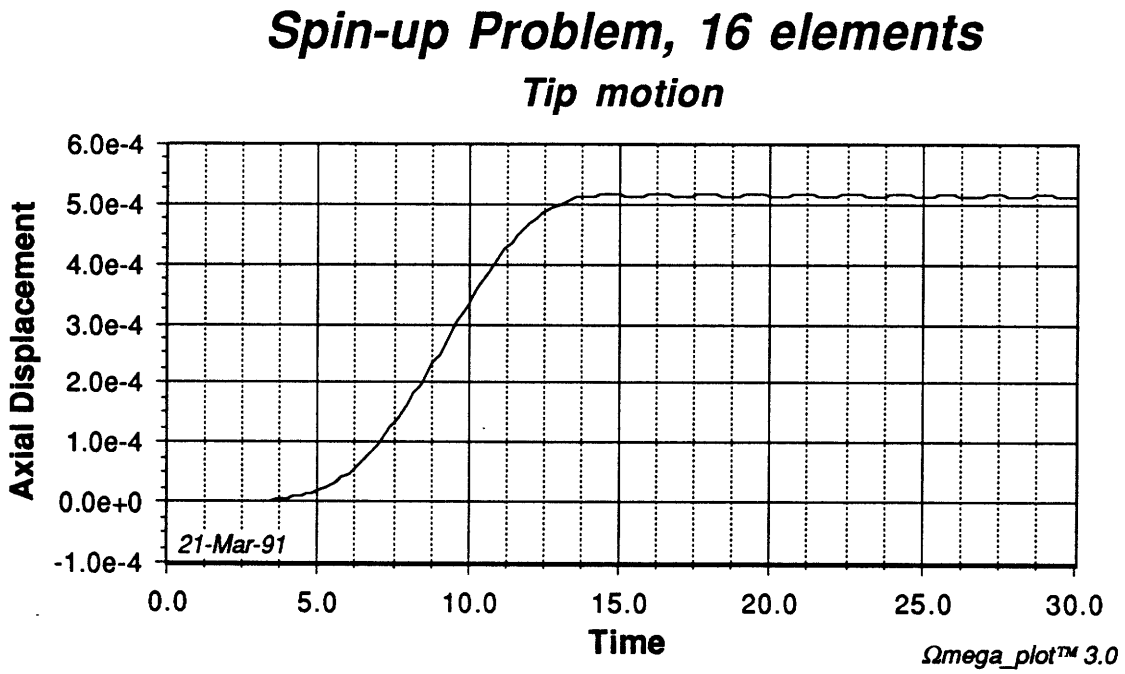

Figure 5.11. Axial displacement of beam tip for case 1, 16 elements.

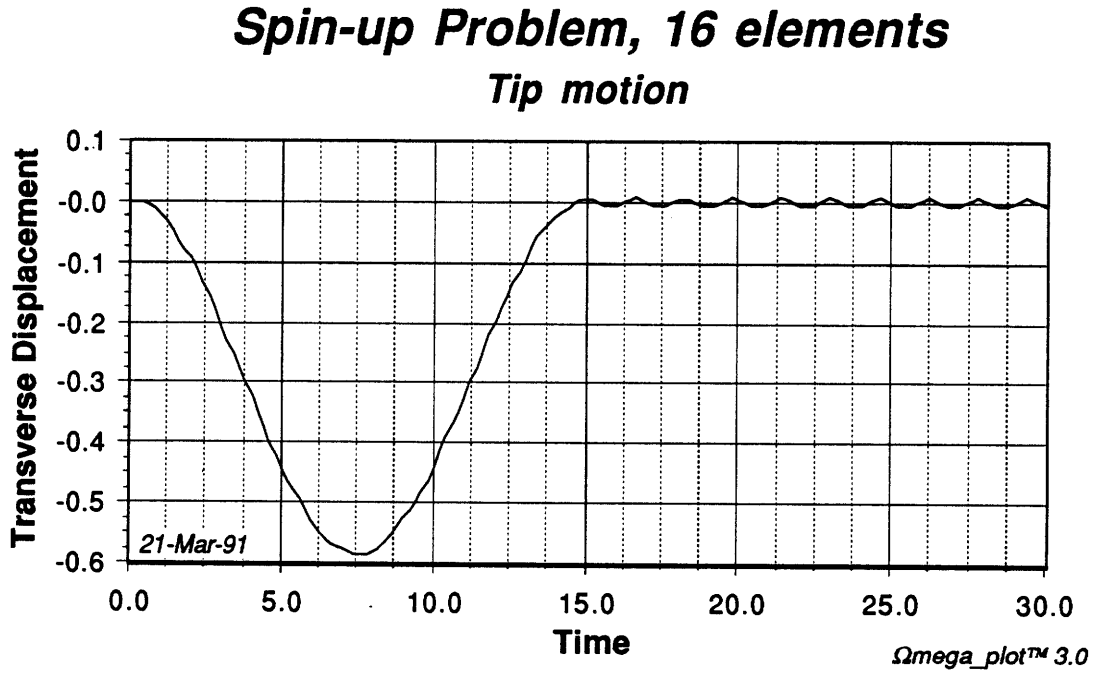

Figure 5.12. Transverse displacement of beam tip for case 1, 16 elements.

Table 5.2. Summary of spin-up problem, case 1.

# of elements	Peak transverse displacement	Steady-state axial displacement	Frequency, bending vibration (rad/sec)
2	- 0.753	5.78×10^{-4}	3.36
4	- 0.660	5.31×10^{-4}	3.56
8	- 0.646	5.18×10^{-4}	3.77
16	- 0.587	5.15×10^{-4}	3.94

The effect of neglecting the Coriolis forcing term is considered in case 2 and displayed in figures 5.13 & 5.14. One can see that the Coriolis term provides the excitation of the axial vibration mode; its removal produces a true steady-state axial elongation. The Coriolis term is not a major contributer to the transverse behavior of the beam (transverse displacements corresponding to figures 5.13 & 5.14 are the same as given for case 1 results).

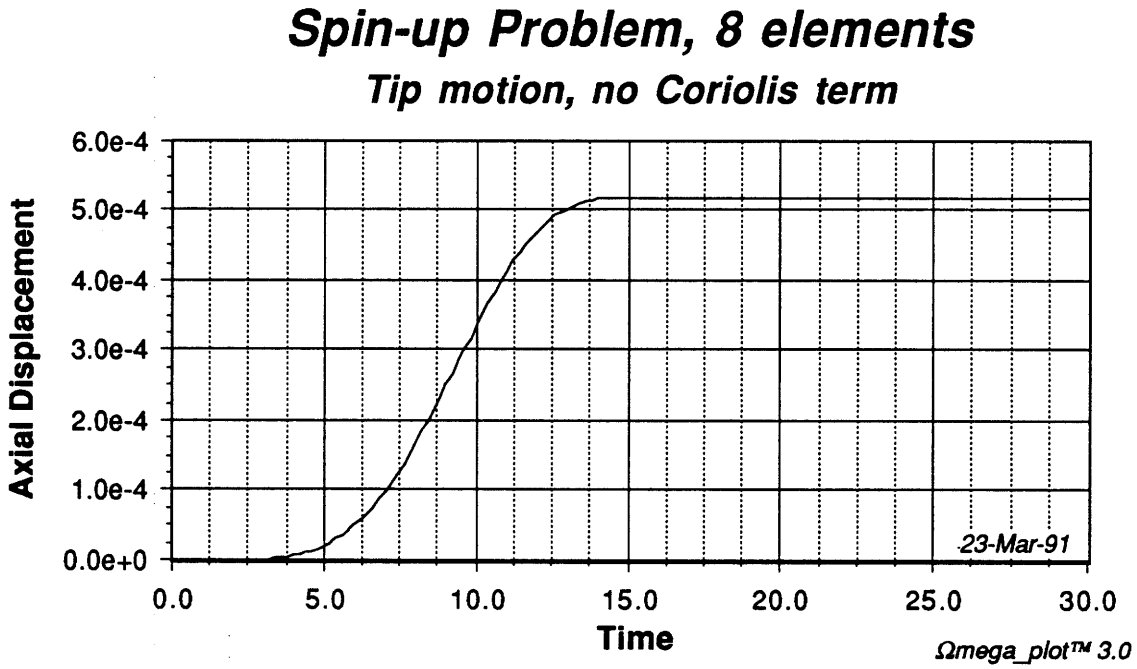

Figure 5.13. Axial displacement of beam tip for case 2, 8 elements.

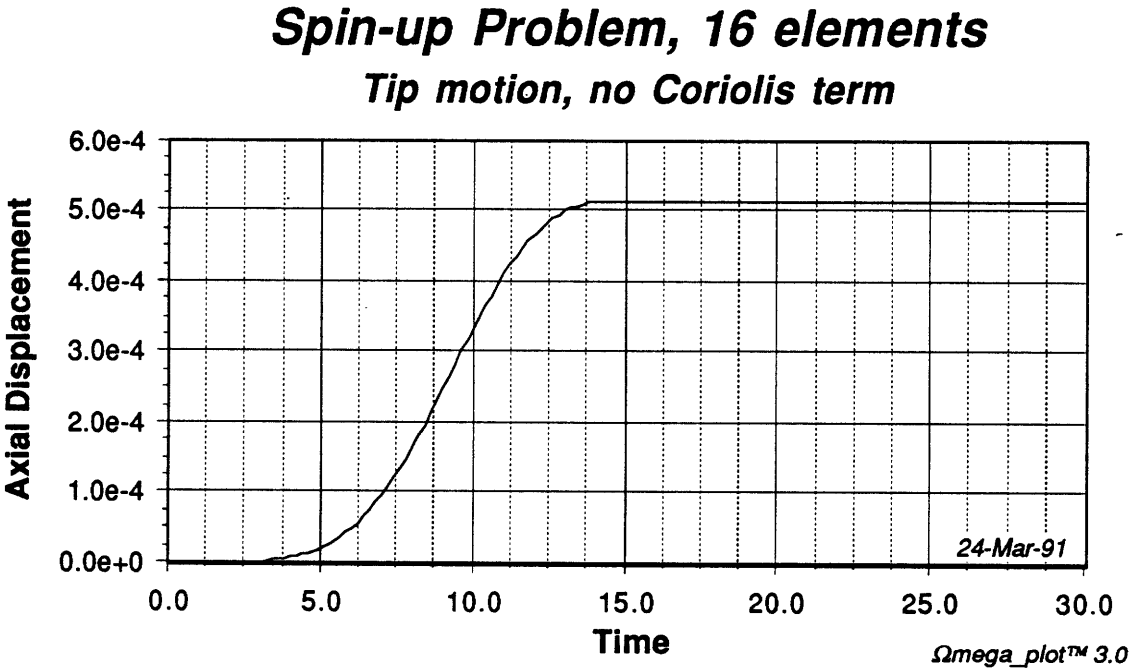

Figure 5.14. Axial displacement of beam tip for case 2, 16 elements.

Case 3 (no centrifugal or Coriolis forcing terms) results are shown in figures 5.15-5.18. Elimination of centrifugal forcing eliminates any axial elongation of the spinning beam. No other effect is observed. The transverse displacement is unaffected by the presence or absence of either centrifugal or Coriolis terms, as shown in the following figures.

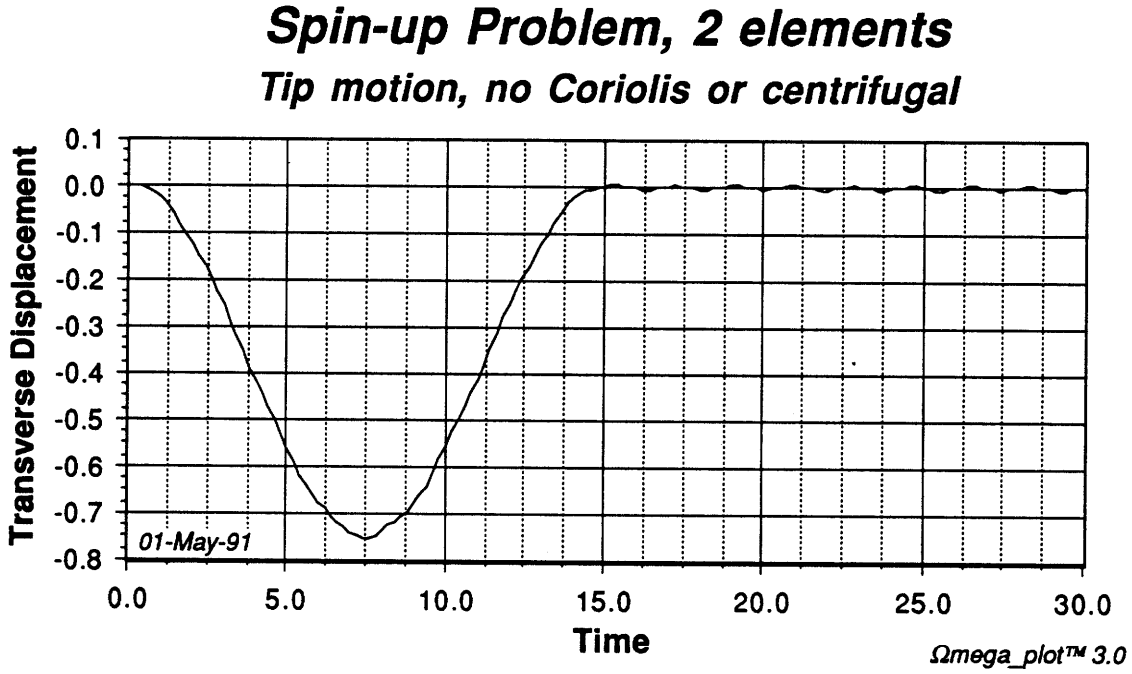

Figure 5.15. Transverse displacement of beam tip for case 3, 2 elements.

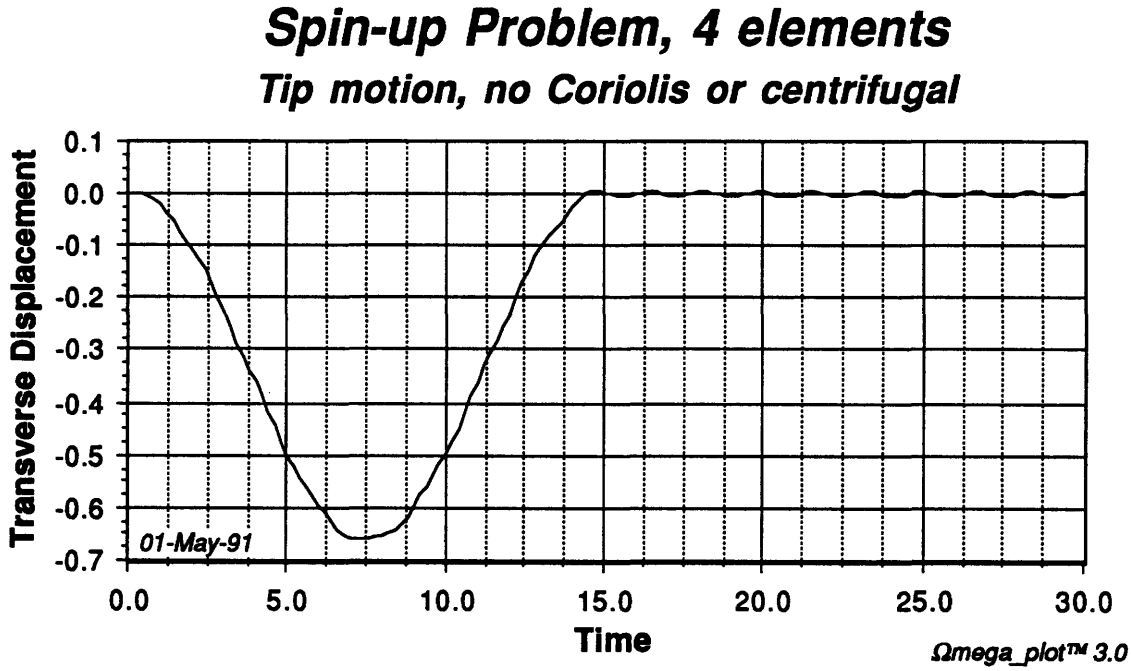

Figure 5.16. Transverse displacement of beam tip for case 3, 4 elements.

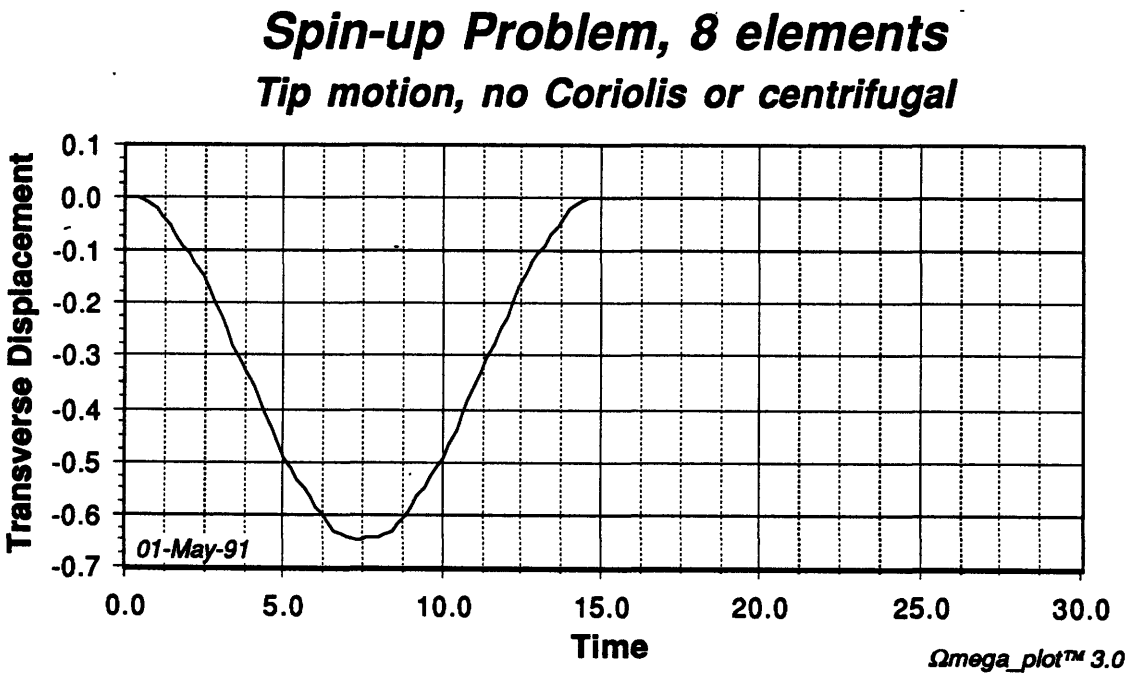

Figure 5.17. Transverse displacement of beam tip for case 3, 8 elements.

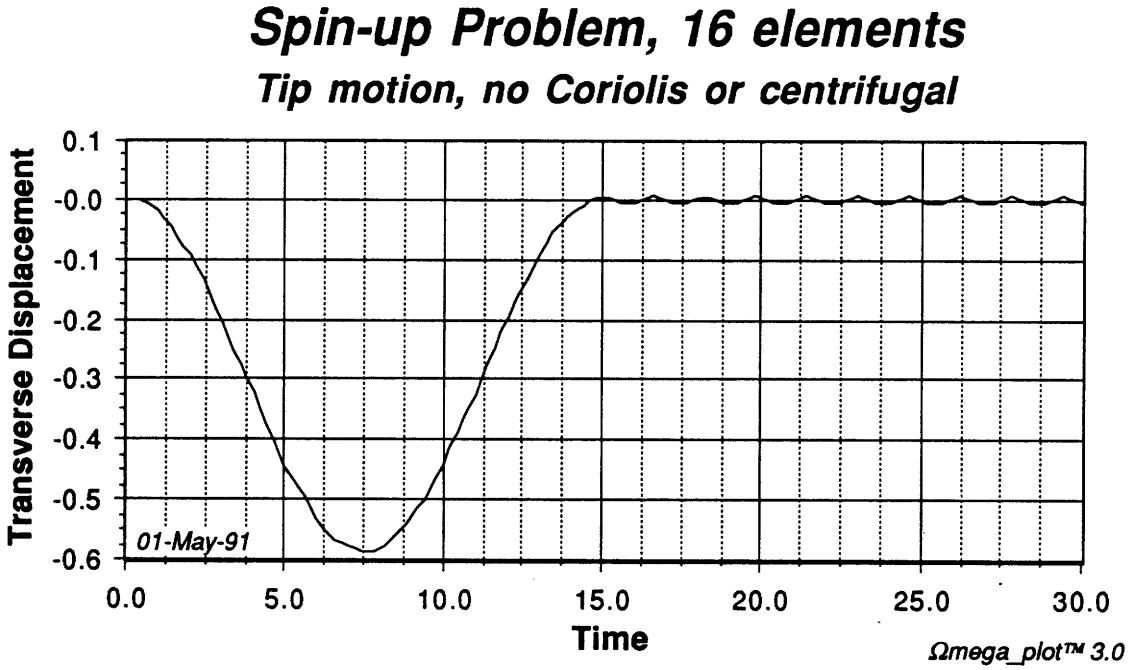

Figure 5.18. Transverse displacement of beam tip for case 3, 16 elements.

Solution of the spin-up problem in the absence of the geometric stiffness matrix (case 4) gives a surprising result. It is interesting that the geometric stiffness matrix apparently has no effect on the solution of the spin-up problem. The formulation as implemented has no dependence on geometric nonlinearity; material stiffness is sufficient to prevent divergent behavior. Different modelling assumptions and solution techniques lead to dynamic instability. Using assumed modes formulations, Ryan [13] and Ider & Amirouche [16] report divergent transverse displacements when geometric stiffening effects are ignored. Simo & Vu-Quoc [15], on the other hand, do not discuss any divergent behavior encountered with their finite element solution.

5.3 Orbiter/Remote Manipulator Arm (RMS)

5.3.1 Problem Description

As a realistic application of the dynamic formulation, an additional example is considered which involves the space shuttle remote manipulator system (RMS). The manipulator arm is assumed to be locked in a fully extended configuration with a typical payload attached to the end effector. The shuttle is constrained against translational and rotation, except for rotation about the body fixed y axis. Orbiter rotation is induced by application of positive/negative pulse torque, shown graphically in figure 5.19. The torque acts about the y axis of figure 5.20 so that the elbow is in the plane of rotation. Angular displacement of the orbiter in response to the torque is heavily influenced by the relative size of the inertias of the shuttle and the flexible (appendage + payload) combination.

Motions are assumed to be small, thus the reference configuration is always taken to be the original configuration.

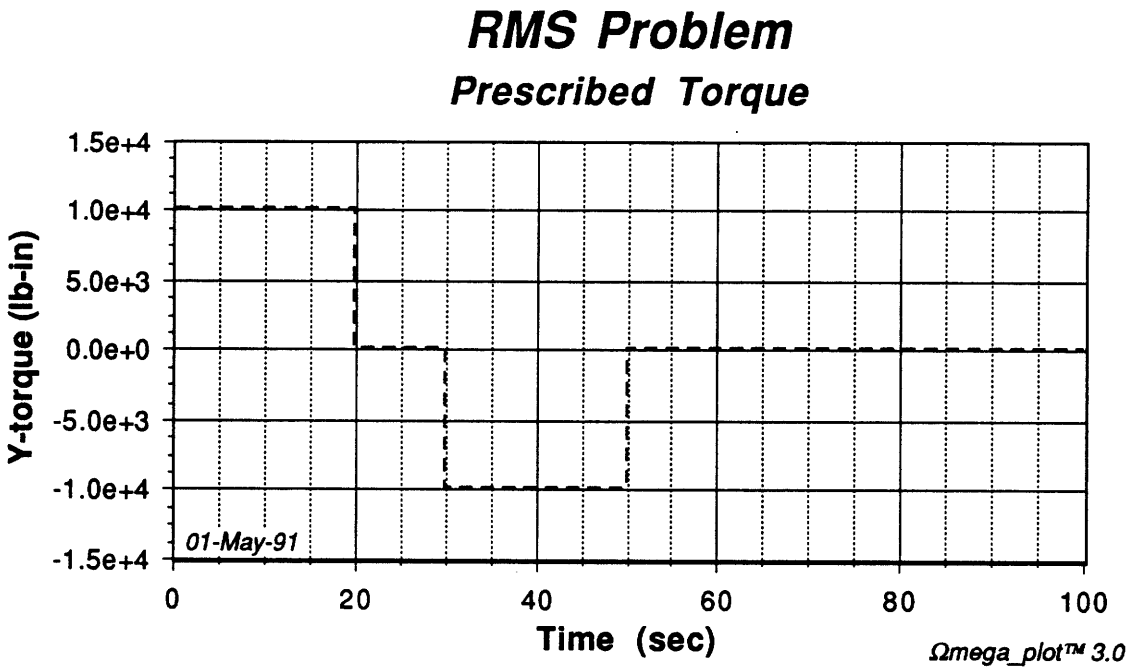

Figure 5.19. Torque time history applied to orbiter.

5.3.2 Finite Element Model

The finite element representation of this system is shown in figure 5.20, where the shuttle c.m. is located at node 1 and payload/end effector are located at node 16. The orbiter and payload are modelled by lumping mass and inertia at their respective nodes, values used are given below. The body fixed frame is coincident with the orbiter c.m. Fifteen elements are used to model the manipulator, which can be numbered consecutively starting from node 1. The finite element model of the remote manipulator arm was extracted and simplified from a NASTRAN model (in-house Draper model) The details of the finite element model are provided in Appendix D.

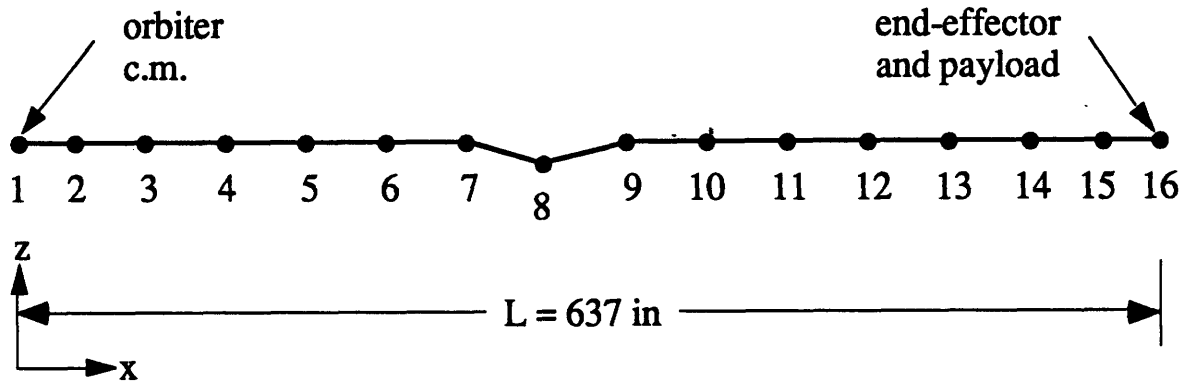

Figure 5.20. Finite element model of remote manipulator arm in straight out position.

$m_{orbiter} = 6397$ slugs

$m_{payload} = 665$ slugs

$$I_{orbiter} = \begin{bmatrix} 1044 & & \\ & 134 & \\ & & 1003.7 \end{bmatrix} x10^6 \text{ slug} \cdot \text{in}^2$$

$$I_{payload} = \begin{bmatrix} 10.4 & & \\ & 10.4 & \\ & & 3.469 \end{bmatrix} x10^6 \text{ slug} \cdot \text{in}^2$$

5.3.3 Orbiter/RMS Results

Orbiter response is obtained assuming a rigid vehicle to provide a baseline for the flexible solution, and provide a greater sense that the flexible solution is correct. The flexible response should (and does) oscillate about the rigid solution.

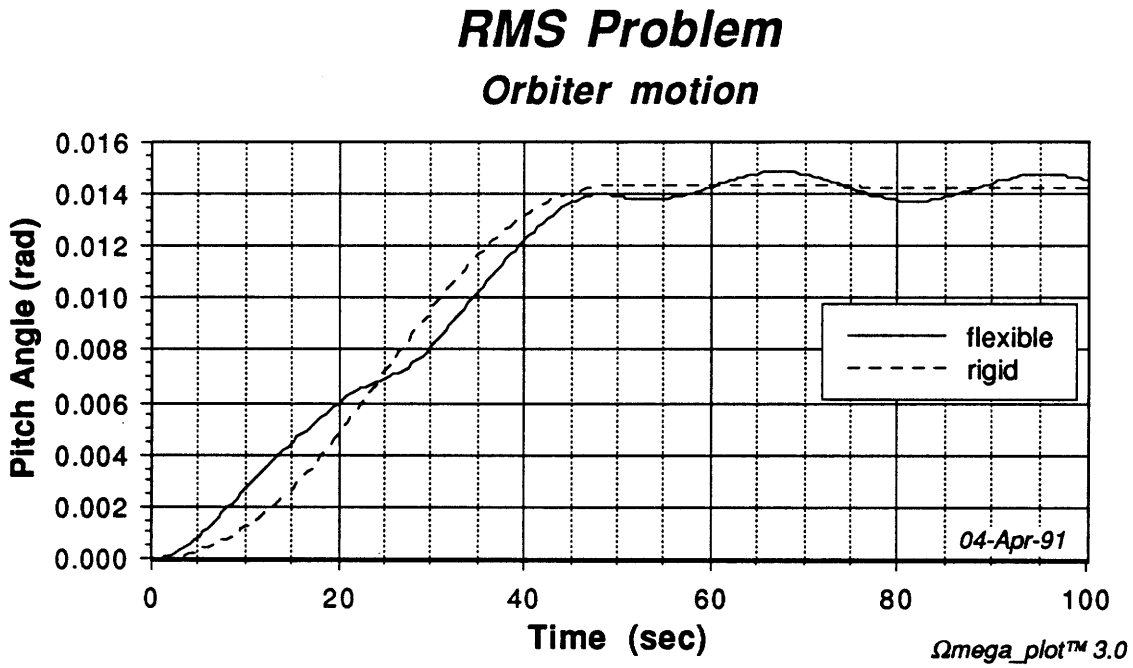

Figure 5.21. Orbiter response to pulse torque, assuming rigid and flexible.

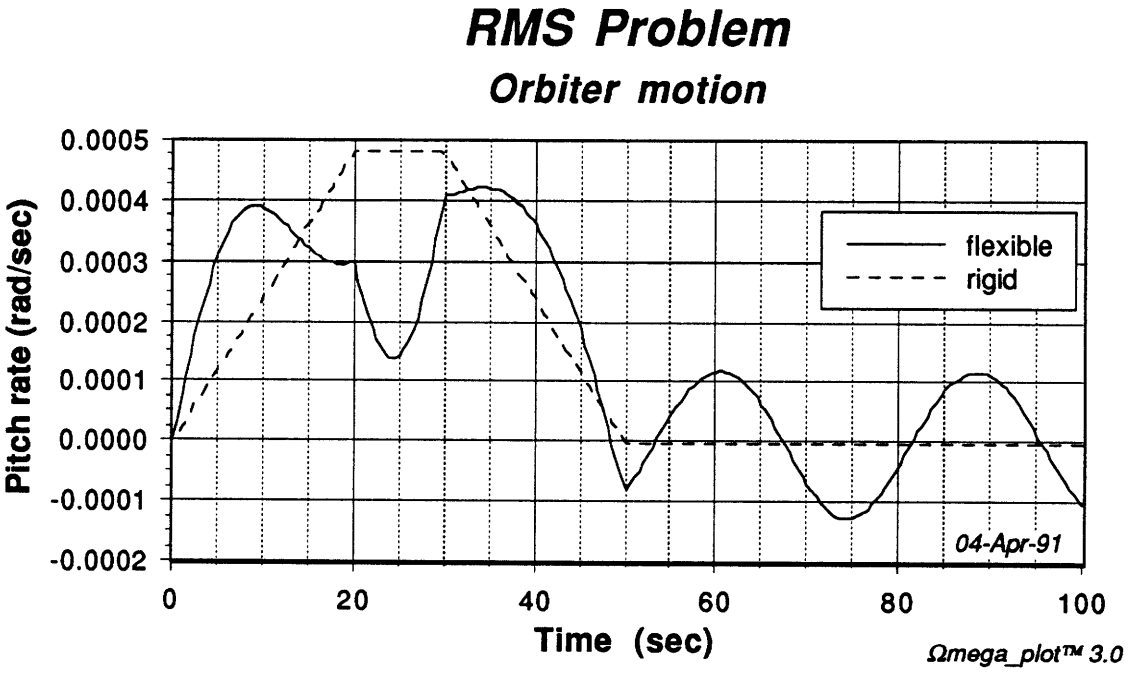

Figure 5.22. Orbiter response to pulse torque, assuming rigid and flexible.

The relative motion of the payload/end effector, in the body fixed frame, is shown in figures 5.23 & 5.24. It is seen that moderate torque input results in payload deflections on the order of 1.5 inches. This may be significant in the context of assembling space station components. Axial displacements are not large. The phase plane shown in figure 5.25 demonstrates the periodic oscillation experienced by the payload after the torques are released.

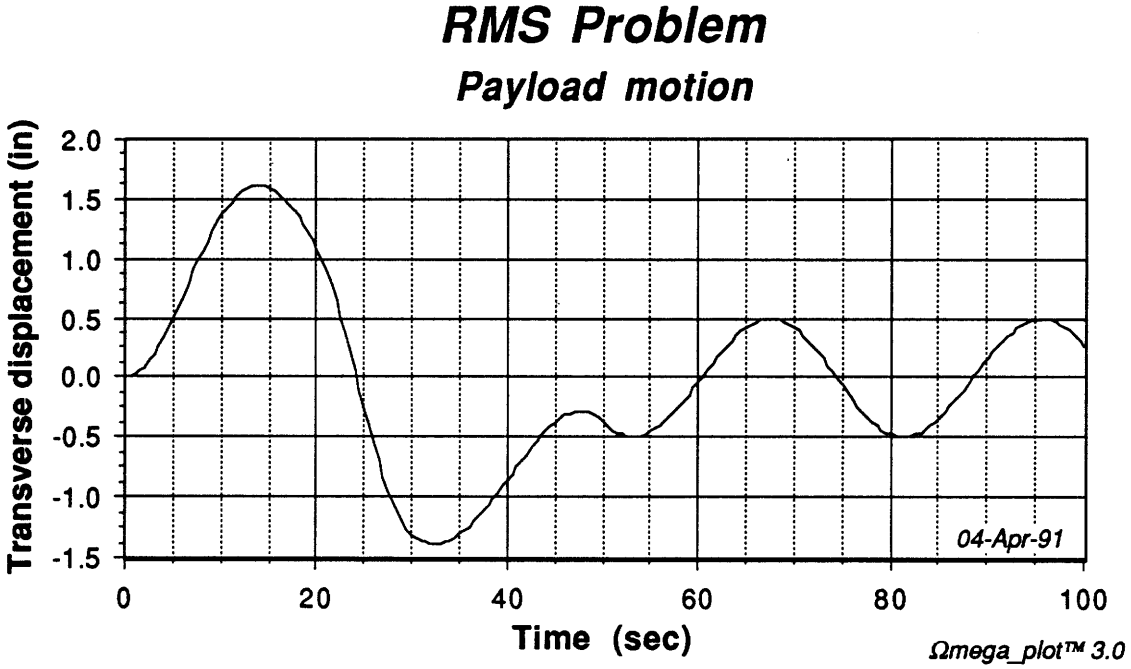

Figure 5.23. End effector response to pulse torque.

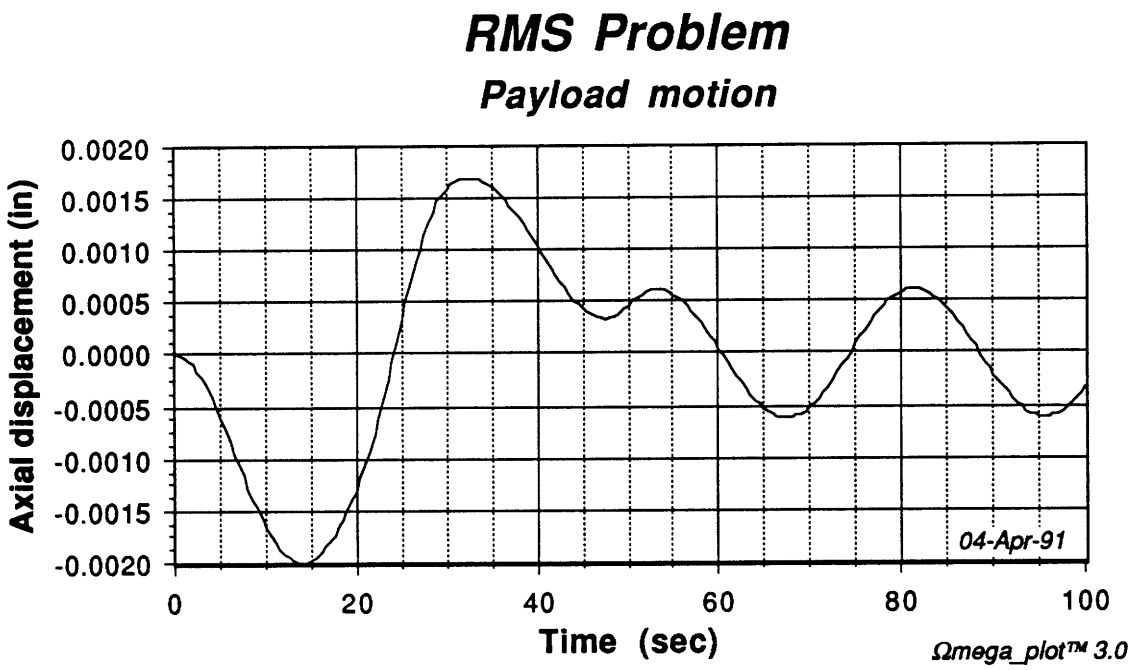

Figure 5.24. End effector response to pulse torque.

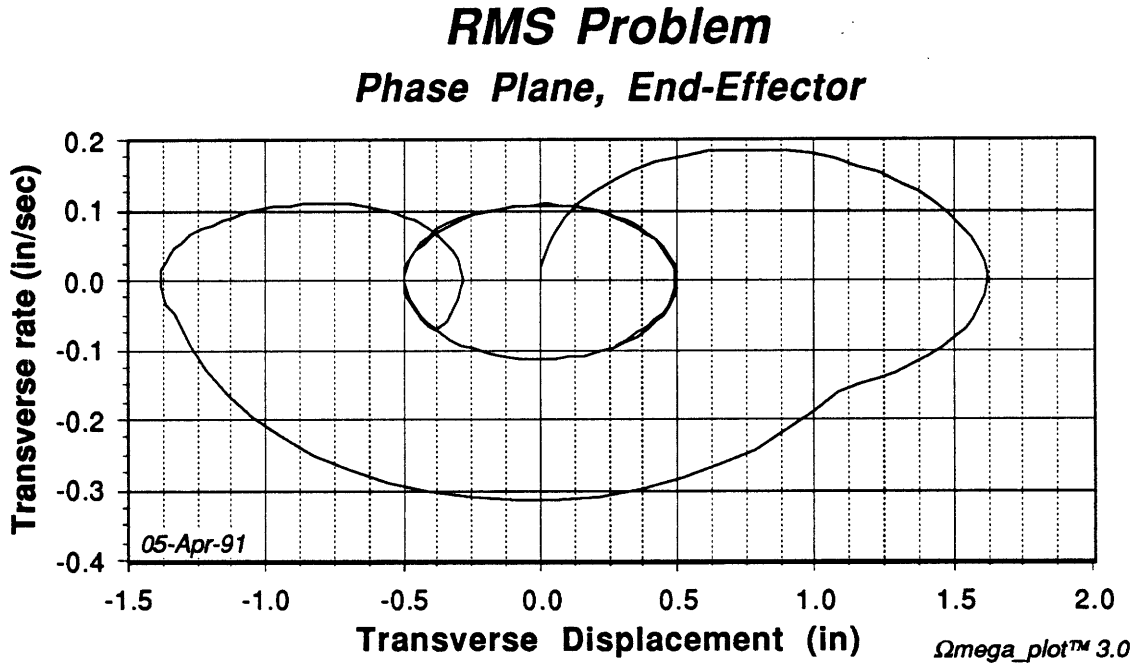

Figure 5.25. Demonstration of periodicity of tip motion (zero damping).

Chapter 6
Conclusion

6.1 Summary and Conclusions

Equations of motion have been consistently derived for a rigid body with attached flexible appendage through application of the virtual work principle. This method allowed a natural and consistent introduction of a finite element discretization for the flexible appendage. Using the assumptions of lumped mass and lumped mass/inertia allowed comparison between the two resulting formulations. The lumped mass formulation required condensing the rotational DOFs from the stiffness matrix.

The nonlinear finite elements used in conjunction with the dynamic equations were consistently derived from the virtual work principle. The consistent derivation using Bernoulli-Euler kinematics lead to a finite element formulation of Rayleigh beam theory. Bernoulli-Euler beam element was recovered by setting the rotatory inertias to zero. All higher order terms were retained in the derivation of the geometric stiffness matrix, which lead to the introduction of higher order stress resultants. Implementation of these elements allowed greater flexibility than was possible with other commercially available finite element codes. This flexibility was exploited in the study of finite element approximations and kinematic assumptions.

Assessment of element behavior was accomplished through eigenvalue problems. The numerous figures generated from the

implementation of the consistently derived finite elements allowed isolation of individual effects such as lumped mass, rotatory inertia, and reduced integration. Some general conclusions are drawn from the results:

- reduced integration of the stiffness matrix in C^0 elements alleviates the problem of shear locking
- lumped mass assumption lowers vibration frequencies
- shear and rotatory inertia lowers the vibration frequencies
- shear and rotatory inertia become increasingly important in higher modes of vibration (as wavelength/thickness decreases)
- shear generally has larger effect upon frequency compared to rotatory inertia
- higher order stress resultants present in the geometric stiffness matrix lower buckling loads

In realistic dynamic analyses, the necessity of using an element with shear and rotatory inertia was shown to be related to the wavelength/thickness ratio. If the vibration modes of interest have large wavelength/thickness ratio, these effects can be neglected.

The lumped mass/inertia equations of motion were employed in the solution of two example problems. In the spin-up problem, the effects of forcing terms and nonlinear flexibility on the solution were systematically addressed. It was shown that the centrifugal term had the effect of producing a steady-state elongation of the beam. The Coriolis term was responsible for the axial oscillations superposed on the steady-state deflection. In the formulation used to solve the spin-up problem, the material stiffness matrix was sufficient to prevent divergent behavior.

In both dynamics problems, the assumption of small flexible displacements was employed, so that the original configuration was the reference configuration. The formulation as presented can be extended to systems undergoing large flexible displacements by updating the configuration. Flexible translations and rotations are referred to the current configuration.

6.2 Future Work

Recommended future work includes full implementation of the rigid/flexible appendage formulation to include configuration updates, allowing solution of problems involving large displacements and rotations of the flexible appendage. This involves updating nodal locations, material and geometric stiffness, vehicle inertia, etc., at each time integration step. Flexible displacements and rotations are referred to the current configuration. Solution of the 'spaghetti' problem, for instance, serves as full demonstration of the equations of motion of chapter 2.

The virtual work principle can be used to derive the governing equations for rigid bodies with articulated flexible appendages [28], and flexible bodies connected to flexible bodies. These formulations have wider application to spacecraft, space structures, and robotics than does the present formulation.

Further study is necessary for complete understanding of the influence of geometric nonlinearities. Investigation should be conducted into the assumed modes formulation with parallel development of finite

element formulation. Systematic study of this type should resolve the question that has arisen regarding the geometric stiffness in the solution of dynamic problems.

References

1. Rayleigh, J.W.S., *The Theory of Sound,* 2nd Ed., Dover Publications, Inc., Mineola, NY, 1945.

2. Timoshenko, S.P., "On the Correction for Shear of the Differential Equation for Transverse Vibrations of Prismatic Bars," *Philosophical Magazine,* Vol. 41, 1921, pp. 744-746.

3. Timoshenko, S.P., "On the Transverse Vibrations of Bars of Uniform Cross-Section," *Philosophical Magazine,* Vol. 43, 1922, pp. 125-131.

4. Huang, T.C., "The Effect of Rotatory Inertia and of Shear Deformation on the Frequency and Normal Mode Equations of Uniform Beams With Simple End Conditions," *Journal of Applied Mechanics,* Vol. 28, 1961, pp. 579-584.

5. Leckie, F.A., and Lindberg, G.M., "The Effect of Lumped Parameters on Beam Frequencies," *The Aeronautical Quarterly,* Vol. 14, 1963, pp. 224-240.

6. Nickel, R.E., and Secor, G.A., "Convergence of Consistently Derived Timoshenko Beam Finite Elements," *International Journal for Numerical Methods in Engineering,* Vol. 5, 1972, pp. 243-253.

7. Thomas, D.L., Wilson, J.M., and Wilson, R.R., "Timoshenko Beam Finite Elements," *Journal of Sound and Vibration,* Vol. 31, No. 3, 1973, pp. 315-330.

8. Thomas, J., and Abbas, B.A.H., "Finite Element Model for Dynamic Analysis of Timoshenko Beam," *Journal of Sound and Vibration,* Vol. 41, No. 3, 1975, pp. 291-299.

9. Hughes, T.J.R., Taylor, R.L., and Kanoknukulchai, W., "A Simple and Efficient Finite Element for Plate Bending," *International Journal for Numerical Methods in Engineering,* Vol. 11, 1977, pp. 1529-1543.

10. Mello, F.J., "Weak Formulations in Analytical Dynamics, with Applications to Multi-Rigid-Body Systems, Using Time Finite Elements," Ph.D. Thesis, Georgia Institute of Technology, December 1989.

11. Han, R.P.S., and Zhao, Z.C., "Dynamics of General Flexible Multibody Systems," *International Journal for Numerical Methods in Engineering,* Vol. 30, 1990, pp. 77-97.

12. Ibrahim, A.M., "Mathematical Modelling of Flexible Multibody Dynamics with Application to Orbiting Systems," Ph.D. Thesis, The University of British Columbia, April 1988.

13. Ryan, R.R., "Flexibility Modeling Methods in Multibody Dynamics," Ph.D. Dissertation, Stanford University, January 1986.

14. Simo, J.C. and Vu-Quoc, L., "On the Dynamics of Flexible Beams Under Large Overall Motions-The Plane Case: Part I," *Journal of Applied Mechanics,* Vol. 53, December 1986, pp. 849-854.

15. Simo, J.C. and Vu-Quoc, L., "On the Dynamics of Flexible Beams Under Large Overall Motions-The Plane Case: Part II," *Journal of Applied Mechanics,* Vol. 53, December 1986, pp. 855-863.

16. Ider, S.K., and Amirouche, F.M.L., "Influence of Geometric Nonlinearities in the Dynamics of Flexible Treelike Structures," *Journal of Guidance, Control, and Dynamics,* Vol. 12, No. 6, 1988, pp. 830-837.

17. Silverberg, L.M., and Park, S., "Interactions Between Rigid-Body and Flexible-Body Motions in Maneuvering Spacecraft," *Journal of Guidance, Control, and Dynamics,* Vol. 13, No. 1, 1990, pp. 73-81.

18. Christensen, E.R., and Lee, S.W., "Nonlinear Finite Element Modeling of the Dynamics of Unrestrained Flexible Structures," *Computers and Structures,* Vol. 23, No. 6, 1986, pp. 819-829.

19. Likins, P.W., "Analytical Dynamics and Nonrigid Spacecraft Simulation," Jet Propulsion Laboratory, Technical Report 32-1593, California Institute of Technology, 1974.

20. Park, K.C., "Flexible Beam Dynamics For Space Structures: - Formulation," Technical Report CU-CSSC-87-03, Appendix C, Center for Space Structures and Controls, May 1987.

21. Hughes, P.C., *Spacecraft Attitude Dynamics,* John Wiley & Sons, New York, NY, 1986.

22. Storch, J., and Gates, S., "Equations of Motion for a Flexible Spacecraft - Lumped Parameter Idealization," Technical Report CSDL-R-1582, Charles Stark Draper Laboratory, 1982.

23. Cook, R.D., Malkus, D.S., and Plesha, M.E., *Concepts and Applications of Finite Element Analysis,* 3rd Ed., John Wiley & Sons, New York, NY, 1989.

24. Bathe, K.J., *Finite Element Procedures in Engineering Analysis,* Prentice-Hall, Englewood Cliffs, NJ, 1982.

25. *SD/FAST User's Manual, Version 88/02/20,* Symbolic Dynamics, Inc., Mountain View, CA, 1988.

26. Sayers, M., *AUTOSIM User's Manual, Version 1.0 B8,* University of Michigan, Transportation Research Institute, Ann Arbor, MI, 1990.

27. Schaechter, D.B., Levinson, D.A., and Kane, T.R., *AUTOLEV User's Manual,* OnLine Dynamics, Inc., Sunnyvale, CA, 1988.

28. Liu, D., Yocum, J., and Kang, D.S., "Control and Dynamics of a Flexible Spacecraft," *4th NASA Workshop on Computational Control of Flexible Aerospace Systems*, Williamsburg, VA, 1990.

29. Kang, D.S., "Extending Symbolic Rigid Body Code to Include Flexibility," *ASME Winter Annual Meeting*, Dallas, TX, 1990.

30. Fung, Y.C., *Foundations of Solid Mechanics,* Prentice-Hall, Englewood Cliffs, NJ, 1965.

31. Washizu, K., *Variational Methods in Elasticity and Plasticity*, 3rd Ed., Pergamon Press, Oxford, England, 1982.

32. Kane, T.R., Likins, P.W., and Levinson, D.A., *Spacecraft Dynamics,* McGraw-Hill, New York, NY, 1983.

33. Crandall, S.H., Dahl, N.C., and Lardner, T.J., *An Introduction to the Mechanics of Solids,* 2nd Ed., McGraw-Hill, New York, NY, 1978.

34. Timoshenko, S.P., and Gere, J.M., *Theory of Elastic Stability,* 2nd Ed., McGraw-Hill, New York, NY, 1961.

35. Storch, J., and Gates, S., "Transverse Vibration and Buckling of a Cantilevered Beam with Tip Body under Axial Acceleration," *Journal of Sound and Vibration,* Vol. 99, No. 1, 1985, pp. 43-52.

36. Kane, T.R., Ryan, R.R., and Banerjee, A.K., "Dynamics of a Cantilever Beam Attached to a Moving Base," *Journal of Guidance, Control, and Dynamics,* Vol. 10, No. 2, March-April 1987, pp. 139-151.

37. Hughes, T.J.R., Pister, K.S., and Taylor, R.L., "Implicit-Explicit Finite Elements in Nonlinear Transient Analysis," Computational Methods and Applications in Mechanical Engineering, Vol. 17/18, 1979, pp. 159-182.

38. Press, W.H., Flannery, B.P., Teukolsky, S.A., and Vetterling, W.T., *Numerical Recipes: The Art of Scientific Computing,* Cambridge University Press, New York, NY, 1986.

39. Kruszewski, E.T., "Effect of Transverse Shear and Rotary Inertia on the Natural Frequency of a Uniform Beam," NACA Technical Note 1909, July 1949.

Appendix A
Stress Resultants

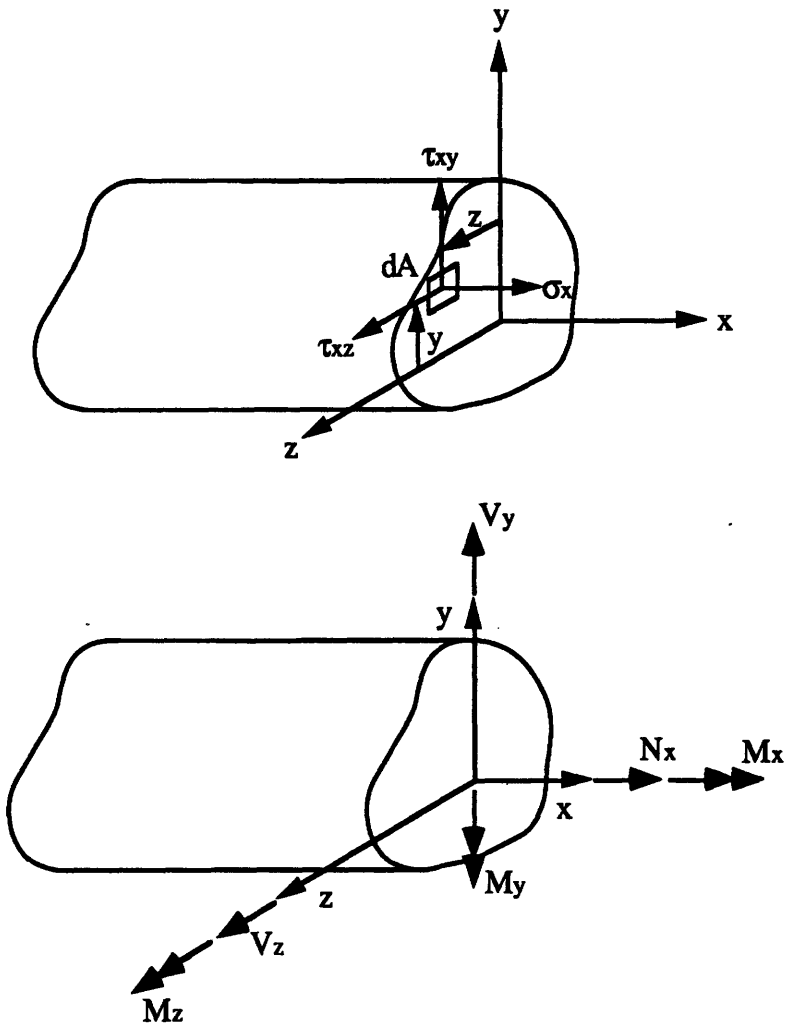

Figure A.1. Definition of stress resultants. (a) Stresses at an arbitrary point, (b) Direction of positive resultants.

Stress resultants provide a convenient measure of the internal force in the beam elements. Positive stresses are shown in figure A.1. Stress resultants are then defined in the following way:

$$N_x = \int_A \sigma_x \, dA \tag{A.1}$$

$$M_x = \int_A (\tau_{xz} y - \tau_{xy} z) \, dA \tag{A.2}$$

$$M_y = -\int_A \sigma_x z \, dA \tag{A.3}$$

$$M_z = -\int_A \sigma_x y \, dA \tag{A.4}$$

$$V_y = \int_A \tau_{xy} \, dA \tag{A.5}$$

$$V_z = \int_A \tau_{xz} \, dA \tag{A.6}$$

The strains are defined as the work conjugates to the stress resultants. The corresponding strains are therefore

C^0	C^1
$\varepsilon_{xo} = u_{o,x}$	$\varepsilon_{xo} = u_{o,x}$
$\kappa_t = \theta_{x,x}$	$\kappa_t = \theta_{x,x}$
$\kappa_y = -\theta_{y,x}$	$\kappa_y = w_{o,xx}$
$\kappa_z = \theta_{z,x}$	$\kappa_z = v_{o,xx}$
$\gamma_{xzo} = w_{o,x} + \theta_y$	
$\gamma_{xyo} = v_{o,x} - \theta_z$	

Let the vector of stress resultants be defined by

C^1: $\underline{\sigma}^T = [\ N_x \quad M_x \quad M_y \quad M_z\ ]$

C^0: $\underline{\sigma}^T = [\ N_x \quad M_x \quad M_y \quad M_z \quad V_y \quad V_z\ ]$

The stress resultants are related to the element strains by the appropriate material matrix. Strains have already been shown to be related to the element nodal DOFs by the $\underline{B}$ matrix. The stress can then be evaluated at any point η within the element from the equation

$$\underline{\sigma}\big|_\eta = \underline{D_k}\,\underline{\varepsilon}\big|_\eta = \underline{D_k}\,\underline{B}\big|_\eta\,\underline{q} \qquad \text{(A.7)}$$

Appendix B
Time Integration Schemes

For direct integration of linear equations of motion, implicit integration schemes have an advantage over explicit schemes in that they are unconditionally stable. The only restriction on time step is due to consideration of solution accuracy, and even then it need not be chosen such that the highest frequency is integrated accurately. Newmark integration is a second order implicit scheme, which makes it an appropriate choice for solution of second order equations of motion. The Newmark method can also be extended to the incremental solution of nonlinear equations of motion. As each increment is a linear step over Δt, the stability holds for nonlinear systems as well. The incremental Newmark scheme is implemented in the dynamic simulations. A brief derivation of the Newmark method follows.

For reference, the fourth-order Runge-Kutta integration scheme is also introduced. Because of its explicit nature, the time step must be chosen for stability as well as accuracy, although for direct integration, the stability requirement is usually strict enough to assure an accurate solution. The Runge-Kutta method is used to solve systems of first order ODEs.

B.1 Newmark Integration for Linear Systems [24]

For a set of ordinary differential equations, consider the state of equilibrium at time t+Δt:

$$\mathbf{M}\,{}^{t+\Delta t}\ddot{\mathbf{U}} + \mathbf{C}\,{}^{t+\Delta t}\dot{\mathbf{U}} + \mathbf{K}\,{}^{t+\Delta t}\mathbf{U} = {}^{t+\Delta t}\mathbf{R} \tag{B.1.1}$$

where **M**, **C**, and **K** are the mass, damping, and stiffness matrices, and **R** is the vector of external loads. The three matrices are constant for linear analyses. Introduce approximations for $\dot{\mathbf{U}}$, and **U** at time t+Δt

$${}^{t+\Delta t}\dot{\mathbf{U}} = {}^{t}\dot{\mathbf{U}} + \left[(1-\delta)\,{}^{t}\ddot{\mathbf{U}} + \delta\,{}^{t+\Delta t}\ddot{\mathbf{U}}\right]\Delta t \tag{B.1.2}$$

$${}^{t+\Delta t}\mathbf{U} = {}^{t}\mathbf{U} + {}^{t}\dot{\mathbf{U}}\Delta t + \left[\left(\frac{1}{2}-\alpha\right){}^{t}\ddot{\mathbf{U}} + \alpha\,{}^{t+\Delta t}\ddot{\mathbf{U}}\right]\Delta t^2 \tag{B.1.3}$$

where α and δ are parameters which govern the accuracy and stability of integration. For δ = 1/2 and α = 1/4, the scheme is second-order accurate, unconditionally stable and equivalent to the trapezoidal rule (also known as the constant-average-acceleration method).

Equation (B.1.3) can be rearranged for ${}^{t+\Delta t}\ddot{\mathbf{U}}$ and substituted into equation (B.1.2). Now expressions for ${}^{t+\Delta t}\ddot{\mathbf{U}}$ and ${}^{t+\Delta t}\dot{\mathbf{U}}$ can be substituted into equation (B.1.1), which can be rearranged to give

$$\hat{\mathbf{K}}\,{}^{t+\Delta t}\mathbf{U} = {}^{t+\Delta t}\hat{\mathbf{R}} \tag{B.1.4}$$

where $\hat{\mathbf{K}}$ is the effective stiffness matrix given by

$$\hat{\mathbf{K}} = \mathbf{K} + a_0\,\mathbf{M} + a_1\,\mathbf{C} \tag{B.1.5}$$

and $\widehat{\mathbf{R}}$ is the effective load vector at time t+Δt

$$^{t+\Delta t}\widehat{\mathbf{R}} = {}^{t+\Delta t}\mathbf{R} + \mathbf{M}\left(a_0{}^{t}\mathbf{U} + a_2{}^{t}\dot{\mathbf{U}} + a_3{}^{t}\ddot{\mathbf{U}}\right) + \mathbf{C}\left(a_1{}^{t}\mathbf{U} + a_4{}^{t}\dot{\mathbf{U}} + a_5{}^{t}\ddot{\mathbf{U}}\right) \tag{B.1.6}$$

Constants are given by

$$a_0 = \frac{1}{\alpha\Delta t^2} \quad a_1 = \frac{\delta}{\alpha\Delta t} \quad a_2 = \frac{1}{\alpha\Delta t} \quad a_3 = \frac{1}{2\alpha} - 1 \quad a_4 = \frac{\delta}{\alpha} - 1$$

$$a_5 = \frac{\Delta t}{2}\left(\frac{\delta}{\alpha} - 2\right) \quad a_6 = \Delta t\left(1 - \delta\right) \quad a_7 = \delta\Delta t$$

Solution of equation (B.1.4) yields displacements $^{t+\Delta t}\mathbf{U}$ at time t+Δt. Velocity and acceleration are then found from equations

$$^{t+\Delta t}\ddot{\mathbf{U}} = a_0\left({}^{t+\Delta t}\mathbf{U} - {}^{t}\mathbf{U}\right) - a_2{}^{t}\dot{\mathbf{U}} - a_3{}^{t}\ddot{\mathbf{U}} \tag{B.1.7}$$

$$^{t+\Delta t}\dot{\mathbf{U}} = {}^{t}\dot{\mathbf{U}} + a_6{}^{t}\ddot{\mathbf{U}} + a_7{}^{t+\Delta t}\ddot{\mathbf{U}} \tag{B.1.8}$$

B.2 Incremental Form of Newmark Integration

The integration scheme developed in the previous section can be viewed as an incremental solution method where successive increments are Δt, 2Δt,..., nΔt; all increments are referred to the original configuration. This is possible for linear equations of motion since the coefficient matrices are constant. In nonlinear problems, the stiffness matrix is interpreted as the tangent stiffness matrix, and accounts for material stiffness as well as geometric stiffness and material nonlinear effects. The tangent stiffness is configuration dependent and is denoted at time t as $^{t}\mathbf{K}_T$. The configuration dependence of nonlinear problems prohibits referring every increment

back to the original configuration, but an incremental procedure can be used to propagate the solution from one known equilibrium state to another, providing the increment is small.

Assume a state of equilibrium is known at time t which can be written as

$$\mathbf{M}\,{}^{t}\ddot{\mathbf{U}} + \mathbf{C}\,{}^{t}\dot{\mathbf{U}} + {}^{t}\mathbf{F} = {}^{t}\mathbf{R} \qquad \text{(B.2.1)}$$

where ${}^{t}\mathbf{F}$ is the internal force vector and is a function of $\mathbf{U}$. With this change of notation, the equilibrium equation (B.1.1) can be written as

$$\mathbf{M}\,{}^{t+\Delta t}\ddot{\mathbf{U}} + \mathbf{C}\,{}^{t+\Delta t}\dot{\mathbf{U}} + {}^{t+\Delta t}\mathbf{F} = {}^{t+\Delta t}\mathbf{R} \qquad \text{(B.2.2)}$$

Now it is assumed that the equilibrium state expressed in equation (B.2.2) can be approximated by a linear increment from the equilibrium expressed in equation (B.2.1). The internal force vector at time t+Δt can thus be written

$${}^{t+\Delta t}\mathbf{F} \cong {}^{t}\mathbf{F} + {}^{t}\mathbf{K}_{T}\,\Delta\mathbf{U} \qquad \text{(B.2.3)}$$

where $\Delta\mathbf{U}$ is a vector of increment displacements. Substitution into equation (B.2.2) yields

$$\mathbf{M}\,{}^{t+\Delta t}\ddot{\mathbf{U}} + \mathbf{C}\,{}^{t+\Delta t}\dot{\mathbf{U}} + {}^{t}\mathbf{K}_{T}\,\Delta\mathbf{U} = {}^{t+\Delta t}\mathbf{R} - {}^{t}\mathbf{F} \qquad \text{(B.2.4)}$$

Displacements corresponding to time t+Δt can then be calculated from

$${}^{t+\Delta t}\mathbf{U} \cong {}^{t}\mathbf{U} + \Delta\mathbf{U} \qquad \text{(B.2.5)}$$

Equations (B.2.4) and (B.2.5) form an approximate incremental solution to the set of nonlinear equations. Equality can be achieved

through iteration at time $t+\Delta t$ by using the full or modified Newton-Raphson technique. Full Newton-Raphson updates the tangent stiffness at *each iteration*, while the modified Newton-Raphson updates only at the start of *each increment*. The full technique converges more rapidly but at the cost of forming the tangent stiffness at every iteration. With the modified Newton-Raphson, the incremental algorithm can be stated as

$$\mathbf{M}\,{}^{t+\Delta t}\ddot{\mathbf{U}}^{k} + \mathbf{C}\,{}^{t+\Delta t}\dot{\mathbf{U}}^{k} + {}^{t}\mathbf{K}_T\,\Delta\mathbf{U}^{k} = {}^{t+\Delta t}\mathbf{R} - {}^{t+\Delta t}\mathbf{F}^{k-1} \tag{B.2.6}$$

$${}^{t+\Delta t}\mathbf{U}^{k} = {}^{t+\Delta t}\mathbf{U}^{k-1} + \Delta\mathbf{U}^{k} \tag{B.2.7}$$

where

$${}^{t+\Delta t}\mathbf{U}^{0} = {}^{t}\mathbf{U} \tag{B.2.8}$$

$${}^{t+\Delta t}\mathbf{F}^{0} = {}^{t}\mathbf{F} \tag{B.2.9}$$

Equation (B.2.6) is an incremental form corresponding to equation (B.1.1), and the Newmark method of section B.1 can be applied. Neglecting the damping matrix and choosing α and δ corresponding to the trapezoidal rule gives

$$\widehat{\mathbf{K}}\,\Delta\mathbf{U}^{k} = {}^{t+\Delta t}\widehat{\mathbf{R}} - {}^{t+\Delta t}\mathbf{F}^{k-1} \tag{B.2.10}$$

where

$$\widehat{\mathbf{K}} = {}^{t}\mathbf{K}_T + \frac{4}{\Delta t^2}\mathbf{M} \tag{B.2.11}$$

$${}^{t+\Delta t}\widehat{\mathbf{R}} = {}^{t+\Delta t}\mathbf{R} - \mathbf{M}\left(\frac{4}{\Delta t^2}\left({}^{t+\Delta t}\mathbf{U}^{k-1} - {}^{t}\mathbf{U}\right) - \frac{4}{\Delta t}\,{}^{t}\dot{\mathbf{U}} - {}^{t}\ddot{\mathbf{U}}\right) \tag{B.2.12}$$

The current state can be obtained from

$$^{t+\Delta t}\mathbf{U}^{k} = {}^{t+\Delta t}\mathbf{U}^{k-1} + \Delta\mathbf{U}^{k} \tag{B.2.13}$$

$$^{t+\Delta t}\ddot{\mathbf{U}}^{k} = \frac{4}{\Delta t^2}\left({}^{t+\Delta t}\mathbf{U}^{k} - {}^{t}\mathbf{U}\right) - \frac{4}{\Delta t}{}^{t}\dot{\mathbf{U}} - {}^{t}\ddot{\mathbf{U}} \tag{B.2.14}$$

$$^{t+\Delta t}\dot{\mathbf{U}}^{k} = {}^{t}\dot{\mathbf{U}} + \frac{\Delta t}{2}{}^{t}\ddot{\mathbf{U}} + \frac{\Delta t}{2}{}^{t+\Delta t}\ddot{\mathbf{U}}^{k} \tag{B.2.15}$$

where the start-up conditions are the same as given by equations (B.2.8) and (B.2.9). Other schemes have been developed for estimating the initial iteration conditions, rather than using the previous equilibrium state as the first estimate of the next equilibrium state [37].

The incremental form of the Newmark method derived in this section for nonlinear problems can be reduced to the result obtained in section B.1 for linear systems by noting that $^{t}\mathbf{K}_{T} \rightarrow \mathbf{K}$ so that the internal force vector becomes

$$^{t+\Delta t}\mathbf{F}^{k-1} = \mathbf{K}\ {}^{t+\Delta t}\mathbf{U}^{k-1}$$

which can be used along with equation (B.2.13) to come up with equation (B.1.4).

B.3 Error Sources in Newmark Integration

For unconditionally stable integration schemes, the choice of time step Δt is governed only by consideration of accuracy. In structural dynamics problems, high frequency modes usually contribute little to the response of the structure. If the time step is chosen to accurately integrate

only some subset of vibration modes, then the errors contributed by the higher modes are also assumed to be small. Solution errors are confined to the upper vibration modes by appropriate choice of the time step Δt.

Since all modes are included in direct integration, solution errors stem only from the use of too large an integration step size. This is in contrast with modal reduction techniques, which also invite errors due to truncation of the modal set.

Integration errors are classified in terms of period elongation and amplitude decay (algorithmic damping). The trapezoidal rule implementation of the Newmark scheme ($\delta = 1/2$, $\alpha = 1/4$) is second-order accurate and introduces only period elongation – no amplitude decay. Thus, all frequencies contribute to the structural response. Amplitude decay can be introduced in the Newmark scheme through alternative choice of parameters δ & α, although accuracy is reduced to first-order.

B.4 Fourth-Order Runge Kutta Integration [38]

The fourth-order accurate Runge-Kutta is an explicit multi-step integration scheme based on the Euler method. It operates on systems of first order ordinary differential equations, in contrast with the Newmark scheme, which operates directly on the second order equations of motion. Thus some additional manipulation is required in order to implement the Runge-Kutta algorithm.

Any system of ordinary differential equations can be reduced to a set of N coupled first order equations. To preserve the dynamics context, the notation of the previous sections is used to express the general form as

$$\frac{dU_i(t)}{dt} = f_i'(t, U_1, \ldots, U_N) \qquad i = 1, \ldots, N \tag{B.4.1}$$

where U_i is the ith component of the vector **U** and the known function f_i' is the corresponding derivative. Note that reduction of the equations of motion to first order form means that N = 2(6+6*Num_nodes).

For convenience only, consider equation (B.4.1) with N=1. Increasing the system size involves a straightforward introduction of a DO loop over i=1,N. The Euler method advances the solution of a first order equation from t to t+Δt by application of the formula

$$^{t+\Delta t}U = {}^{t}U + \Delta t f'(t, {}^{t}U) \tag{B.4.2}$$

where it should be noted that the solution at time t+Δt is based entirely on information known at time t. Thus no iterations are necessary in the explicit algorithm. The accuracy and stability of the one step Euler method can be improved by introducing multiple steps. The break-even point is the fourth-order Runge-Kutta, which makes use of four steps, and is given by

$$^{t+\Delta t}U = {}^{t}U + \frac{k_1}{6} + \frac{k_2}{3} + \frac{k_3}{3} + \frac{k_4}{6} \tag{B.4.3}$$

where

$$k_1 = \Delta t f'({}^tU, t) \tag{B.4.4}$$

$$k_2 = \Delta t f'\left({}^tU + \frac{k_1}{2}, t + \frac{\Delta t}{2}\right) \tag{B.4.5}$$

$$k_3 = \Delta t f'\left({}^tU + \frac{k_2}{2}, t + \frac{\Delta t}{2}\right) \tag{B.4.6}$$

$$k_4 = \Delta t f'({}^tU + k_3, t + \Delta t) \tag{B.4.7}$$

B.5 Implementation with Equations of Motion

As noted earlier, use of Runge-Kutta requires some manipulation that the Newmark method does not. This section shows the details of this manipulation. The equations of motion (2.6.6) or (2.7.7) can be rewritten as a system of matrix equations

$$\mathbf{M_{RR}}\,\ddot{\mathbf{U}}_R + \mathbf{M_{RF}}\,\ddot{\mathbf{U}}_F = \mathbf{R_R} + \mathbf{R_{RF}} \tag{B.5.1}$$

$$\mathbf{M_{FR}}\,\ddot{\mathbf{U}}_R + \mathbf{M_{FF}}\,\ddot{\mathbf{U}}_F + \mathbf{K_{FF}}\,\mathbf{U_F} = \mathbf{R_F} \tag{B.5.2}$$

Equation (B.5.2) can be rewritten as

$$\ddot{\mathbf{U}}_F = \mathbf{M_{FF}}^{-1}\left[\mathbf{R_F} - \mathbf{M_{FR}}\,\ddot{\mathbf{U}}_R - \mathbf{K_{FF}}\,\mathbf{U_F}\right] \tag{B.5.3}$$

Substitution into equation (B.5.1) yields

$$\left[\mathbf{M_{RR}} - \mathbf{M_{RF}}\,\mathbf{M_{FF}}^{-1}\,\mathbf{M_{FR}}\right]\ddot{\mathbf{U}}_R = \mathbf{R_R} + \mathbf{R_{RF}} - \mathbf{M_{RF}}\,\mathbf{M_{FF}}^{-1}\,\mathbf{R_F} + \mathbf{M_{RF}}\,\mathbf{M_{FF}}^{-1}\,\mathbf{K_{FF}}\,\mathbf{U_F} \tag{B.5.4}$$

A set of first order equations can be formed by letting $\widetilde{U}_R = \dot{U}_R$ and $\widetilde{U}_F = \dot{U}_F$. The set of derivatives (at time t) to be evaluated in the course of the Runge-Kutta scheme can be summarized as follows:

$$\dot{U}_R = \widetilde{U}_R \tag{B.5.5}$$

$$\dot{U}_F = \widetilde{U}_F \tag{B.5.6}$$

$$\left[M_{RR} - M_{RF} M_{FF}^{-1} M_{FR}\right] \dot{\widetilde{U}}_R = R_R + R_{RF} - M_{RF} M_{FF}^{-1} R_F + M_{RF} M_{FF}^{-1} K_{FF} U_F \tag{B.5.7}$$

$$M_{FF} \dot{\widetilde{U}}_F = R_F - M_{FR} \dot{\widetilde{U}}_R - K_{FF} U_F \tag{B.5.8}$$

Both of equations (B.5.5) & (B.5.7) encompass six scalar equations governing the rigid body DOFs. Equations (B.5.6) & (B.5.8) encompass (6*Num_nodes) scalar equations relating the flexible DOFs. Thus the total number of derivatives evaluated at each step is 2(6 + 6*Num_nodes).

The Runge-Kutta method is well suited for nonlinear analysis since it is a natural incremental scheme; each increment is referred to the previous equilibrium state. Nonlinear solutions are obtained by interpreting the K_{FF} matrix as the tangent stiffness matrix ${}^tK_T$, evaluated at time t. A typical step (evaluation of the functions f_i') of the Runge-Kutta algorithm in the dynamics simulation is as follows:

Given initial conditions (at time t): $\mathbf{U}_R$, $\mathbf{U}_F$, $\tilde{\mathbf{U}}_R$, $\tilde{\mathbf{U}}_F$

1) calculate tangent stiffness based on $\mathbf{U}_F$
2) evaluate equations (B.5.5) & (B.5.6) for $\dot{\mathbf{U}}_R$, $\dot{\mathbf{U}}_F$
3) evaluate equation (B.5.7) for $\dot{\tilde{\mathbf{U}}}_R$
4) evaluate equation (B.5.8) for $\dot{\tilde{\mathbf{U}}}_F$
5) use these results in calculation of k_i's

A typical increment implements this sequence four times and employs equation (B.4.3). The tangent stiffness matrix need only be calculated at the beginning of each increment.

Appendix C
Convergence Data

Convergence data is tabulated for the figures shown in chapter 4.

C.1 Free Vibration

As a reminder, the following cases were considered:

1) C^0: consistent mass, full integration of mass and stiffness
2) C^0: consistent mass, reduced integration of stiffness
3) C^0: consistent mass, 1-point integration of mass and stiffness
4) C^0: lumped mass, full integration of mass and stiffness
5) C^0: lumped mass, reduced integration of stiffness
6) C^0: lumped mass, 1-point integration of mass and stiffness
7) C^1: consistent mass, full integration of mass and stiffness (with rotatory inertia - Rayleigh)
8) C^1: consistent mass, full integration of mass and stiffness (without rotatory inertia - Bernoulli-Euler)

Table C.1. Free vibration, case 1, parameter set 1.

Mode	Numel=1	Numel=2	Numel=4	Numel=8	Numel=16	Numel=32	B. E.
1	171.0	101.0	58.5	40.3	34.2	32.5	32.1
2	6820.0	687.0	375.0	247.0	207.0	196.0	201.1
3		6860.0	1100.0	678.0	553.0	520.0	563.2
4		7040.0	2310.0	1310.0	1030.0	953.0	1103.7
5			6870.0	2130.0	1600.0	1470.0	1824.5
6			7100.0	3110.0	2260.0	2040.0	
7			7510.0	4170.0	3000.0	2660.0	
8			7980.0	5070.0	3800.0	3310.0	
9				6880.0	4660.0	3980.0	
10				7140.0	5570.0	4680.0	

Table C.2. Free vibration, case 2, parameter set 1.

Mode	Numel=1	Numel=2	Numel=4	Numel=8	Numel=16	Numel=32	B. E.
1	31.4	32.6	32.1	31.9	31.9	31.9	32.1
2	5920.0	331.0	222.0	199.0	194.0	192.0	201.1
3		4400.0	745.0	560.0	521.0	512.0	563.2
4		6680.0	1820.0	1110.0	972.0	940.0	1103.7
5			4810.0	1870.0	1530.0	1450.0	1824.5
6			6100.0	2830.0	2170.0	2020.0	
7			6650.0	3940.0	2890.0	2630.0	
8			6900.0	4970.0	3680.0	3280.0	
9				6850.0	4530.0	3950.0	
10				7000.0	5440.0	4640.0	

Table C.3. Free vibration, case 3, parameter set 1.

Mode	Numel=1	Numel=2	Numel=4	Numel=8	Numel=16	Numel=32	B. E.
1	36.3	34.2	32.5	32.0	31.9	31.9	32.1
2	6830.0	549.0	245.0	203.0	195.0	193.0	201.1
3		6930.0	1020.0	591.0	527.0	513.0	563.2
4		7570.0	4190.0	1240.0	994.0	945.0	1103.7
5			6920.0	2280.0	1580.0	1460.0	1824.5
6			7300.0	4020.0	2290.0	2040.0	
7			9800.0	6700.0	3130.0	2680.0	
8			14700.0	6910.0	4120.0	3350.0	
9				7390.0	5290.0	4070.0	
10				7820.0	6590.0	4830.0	

Table C.4. Free vibration, case 4, parameter set 1.

Mode	Numel=1	Numel=2	Numel=4	Numel=8	Numel=16	Numel=32	B. E.
1	140.0	93.5	57.3	40.1	34.2	32.5	32.1
2		468.0	328.0	240.0	207.0	198.0	201.1
3			825.0	634.0	554.0	530.0	563.2
4			1340.0	1150.0	1020.0	979.0	1103.7
5				1720.0	1570.0	1510.0	1824.5
6				2270.0	2160.0	2100.0	
7				2730.0	2760.0	2720.0	
8				3030.0	3360.0	3360.0	
9					3930.0	4000.0	
10					4450.0	4640.0	

Table C.5. Free vibration, case 5, parameter set 1.

Mode	Numel=1	Numel=2	Numel=4	Numel=8	Numel=16	Numel=32	B. E.
1	25.7	29.9	31.4	31.8	31.9	31.9	32.1
2		229.0	193.0	194.0	194.0	194.0	201.1
3			562.0	524.0	522.0	521.0	563.2
4			1210.0	982.0	967.0	965.0	1103.7
5				1530.0	1500.0	1490.0	1824.5
6				2110.0	2080.0	2080.0	
7				2630.0	2680.0	2700.0	
8				3000.0	3280.0	3340.0	
9					3860.0	3970.0	
10					4390.0	4610.0	

Table C.6. Free vibration, case 6, parameter set 1.

Mode	Numel=1	Numel=2	Numel=4	Numel=8	Numel=16	Numel=32	B. E.
1	25.7	29.9	31.4	31.8	31.9	31.9	32.1
2		229.0	193.0	194.0	194.0	194.0	201.1
3			562.0	524.0	522.0	521.0	563.2
4			1210.0	982.0	967.0	965.0	1103.7
5				1530.0	1500.0	1490.0	1824.5
6				2110.0	2080.0	2080.0	
7				2630.0	2680.0	2700.0	
8				3000.0	3280.0	3340.0	
9					3860.0	3970.0	
10					4390.0	4610.0	

Table C.7. Free vibration, case 7, parameter set 1.

Mode	Numel=1	Numel=2	Numel=4	Numel=8	Numel=16	Numel=32	B. E.
1	32.2	32.0	32.0	32.0	32.0	32.0	32.1
2	310.0	200.0	199.0	198.0	198.0	198.0	201.1
3		661.0	550.0	546.0	546.0	546.0	563.2
4		1770.0	1060.0	1050.0	1040.0	1040.0	1103.7
5			1900.0	1680.0	1670.0	1670.0	1824.5
6			2920.0	2440.0	2410.0	2410.0	
7			4370.0	3300.0	3250.0	3240.0	
8			6130.0	4220.0	4150.0	4140.0	
9				5630.0	5110.0	5090.0	
10				6800.0	6120.0	6090.0	

Table C.8. Free vibration, case 8, parameter set 1.

Mode	Numel=1	Numel=2	Numel=4	Numel=8	Numel=16	Numel=32	B. E.
1	32.2	32.1	32.1	32.1	32.1	32.1	32.1
2	318.0	203.0	201.0	201.0	201.0	201.0	201.1
3		686.0	568.0	564.0	563.0	563.0	563.2
4		1990.0	1120.0	1110.0	1100.0	1100.0	1103.7
5			2080.0	1840.0	1830.0	1820.0	1824.5
6			3340.0	2760.0	2730.0	2730.0	
7			5300.0	3880.0	3810.0	3810.0	
8			8700.0	5160.0	5080.0	5070.0	
9				7250.0	6540.0	6510.0	
10				9200.0	8190.0	8140.0	

Table C.9. Free vibration, case 1, parameter set 2.

Mode	Numel=1	Numel=2	Numel=4	Numel=8	Numel=16	Numel=32	B. E.
1	53.7	30.7	15.7	7.9	4.1	2.2	1.0
2	67900.0	215.0	105.0	50.5	25.6	13.9	6.4
3		67900.0	325.0	147.0	72.3	39.0	17.8
4		68000.0	661.0	306.0	144.0	76.6	34.9
5			67900.0	541.0	243.0	127.0	57.7
6			68000.0	863.0	373.0	191.0	
7			68000.0	1240.0	538.0	269.0	
8			68100.0	1580.0	741.0	362.0	
9				67900.0	989.0	469.0	
10				68000.0	1280.0	592.0	

Table C.10. Free vibration, case 2, parameter set 2.

Mode	Numel=1	Numel=2	Numel=4	Numel=8	Numel=16	Numel=32	B. E.
1	1.0	1.0	1.0	1.0	1.0	1.0	1.0
2	58800.0	11.7	7.4	6.6	6.4	6.4	6.4
3		39600.0	28.4	19.9	18.3	17.9	17.8
4		66100.0	121.0	43.9	36.8	35.3	34.9
5			22500.0	86.0	63.2	58.9	57.7
6			51500.0	163.0	99.2	88.9	
7			63400.0	331.0	147.0	126.0	
8			67500.0	913.0	210.0	170.0	
9				14400.0	294.0	222.0	
10				32600.0	406.0	283.0	

Table C.11. Free vibration, case 3, parameter set 2.

Mode	Numel=1	Numel=2	Numel=4	Numel=8	Numel=16	Numel=32	B. E.
1	1.2	1.1	1.0	1.0	1.0	1.0	1.0
2	67900.0	19.5	8.2	6.8	6.5	6.4	6.4
3		67900.0	41.3	21.1	18.5	18.0	17.8
4		68000.0	324.0	49.7	37.8	35.5	34.9
5			67900.0	109.0	65.9	59.5	57.7
6			68000.0	255.0	106.0	90.2	
7			68100.0	773.0	161.0	128.0	
8			69100.0	4320.0	240.0	175.0	
9				67900.0	354.0	230.0	
10				68000.0	525.0	296.0	

Table C.12. Free vibration, case 4, parameter set 2.

Mode	Numel=1	Numel=2	Numel=4	Numel=8	Numel=16	Numel=32	B. E.
1	43.9	28.3	15.3	7.9	4.1	2.2	1.0
2		146.0	90.1	48.5	25.3	13.8	6.4
3			238.0	134.0	70.5	38.7	17.8
4			415.0	257.0	138.0	75.7	34.9
5				417.0	226.0	125.0	57.7
6				604.0	336.0	186.0	
7				793.0	466.0	259.0	
8				939.0	616.0	344.0	
9					784.0	441.0	
10					967.0	549.0	

Table C.13. Free vibration, case 5, parameter set 2.

Mode	Numel=1	Numel=2	Numel=4	Numel=8	Numel=16	Numel=32	B. E.
1	0.8	0.9	1.0	1.0	1.0	1.0	1.0
2		7.9	6.3	6.3	6.4	6.4	6.4
3			20.4	18.0	17.8	17.8	17.8
4			78.4	36.7	35.2	34.9	34.9
5				65.6	58.8	57.8	57.7
6				114.0	89.1	86.6	
7				212.0	127.0	121.0	
8				559.0	174.0	162.0	
9					232.0	209.0	
10					305.0	262.0	

Table C.14. Free vibration, case 6, parameter set 2.

Mode	Numel=1	Numel=2	Numel=4	Numel=8	Numel=16	Numel=32	B. E.
1	0.8	0.9	1.0	1.0	1.0	1.0	1.0
2		7.9	6.3	6.3	6.4	6.4	6.4
3			20.4	18.0	17.8	17.8	17.8
4			78.4	36.7	35.2	34.9	34.9
5				65.6	58.8	57.8	57.7
6				114.0	89.1	86.6	
7				212.0	127.0	121.0	
8				559.0	174.0	162.0	
9					232.0	209.0	
10					305.0	262.0	

Table C.15. Free vibration, case 7, parameter set 2.

Mode	Numel=1	Numel=2	Numel=4	Numel=8	Numel=16	Numel=32	B. E.
1	1.0	1.0	1.0	1.0	1.0	1.0	1.0
2	10.0	6.4	6.4	6.4	6.4	6.4	6.4
3		21.7	17.9	17.8	17.8	17.8	17.8
4		63.0	35.4	35.0	34.9	34.9	34.9
5			65.9	58.0	57.7	57.7	57.7
6			106.0	87.2	86.3	86.2	
7			168.0	123.0	121.0	120.0	
8			275.0	163.0	161.0	160.0	
9				229.0	207.0	206.0	
10				291.0	259.0	257.0	

Table C.16. Free vibration, case 8, parameter set 2.

Mode	Numel=1	Numel=2	Numel=4	Numel=8	Numel=16	Numel=32	B. E.
1	1.0	1.0	1.0	1.0	1.0	1.0	1.0
2	10.0	6.4	6.4	6.4	6.4	6.4	6.4
3		21.7	17.9	17.8	17.8	17.8	17.8
4		63.0	35.4	35.0	34.9	34.9	34.9
5			65.9	58.0	57.7	57.7	57.7
6			106.0	87.2	86.3	86.2	
7			168.0	123.0	121.0	120.0	
8			275.0	163.0	161.0	160.0	
9				229.0	207.0	206.0	
10				291.0	259.0	257.0	

C.2 Static Buckling

Static buckling results were obtained for the following cases:

1) C^0: full integration of stiffness matrices
2) C^0: reduced integration of material stiffness
3) C^1: full integration of stiffness matrices

Included among the tabulated data are the results using the higher order stress resultants. Table entries have units of stress.

Table C.17. Static buckling, case 1, parameter set 1.

Mode	Numel=1	Numel=2	Numel=4	Numel=8	Numel=16	Numel=32	B. E.
1	9.80E+05	2.28E+05	7.05E+04	3.28E+04	2.35E+04	2.12E+04	2.06E+04
2		2.62E+06	6.69E+05	2.91E+05	2.04E+05	1.84E+05	1.85E+05
3			1.98E+06	7.78E+05	5.31E+05	4.73E+05	5.14E+05
4			3.55E+06	1.44E+06	9.47E+05	8.35E+05	1.01E+06
5				2.19E+06	1.40E+06	1.22E+06	1.67E+06

Table C.18. Static buckling, case 2, parameter set 1.

Mode	Numel=1	Numel=2	Numel=4	Numel=8	Numel=16	Numel=32	B. E.
1	3.30E+04	2.27E+04	2.10E+04	2.06E+04	2.05E+04	2.05E+04	2.06E+04
2		6.46E+05	2.24E+05	1.87E+05	1.79E+05	1.77E+05	1.85E+05
3			9.11E+05	5.26E+05	4.70E+05	4.57E+05	5.14E+05
4			2.99E+06	1.05E+06	8.51E+05	8.11E+05	1.01E+06
5				1.74E+06	1.28E+06	1.19E+06	1.67E+06

Table C.19. Static buckling, case 3, parameter set 1.

Mode	Numel=1	Numel=2	Numel=4	Numel=8	Numel=16	Numel=32	B. E.
1	2.07E+04	2.06E+04	2.06E+04	2.06E+04	2.06E+04	2.06E+04	2.06E+04
2	2.68E+05	1.91E+05	1.86E+05	1.85E+05	1.85E+05	1.85E+05	1.85E+05
3		6.42E+05	5.23E+05	5.15E+05	5.14E+05	5.14E+05	5.14E+05
4		1.66E+06	1.06E+06	1.01E+06	1.01E+06	1.01E+06	1.01E+06
5			1.97E+06	1.68E+06	1.67E+06	1.67E+06	1.67E+06

Table C.20. Static buckling, case 1, parameter set 2.

Mode	Numel=1	Numel=2	Numel=4	Numel=8	Numel=16	Numel=32	B. E.
1	9.62E+05	2.08E+05	5.03E+04	1.26E+04	3.30E+03	9.78E+02	2.06E+02
2		2.54E+06	5.00E+05	1.16E+05	2.99E+04	8.81E+03	1.85E+03
3			1.65E+06	3.40E+05	8.39E+04	2.45E+04	5.14E+03
4			3.44E+06	7.15E+05	1.67E+05	4.83E+04	1.01E+04
5				1.29E+06	2.83E+05	8.02E+04	1.67E+04

Table C.21. Static buckling, case 2, parameter set 2.

Mode	Numel=1	Numel=2	Numel=4	Numel=8	Numel=16	Numel=32	B. E.
1	3.33E+02	2.29E+02	2.11E+02	2.07E+02	2.06E+02	2.06E+02	2.06E+02
2		7.76E+03	2.38E+03	1.96E+03	1.88E+03	1.86E+03	1.85E+03
3			1.19E+04	6.09E+03	5.35E+03	5.19E+03	5.14E+03
4			1.30E+05	1.43E+04	1.09E+04	1.02E+04	1.01E+04
5				3.14E+04	1.90E+04	1.71E+04	1.67E+04

Table C.22. Static buckling, case 3, parameter set 2.

Mode	Numel=1	Numel=2	Numel=4	Numel=8	Numel=16	Numel=32	B. E.
1	2.07E+02	2.06E+02	2.06E+02	2.06E+02	2.06E+02	2.06E+02	2.06E+02
2	2.68E+03	1.91E+03	1.86E+03	1.85E+03	1.85E+03	1.85E+03	1.85E+03
3		6.42E+03	5.23E+03	5.15E+03	5.14E+03	5.14E+03	5.14E+03
4		1.66E+04	1.06E+04	1.01E+04	1.01E+04	1.01E+04	1.01E+04
5			1.97E+04	1.68E+04	1.67E+04	1.67E+04	1.67E+04

Table C.23. Static buckling, case 1, parameter set 1, higher order terms.

Mode	Numel=1	Numel=2	Numel=4	Numel=8	Numel=16	Numel=32	B. E.
1	9.78E+05	2.28E+05	7.04E+04	3.28E+04	2.35E+04	2.12E+04	2.06E+04
2		2.60E+06	6.59E+05	2.86E+05	2.01E+05	1.80E+05	1.85E+05
3			1.92E+06	7.49E+05	5.10E+05	4.54E+05	5.14E+05
4			3.52E+06	1.36E+06	8.91E+05	7.85E+05	1.01E+06
5				2.06E+06	1.29E+06	1.13E+06	1.67E+06

Table C.24. Static buckling, case 2, parameter set 1, higher order terms.

Mode	Numel=1	Numel=2	Numel=4	Numel=8	Numel=16	Numel=32	B. E.
1	3.29E+04	2.27E+04	2.09E+04	2.05E+04	2.04E+04	2.04E+04	2.06E+04
2		6.13E+05	2.20E+05	1.84E+05	1.76E+05	1.74E+05	1.85E+05
3			8.51E+05	5.03E+05	4.51E+05	4.40E+05	5.14E+05
4			2.76E+06	9.70E+05	7.97E+05	7.61E+05	1.01E+06
5				1.58E+06	1.17E+06	1.10E+06	1.67E+06

Table C.25. Static buckling, case 3, parameter set 1, higher order terms.

Mode	Numel=1	Numel=2	Numel=4	Numel=8	Numel=16	Numel=32	B. E.
1	2.07E+04	2.05E+04	2.05E+04	2.05E+04	2.05E+04	2.05E+04	2.06E+04
2	2.61E+05	1.88E+05	1.82E+05	1.82E+05	1.82E+05	1.82E+05	1.85E+05
3		6.03E+05	4.97E+05	4.89E+05	4.89E+05	4.89E+05	5.14E+05
4		1.42E+06	9.60E+05	9.19E+05	9.16E+05	9.15E+05	1.01E+06
5			1.65E+06	1.44E+06	1.43E+06	1.43E+06	1.67E+06

Table C.26. Static buckling, case 1, parameter set 2, higher order terms.

Mode	Numel=1	Numel=2	Numel=4	Numel=8	Numel=16	Numel=32	B. E.
1	9.62E+05	2.08E+05	5.03E+04	1.26E+04	3.30E+03	9.78E+02	2.06E+02
2		2.54E+06	5.00E+05	1.16E+05	2.98E+04	8.81E+03	1.85E+03
3			1.65E+06	3.39E+05	8.39E+04	2.45E+04	5.14E+03
4			3.44E+06	7.14E+05	1.67E+05	4.82E+04	1.01E+04
5				1.29E+06	2.83E+05	8.00E+04	1.67E+04

Table C.27. Static buckling, case 2, parameter set 2, higher order terms.

Mode	Numel=1	Numel=2	Numel=4	Numel=8	Numel=16	Numel=32	B. E.
1	3.33E+02	2.29E+02	2.11E+02	2.07E+02	2.06E+02	2.06E+02	2.06E+02
2		7.75E+03	2.38E+03	1.96E+03	1.88E+03	1.86E+03	1.85E+03
3			1.19E+04	6.08E+03	5.34E+03	5.18E+03	5.14E+03
4			1.29E+05	1.43E+04	1.09E+04	1.02E+04	1.01E+04
5				3.13E+04	1.90E+04	1.71E+04	1.67E+04

Table C.28. Static buckling, case 3, parameter set 2, higher order terms.

Mode	Numel=1	Numel=2	Numel=4	Numel=8	Numel=16	Numel=32	B. E.
1	2.07E+02	2.06E+02	2.06E+02	2.06E+02	2.06E+02	2.06E+02	2.06E+02
2	2.68E+03	1.91E+03	1.85E+03	1.85E+03	1.85E+03	1.85E+03	1.85E+03
3		6.42E+03	5.23E+03	5.14E+03	5.14E+03	5.14E+03	5.14E+03
4		1.65E+04	1.06E+04	1.01E+04	1.01E+04	1.01E+04	1.01E+04
5			1.97E+04	1.68E+04	1.66E+04	1.66E+04	1.67E+04

C.3 Dynamic Buckling

Results tabulated below correspond to the convergence plot shown in figure 4.23. The exact solution is that of Timoshenko [34].

Table C.29. Dynamic buckling, parameter set 1.

# Elements	Critical Acceleration				
	C^1 (B.E.)	C^1 Rayleigh	C^0 Full	C^0 Reduced	Exact B.E.
1	6574.1	6574.1	196033	6609.3	6530.8
2	6547.4	6547.4	68564	6957.6	
4	6532.4	6532.4	22159	6635.2	
8	6531.1	6531.1	10388	6520.0	
16	6531.1	6531.1	7455	6489.3	
32	6531.0	6531.0	6722	6481.5	

Appendix D

RMS Finite Element Model

Details are provided for the simplified finite element model of the remote manipulator arm extracted from the NASTRAN model. Information given here was used in the finite element formulations derived in chapter 3 and subsequently used in the dynamic formulation of chapter 2. An example problem is given in chapter 5.

Table D.1. Nodal data for RMS model.

Node #	x (in)	y (in)	z (in)
1	0.	0.	0.
2	22.5396	0.	0.
3	34.5396	0.	0.
4	84.7495	0.	0.
5	134.9594	0.	0.
6	185.1694	0.	0.
7	235.3793	0.	0.
8	285.6156	0.	- 6.
9	341.2056	0.	0.
10	396.7956	0.	0.
11	452.3856	0.	0.
12	507.9756	0.	0.
13	563.5956	0.	0.
14	581.5956	0.	0.
15	611.5512	0.	0.
16	637.5962	0.	0.

Table D.2. Element data for RMS model.

Element #	Prop Set #	Mat'l Set #
1	1	1
2	2	1
3	3	2
4	3	2
5	3	2
6	3	2
7	3	2
8	4	2
9	4	2
10	4	2
11	4	2
12	4	2
13	5	1
14	6	1
15	7	1

Table D.3. Cross section Properties for RMS model.

Prop. Set #	I_{my} (slg•in^2)	I_{mz} (slg•in^2)	I_y (in^4)	I_z (in^4)	A (in^2)	m (slg/in)	k
1	.03346	.02792	54.91	45.81	26.27	.01601	.53
2	.03653	.06155	71.81	121.00	30.04	.01528	.53
3	.007259	.007259	66.21	66.21	28.84	.003162	.53
4	.003367	.003367	44.27	44.27	23.59	.001794	.53
5	.002035	.002035	7.22	7.22	9.53	.002685	.53
6	.01025	.01025	17.20	17.20	14.70	.008762	.53
7	.02741	.02741	9.7	9.7	3.51	.009917	.53

Table D.4. Material Properties for RMS model.

Mat'l Set #	E (lb/in^2)	ν
1	1 x 10^7	.3
2	2.22.x 10^7	.495

Appendix E

Solution of Timoshenko Frequency Equation

The analytical formulation of Timoshenko beam theory leads to much more complicated differential equations than does classical Bernoulli-Euler beam theory. Kruszewski [39] gives the frequency equation for a uniform beam with cantilevered boundary conditions as

$$2 - \frac{k_B\left(k_S^2 + k_{RI}^2\right)}{\sqrt{1 - k_S^2\, k_{RI}^2\, k_B^2}} \sin k_B\beta \sinh k_B\alpha + \left[k_B^2\left(k_S^2 - k_{RI}^2\right)^2 + 2\right] \cos k_B\beta \cosh k_B\alpha = 0 \tag{E.1}$$

where

$$k_S = \frac{1}{L}\sqrt{\frac{EI}{A_S G}} \tag{E.2}$$

$$k_{RI} = \frac{1}{L}\sqrt{\frac{I}{A_T}} \tag{E.3}$$

$$k_B = \omega\sqrt{\frac{mL^4}{EI}} \tag{E.4}$$

$$\alpha = \sqrt{\frac{-\left(k_S^2 + k_{RI}^2\right) + \sqrt{\left(k_S^2 - k_{RI}^2\right)^2 + \frac{4}{k_B^2}}}{2}} \tag{E.5}$$

$$\beta = \sqrt{\frac{\left(k_S^2 + k_{RI}^2\right) + \sqrt{\left(k_S^2 - k_{RI}^2\right)^2 + \frac{4}{k_B^2}}}{2}} \tag{E.6}$$

along with the definitions:

m = mass of the beam per unit length
A_S = effective shear-carrying area
A_T = effective total cross-sectional area
k_S = coefficient of shear rigidity
k_{RI} = coefficient of rotary inertia
k_B = frequency coefficient
ω = natural frequency (rad/sec)

For the beam used in the eigenvalue problems of chapter 4, $A_S = A_T$. The roots of the frequency equation (E.1) must be determined by numerical methods, and natural frequencies subsequently found using equation (E.4). For the property sets defined in chapter 4, the natural frequencies corresponding to the first 5 vibration modes are obtained from Timoshenko beam theory and are shown in table E.1.

Table E.1. Natural frequencies from Timoshenko beam theory.

Mode	Natural Frequency	
	Parameter Set 1	Parameter Set 2
1	31.88	1.01
2	192.07	6.36
3	508.58	17.79
4	929.37	34.83
5	1424.45	57.50

These values may be compared with the Bernoulli-Euler results tabulated in Appendix C. Note that shear and rotatory inertia have the effect of reducing the natural frequencies. For parameter set 1, the

frequency of mode 5 is reduced by 20%. Almost no difference is observed for parameter set 2.

The natural frequency data for the C^0 element (parameter set 1 only) is normalized by the Timoshenko solution and shown in figures E.1-E.5 below. The analogous figure from chapter 4 is indicated, and serves as comparison. The magnitude of the shear and rotatory inertia effects was demonstrated earlier. Normalization by the Timoshenko solution validates that the finite elements are producing the correct result.

The slow convergence of all modes using full integration is again noted in figure E.1. This demonstrates the problem of 'shear locking.' Figure E.2 shows the improvement in mode 1 convergence achieved through the use of reduced integration of the stiffness matrix.

Note figures E.4 and E.5. Rotatory inertia is not present in the lumped mass assumption. The convergence to higher frequencies than predicted by the Timoshenko solution are directly attributable to the exclusion of rotatory inertia in the finite element model.

The Rayleigh and Bernoulli-Euler finite element results are shown in figures E.6 and E.7. From these figures it is seen that, (a) the frequencies are higher than predicted by Timoshenko beam theory, and (b) the frequencies are reduced by the inclusion of rotatory inertia (figure E.6). The difference remaining in figure E.6 is attributable to the exclusion of shear in the finite element model.

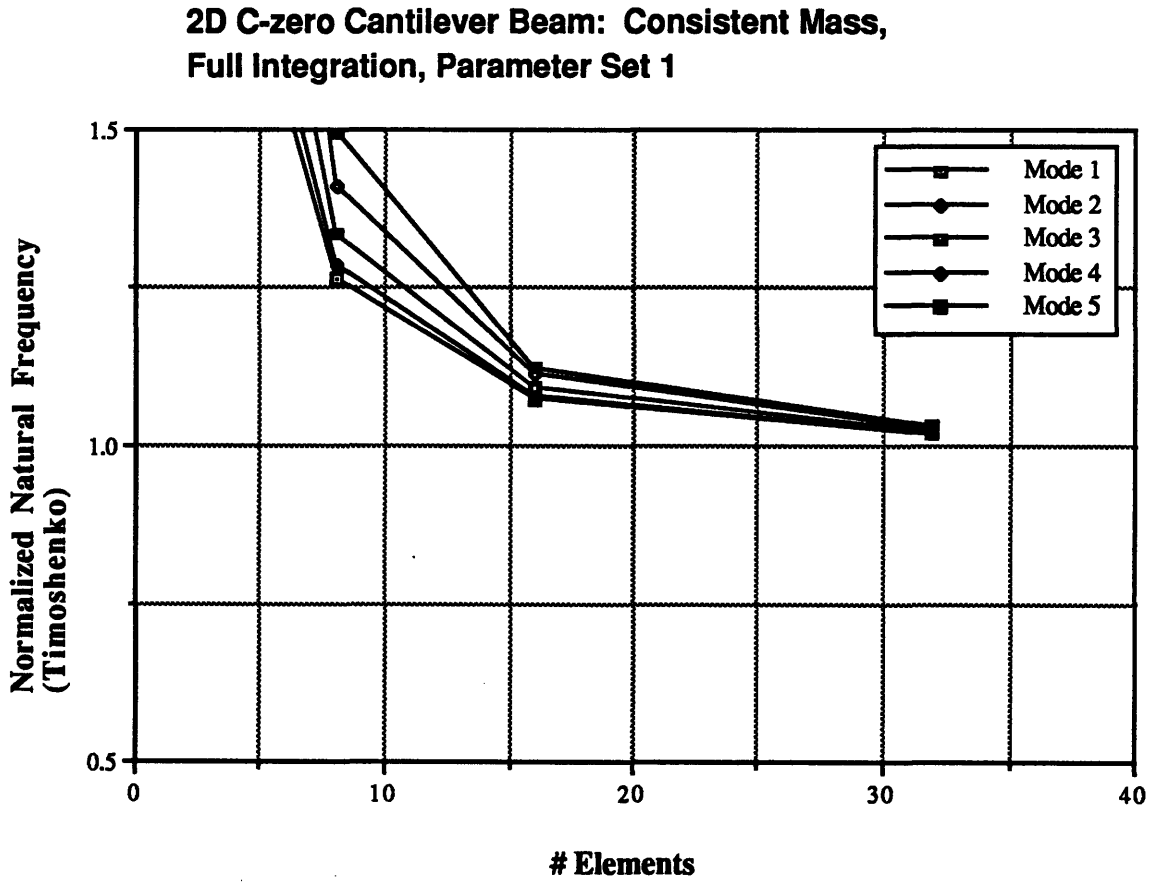

Figure E.1. Convergence plot normalized by Timoshenko frequencies; analogous to figure 4.1.

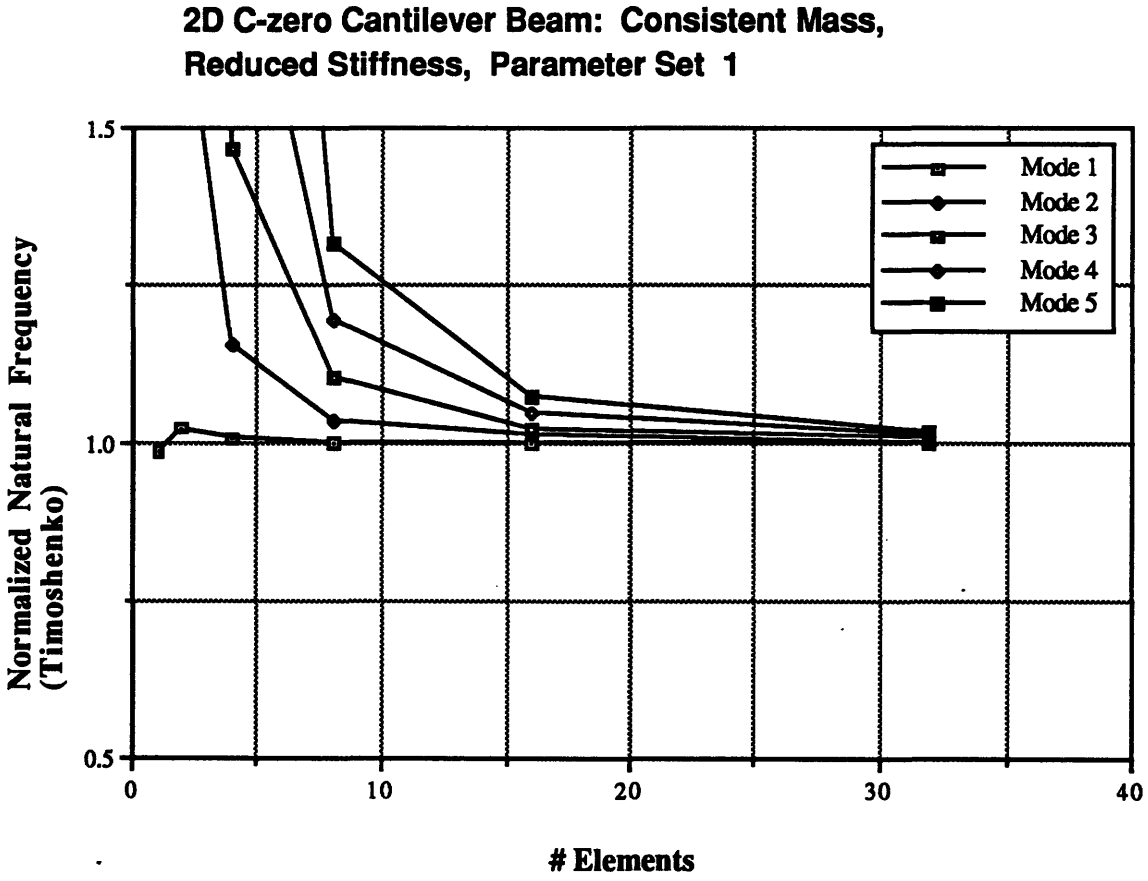

Figure E.2. Convergence plot normalized by Timoshenko frequencies; analogous to figure 4.3.

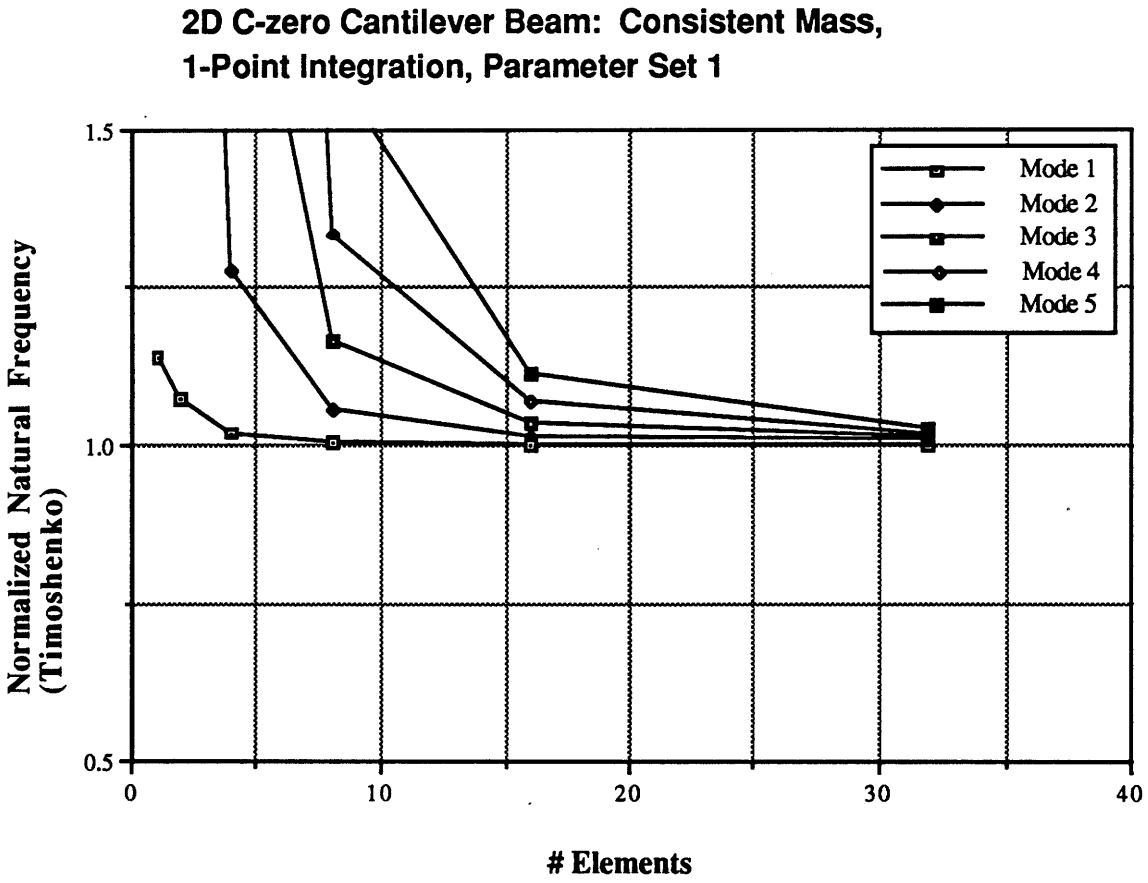

Figure E.3. Convergence plot normalized by Timoshenko frequencies; analogous to figure 4.5.

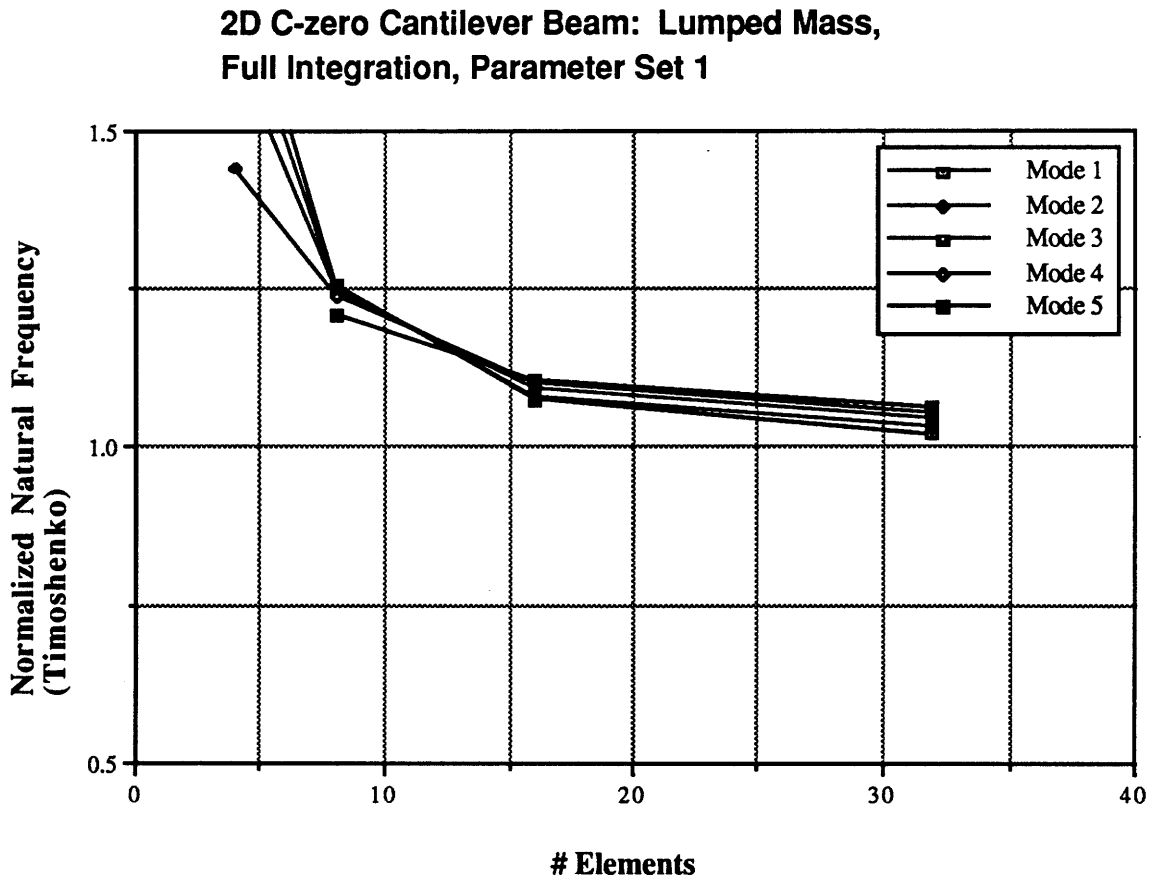

Figure E.4. Convergence plot normalized by Timoshenko frequencies; analogous to figure 4.7.

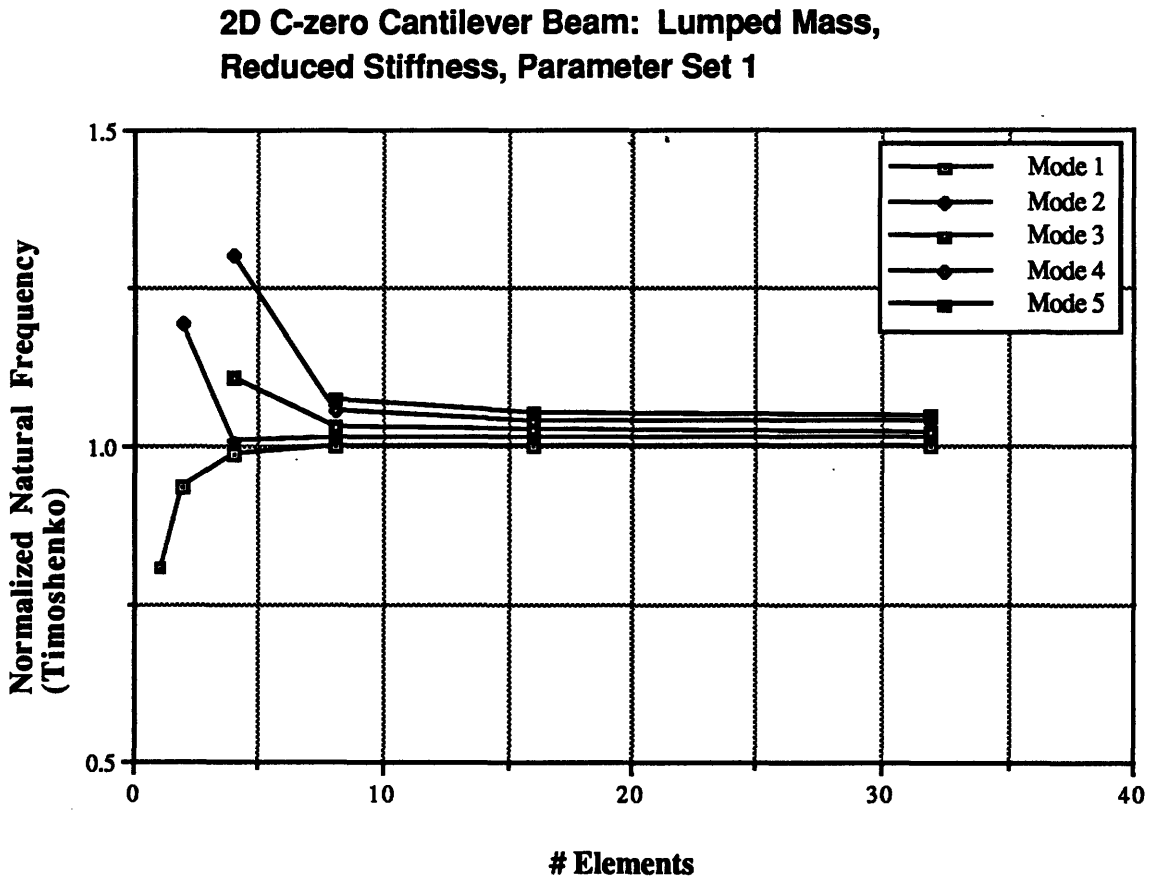

Figure E.5. Convergence plot normalized by Timoshenko frequencies; analogous to figure 4.9.

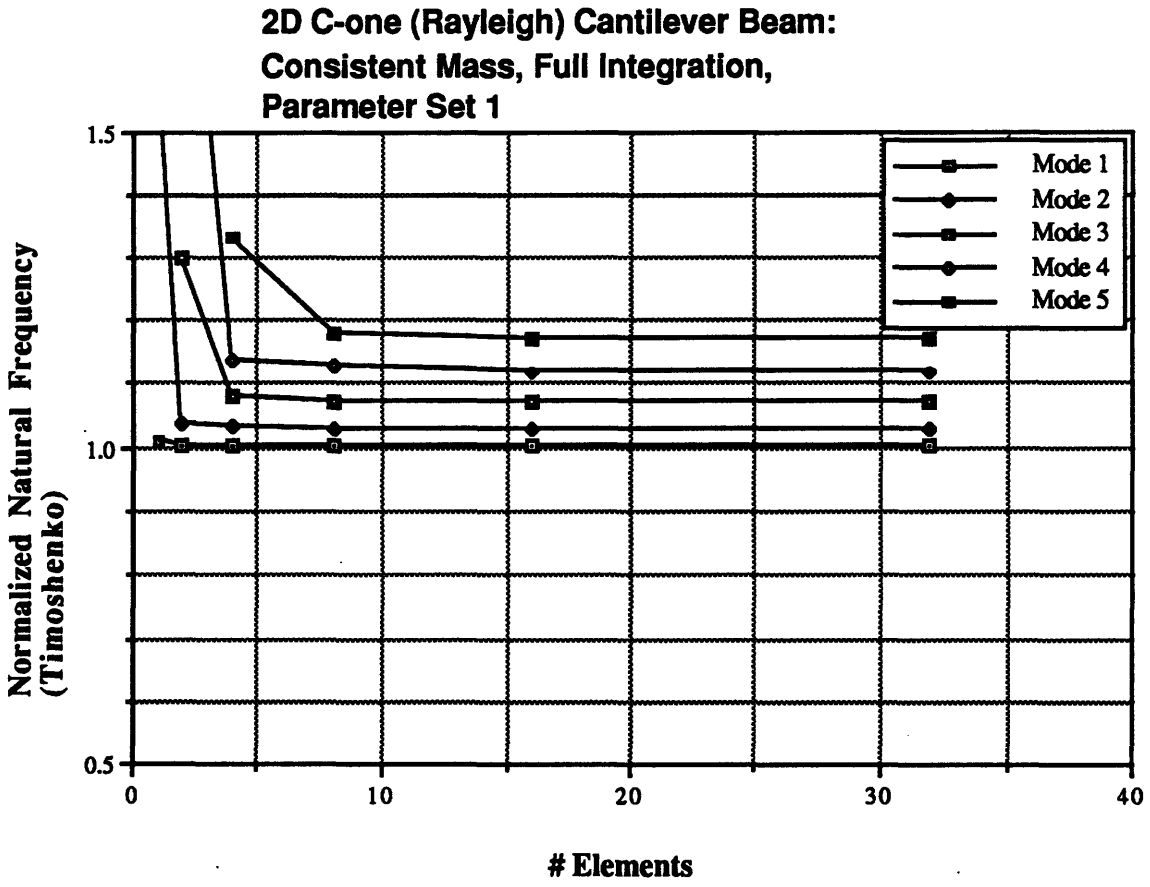

Figure E.6. Convergence plot normalized by Timoshenko frequencies; analogous to figure 4.11.

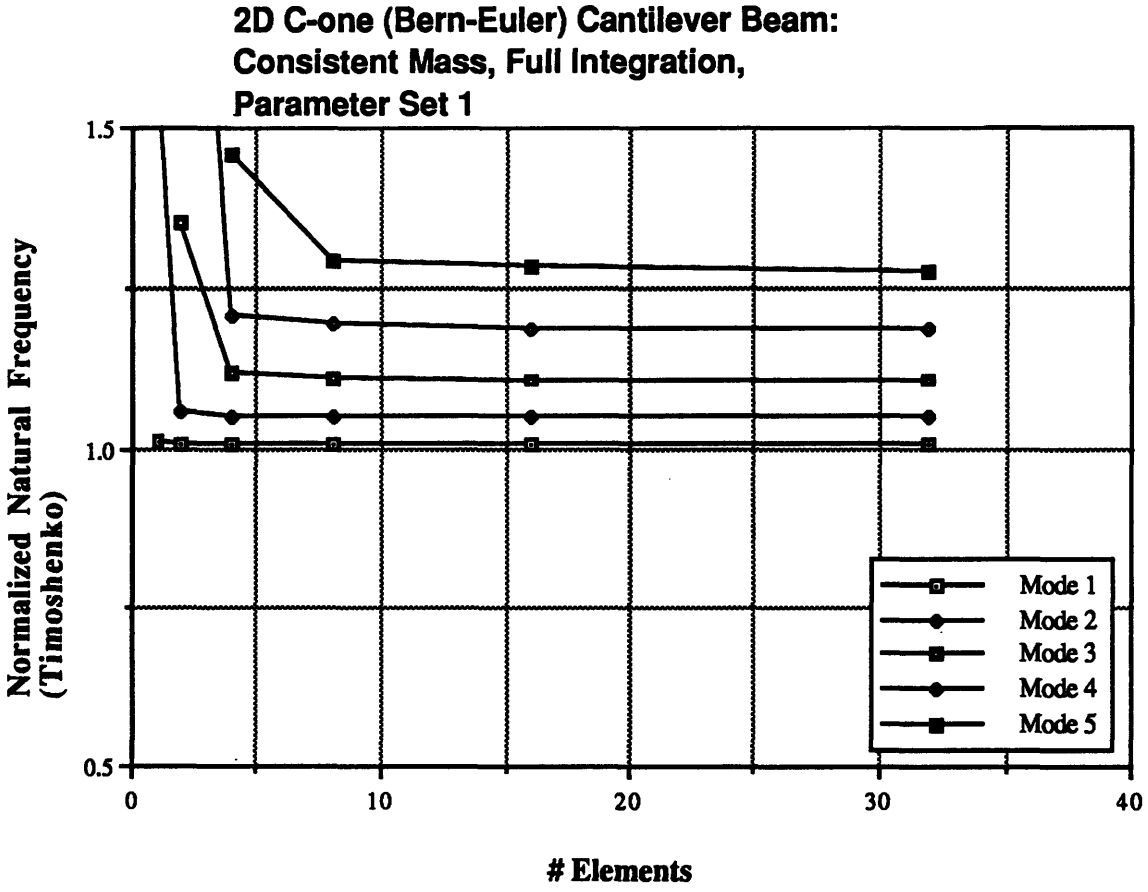

Figure E.7. Convergence plot normalized by Timoshenko frequencies; analogous to figure 4.12.

Appendix F

Gauss Quadrature [23]

The spatial integrals arising in the finite element method are conveniently evaluated using numerical integration procedures. An efficient scheme is of considerable importance in reduction of both computational time and cost. Gauss quadrature is such an optimal procedure. Integrals such as given by equations (3.3.15), (3.3.16), and (3.5.5) are transformed such that

$$I = \int_a^b f(x)\,dx \quad \rightarrow \quad I = \int_{-1}^{+1} g(\xi)\,d\xi \tag{F.1}$$

where $f(x)$ is representative of an arbitrary element of the matrix triple product and $g(\xi)$ is the transformed integrand. The transformation involves the Jacobian, which was discussed in chapter 3. In one dimension, the quadrature formula is given by

$$I = \int_{-1}^{+1} g(\xi)\,d\xi = w_1\, g(\xi_1) + w_2\, g(\xi_2) + \cdots + w_n\, g(\xi_n) \tag{F.2}$$

where

$g(\xi)$ = transformed function to be integrated
ξ_i = sampling points
w_i = weights

In Gauss quadrature, the sampling points and weights are prescribed such that maximum accuracy is achieved for a given n. Sampling points are symmetric about the center of the interval and are unevenly spaced. Symmetric points have the same weight. Exact integration is often referred to as 'full integration', whereas 'reduced integration' usually refers to an order of integration one less than required for full integration. The order of integration is governed by the rule: *a polynomial of degree (2n - 1) is integrated exactly by n-point Gauss quadrature.*

The mass and material and geometric stiffness matrices, derived in chapter 3, are evaluated by Gauss quadrature. The integration order required for exact integration can be determined from examination of the matrix elements which constitute the integrand, along with the above rule. The integration rule for the beam elements is summarized in table F.1.

Table F.1. Integration rule for beam finite elements.

Element Formulation	Mass Matrix	Stiffness Matrix	
	Full	Full	Reduced
C^1	4-point	3-point	2-point†
C^0	2-point	2-point	1-point

†In practice, reduced integration is not necessary in C^1 elements.